Program and Abstract Volume

LPI Contribution No. 1646

LUNAR AND PLANETARY INSTITUTE

USRA

ANNUAL MEETING OF THE LUNAR EXPLORATION ANALYSIS GROUP

November 7–9, 2011 • Houston, Texas

Sponsors

Universities Space Research Association/Lunar and Planetary Institute
National Aeronautics and Space Administration
NASA Lunar Exploration Analysis Group

Conveners

Charles Shearer, *University of New Mexico*
Clive Neal, *University of Notre Dame*
Stephen Mackwell, *Lunar and Planetary Institute*

Scientific Organizing Committee

Charles Shearer,*University of New Mexico*
Jeffrey Plescia, *John Hopkins, Advanced Physics Laboratory*
Clive Neal, *University of Notre Dame*
Michael Wargo, *NASA Headquarters*
Stephen Mackwell, *Lunar and Planetary Institute*
Dallas Bienhoff, *The Boeing Corportation*
John Crusan, *NASA Headquarters*
Kurt Sacksteder, *NASA Glenn Research Center*
Greg Schmidt, *NASA Lunar Science Institute, NASA Ames Research Center*
George Tahu, *NASA Headquarters*

Lunar and Planetary Institute 3600 Bay Area Boulevard Houston TX 77058-1113

LPI Contribution No. 1646

Compiled in 2011 by

Meeting and Publication Services
Lunar and Planetary Institute
USRA Houston
3600 Bay Area Boulevard, Houston TX 77058-1113

The Lunar and Planetary Institute is operated by the Universities Space Research Association under a cooperative agreement with the Science Mission Directorate of the National Aeronautics and Space Administration.

Abstracts in this volume may be cited as

Author A. B. (2011) Title of abstract. In *Annual Meeting of the Lunar Exploration Analysis Group,* p. XX. LPI Contribution No. 1646, Lunar and Planetary Institute, Houston.

ISSN No. 0161-5297

Preface

This volume contains abstracts that have been accepted for presentation at the Annual Meeting of the Lunar Exploration Analysis Group, November 7–9, 2011, Houston, Texas.

Administration and publications support for this meeting were provided by the staff of the Meeting and Publication Services Department at USRA's Lunar and Planetary Institute.

Contents

Program

Monday, November 7, 2011
BREAKTHROUGHS IN LUNAR SCIENCE AND EXPLORATION
8:30 a.m. Lecture Hall

New Science and Exploration Results from Missions, Terrestrial Laboratories, and NLSI Nodes

Chairs: **Charles Shearer**
Bradley Jolliff

8:30 a.m. Shearer C. K. *
Welcome to the LEAG Annual Meeting and LEAG Updates

8:45 a.m. Jolliff B. L. * Lawrence S. J. Robinson M. S. Scholten F. Hawke B. R. Greenhagen B. T. Glotch T. D. Hiesinger H. van der Bogert C. H.
Compton-Belkovich Volcanic Complex: Nonmare Volcanism on the Moon's Far Side **[#2031]**

9:00 a.m. Dhingra D. * Pieters C. M.
Mg-Spinel Rich Lithology at Crater Copernicus **[#2024]**

9:15 a.m. Allen C. C. * Greenhagen B. T. Donaldson Hanna K. L. Paige D. A.
Analysis of Lunar Pyroclastic Glass Deposit FeO Abundances by LRO Diviner **[#2022]**

9:30 a.m. Retherford K. D. * Gladstone G. R. Stern S. A. Egan A. F. Miles P. F. Parker J. Wm. Kaufmann D. E. Horvath D. G. Greathouse T. K. Versteeg M. H. Steffl A. J. Mukherjee J. Davis M. W. Slater D. C. Bayless A. J. Rojas P. M. Feldman P. D. Hurley D. M. Pryor W. R. Hendrix A. R.
LRO — Lyman Alpha Mapping Project (LAMP) Far-UV Maps of the Lunar Poles **[#2032]**

9:45 a.m. Mitrofanov I. * Litvak M. Sanin A. Malakhov A. Golovin D. Boynton W. Droege G. Chin G. Evans L. Harshman K. Garvin J. Kozyrev A. McClanahan T. Milih G. Mokrousov M. Starr R. Sagdeev R. Shevchenko V. Shvetsov V. Tret'yakov V. Trombka J. Varenikov A. Vostrukhin A.
Local Spots of Lunar Water-Ice Permafrost in Shadow and in Sunlight, as Seen by LEND/LRO **[#2015]**

10:00 a.m. Bussey D. B. J. * Cahill J. T. S. McGovern J. A. Green A. Spudis P. D.
Landing Site Selection Based on Polar Illumination Analysis **[#2029]**

10:15 a.m. BREAK

10:30 a.m. Stopar J. D. * Denevi B. W. Robinson M. S. Hawke B. R. Lawrence S. J. Koeber S.
Impact Melt Properties and Characteristics as Observed with the LROC Narrow Angle Cameras **[#2050]**

10:45 a.m. Joy K. H. * Kring D. A. Zolensky M. E. Ross D. K. McKay D. S.
Projectile Fragments in Ancient Lunar Regolith Breccias: Exploring the Sources and Temporal Record of Lunar Impacts **[#2036]**

11:00 a.m. Petro N. E. *
Volume of Impact Melt Generated by the Formation of the South Pole-Aitken Basin **[#2051]**

11:15 a.m. Harris I. E. * **CANCELED**
Planetary Dynamics of the Moon's Surface **[#2003]**

11:30 a.m. Shearer C. K. * Sharp Z. D. McCubbin F. Steele A.
Chlorine Isotope Composition and Carbon Mineralogy of "Rusty Rock" 66095. Implications for the Petrogenesis of Rusty Rock, Origin of "Rusty" Alteration, and Volatile Element Behavior on the Moon **[#2047]**

11:45 a.m. Zhong S. J. *
A New Hypothesis for Mare Basalt Volcanism, Volatile Distribution in the Lunar Mantle, and Moonquakes **[#2009]**

Monday, November 7, 2011
LUNAR COMMUNITY UPDATES
1:30 p.m. Lecture Hall

Updates to the Lunar Community About NASA and NLSI Node Activities

Chairs: **Charles Shearer**
Michael Wargo

1:30 p.m. Charles Shearer and Michael Wargo
Introduction

1:35 p.m. TBA
HEOMD — Community Update

2:05 p.m. James Green [INVITED]
SMD and Planetary Science — Community Update

2:25 p.m. TBA
Office of the Chief Technologist — Community Update

2:45 p.m. Gordon Johnston [INVITED]
SMD Technology Program — Community Update

3:05 p.m. TBD [INVITED]
International Collaboration and the Global Exploration Roadmap — Community Update

3:25 p.m. John Connolly [INVITED]
Human Space Flight Architecture Team-Destination Leads—- Community Update

3:45 p.m. Robert Kelso [INVITED]
Understanding Preservation and Scientific Value of Apollo Sites Relative to Spacecraft Visits — Community Update

4:00 p.m. Yvonne Pendleton [INVITED]
NLSI — Community Update

4:15 p.m. Burns J. O. Lazio J. *
Science Of and On the Moon with the Lunar University Network for Astrophysics Research **[#2014]**

4:30 p.m. Horanyi M. * Munsat T. Sternovsky Z. Kempf S. Colette A. Wang X. Robertson S. Mocker A. Gruen E.
NASA Lunar Science Institute: Colorado Center for Lunar Dust and Atmospheric Studies **[#2035]**

4:45 p.m. Neish C. D. Besse S. Kramer G. * Farrell W. Pieters C. Horanyi M. Pendleton Y.
Virtual Swirls: Highlights from NLSI's First Workshop Without Walls **[#2034]**

5:00 p.m. Kring D. A. *
Developing an Integrated, Multi-Institutional Approach for Studies of Fundamental Planetary Processes on the Moon: The Giant Impact, Lunar Magma Ocean, and Lunar Cataclysm Hypotheses **[#2017]**

5:15 p.m. Farrell W. M. * Killen R. M. Delory G. T. Bleacher L. V. Halekas J. S. Krauss-Varben D. Travnicek P. Zimmerman M. I. Hurley D. M. Stubbs T. J. Sarantos M. Gross N. Glenar D. A. Jordan A. P. Spence H. E. Bleacher J . E. Petro N. E. Jackson T. L. Dream N. L. S. I.
Solar Storm-Lunar Interaction Modeling: A Focus Study by the DREAM Lunar Science Institute **[#2013]**

Monday, November 7, 2011
POSTER SESSION: LUNAR EXPLORATION AND SCIENCE
6:00 p.m. Great Room

Spudis P. D. Lavoie T.
Using the Resources of the Moon to Create a Permanent Cislunar Space Faring System **[#2021]**

Wilson J. K. Spence H. E. Case A. W. Blake J. B. Golightly M. J. Kasper J. Looper M. D. Mazur J. E. Schwadron N. Townsend L. W. Zeitlin C.
First Cosmic Ray Albedo Proton Map of the Moon **[#2004]**

Eubanks T. M. Laine M.
LADDER: The Development of a Prototype Lunar Space Elevator **[#2043]**

Li R. He S. Skopljak B. Meng X. Yilmaz A. Jiang J. Banks M. S. Kim S. Oman C.
Lunar Astronaut Navigation Using LASOIS: Performance of a Simulated Apollo-14 Traverse at Haleakala National Park, Hawaii **[#2019]**

Mader M. M. Osinski G. R. Antoneko I. Barfoot T. Battler M. Beauchamp M. Chanou A. Cloutis E. Daly M. Capitan R-D. Francis R. Ghafoor N. Grieve R. A. F. Hodges K. Joliff B. L. Kerrigan M. McCullough E. Moores J. Otto C. Pickergill A. Pontefact A. Preston L. Redman D. Sapers H. Shankar B. Singleton A. Sylvester P. Tornabene L. L. Unrau T. Young K. Zanetti M.
Use of Robotitc Precursor Mission for Follow-On Human Exploration: Case Study Lunar Analogue Mission at the Mistastin Lake Impact Structure **[#2033]**

Lester D. F. Hodges K. V. Raftery M. L.
On-Orbit Control of Lunar Surface Telerobots from Earth-Moon Lagrange Points **[#2012]**

Li R. Lin L. Wang W. Crawford J. Meng X. He S. Robinson M. S. the LROC Science Team
Recent Progress in Lunar Topographic Mapping Using OrbiterMapper and LROC NAC Stereo Images **[#2018]**

Zacny K. Paulsen G. Shasho J. Hedlund M. Mellerowicz B. Makai T. Szwarc T. Nagihara S. Taylor P. Milam B.
Testing of a Pneumatic Proboscis Heat Flow Probe in a Vacuum Chamber and JSC-1A Lunar Soil Simulant **[#2028]**

Zacny K. Currie D. Paulsen G. Avanesyan A. Chu P. Makai T. Szwarc T.
Development and Testing of Gas Assisted Drill for the Emplacement of the Corner Cube Reflector System on the Moon **[#2008]**

Nandikotkur G. Milikh G. M. Sagdeev R. Chin G. Boynton W. Harshman K. Droege J. G. Mitrofanov I. G. Litvak M. L. Sanin A. B. Golovin D. Evans L. G. Starr R. McClanahan T.
Effect of Solar Activity on the Neutron Flux Detected by LEND **[#2010]**

Dhingra D. Pieters C. M.
Mineralogical Diversity of Impact Melts on Central Peak of Tycho and its Vicinity **[#2025]**

Joy K. H. Ross D. K. Zolensky M. E. Kring D. A.
Reconnaissance Element Mapping of Lunar Regolith Breccias **[#2007]**

Miura Yas.
Carbon and Rare-Earth Elements Contents on the Moon: As New Resources **[#2001]**

Tuesday, November 8, 2011
RESULTS AND STATUS OF CURRENT MISSIONS
8:30 a.m. Lecture Hall

Recent Results and Status of Current Lunar Missions and Activities

Chairs: **Clive Neal**
Noah Petro

8:30 a.m. Zuber M. T. * Smith D. E. Watkins M. Asmar S. C.
Update on the GRAIL Twin Spacecraft Mission to the Moon **[#2039]**

8:50 a.m. Pieters C. M. *
Scientific Breakthroughs from the Moon Mineralogy Mapper **[#2027]**

9:10 a.m. Vondrak R. R. * Keller J. W. Chin G. Garvin J. B. Rice J. W. Jr. Petro N. E.
The Lunar Reconnaissance Orbiter: Plans for the Science Phase **[#2040]**

9:25 a.m. Robinson M. S. * Team L. R. O. C.
The Lunar Reconnaissance Orbiter Camera: Two Years Exploring the Moon **[#2053]**

9:40 a.m. Greenhagen B. T. * Paige D. A. Diviner Science Team
Constaints from Diviner Lunar Radiometer Data for Future Lunar Landing Sites **[#2054]**

9:55 a.m. Boynton W. V. * Droege G. F. Harshman K. Mitrofanov I. G.
Results of LEND High Resolution Epithermal Neutron Measurements: Evidence for Two Hydrogen Emplacement Mechanisms **[#2044]**

10:10 a.m. BREAK

10:25 a.m. Litvak M. L. * Mitrofanov I. G. Sanin A. B. Boynton W. V. Chin G. Garvin J. B. Golovin D. V. Droege G. Evans L. Harshman K. Kozyrev A. S. Malakhov A. V. McClanahan T. Milikh G. Mokrousov M. I. Sagdeev R. Z. Starr R.
Global Mapping of Neutrons from the Moon by LEND Instrument Onboard LRO **[#2020]**

10:40 a.m. Smith D. E. * Zuber M. T. Neumann G. A. Mazarico E. Head J. W. III LOLA Science Team
Surface Roughness and Slopes on the Moon at 5-Meter Scale **[#2037]**

10:55 a.m. Mazarico E. * Neumann G. A. Smith D. E. Zuber M. T. Torrence M. H.
Illumination Conditions of the Lunar Poles to 65 Degrees Latitude from Lunar Orbiter Laser Altimeter Data **[#2030]**

11:10 a.m. Schwadron N. A. * Case A. W. Golightly M. Jordan A. Joyce C. Kasper J. Kozarev K. Mislinski J. Spence H. E. Townsend L. W. Wilson J.
The Lunar Radiation Environment from the Cosmic Ray Telescope for the Effects of Radiation (CRaTER) and from Earth-Moon-Mars Radiation Environment Modules (EMMREM) **[#2005]**

11:25 a.m. Mislinski J. F. * Schwadron N. A. Townsend L. Spence H. E. Rother O. M. Posner A. Squier R. Wilson J. K. Jordan A. P. Anderson R. Baker T. Kozarev K. A. Joyce C.
Radiation Risks for Future Manned and Robotic Missions: PREDICCS: Predictions of Radiation from REleASE, EMMREM, and Data Incorporating CRaTER, COSTEP, and Other SEP Measurements — An Online Nowcasting and Forecasting System **[#2023]**

11:40 a.m. Eppler D. B. *
The 2010 Desert RATS Science Operations Test: Outcomes and Lessons Learned **[#2049]**

11:55 a.m. Shearer C. K. * Neal C. R. Christoffersen R. Keller L. P. Clemett S. J. Noble S. K.
Exploring a "New" Moon Now and Preparing for Future Lunar Exploration. A Consortium Study of "Special" Lunar Samples **[#2006]**

Tuesday, November 8, 2011
FORGING INNOVATIVE PARTNERSHIPS I:
COMMERCIAL LUNAR EXPLORATION
1:30 p.m. Lecture Hall

Teams Address Commercial Approaches Behind Their Effort to Win the GLXP and Earn a Profit

Moderators: **Dallas Bienhoff**

Panel Members: **David Gump**
Michael Joyce
Robert Richards

Tuesday, November 8, 2011
FORGING INNOVATIVE PARTNERSHIPS II:
ALTERNATIVE APPROACHES TO LUNAR DEVELOPMENT
3:00 p.m. Lecture Hall

Four Unique Views on Lunar Development, Including Government Outpost, International Research Park, Commercial Outpost/Research Facility, and Commercial Resource Extraction Plus Potential Funding Approaches

Moderators: **Dallas Bienhoff**

Panel Members: **John Connolly**
John Hamilton
Mike Gold
Jim Keravala

Wednesday, November 9, 2011
FUTURE MISSIONS OF EXPLORATION AND SCIENCE
8:30 a.m. Lecture Hall

Explore Concepts for Future Missions, from Around the World,
that Fulfill Lunar Science Goals and Enable Human Exploration of the Solar System

Chairs: **Richard Elphic**
Mark Robinson

8:30 a.m. Pieters C. M. *
What's Next? Building on Recent Results **[#2026]**

8:45 a.m. Elphic R. C. * Delory G. T. Grayzeck E. J. Colaprete T. Horanyi M. Mahaffy P. Hine B. Boroson D. Salute J. S.
The Science Behind NASA's Lunar Atmosphere and Dust Environment Explorer **[#2056]**

9:00 a.m. Carpenter J. D. * Pradier A. Fisackerly R. Houdou B. De Rosa D. Gardini B. Philippe C.
The European Lunar Lander: A Human Exploration Precursor Mission **[#2046]**

9:15 a.m. Mitrofanov I. *
Science Mission LUNA GLOB **[#2016]**

9:30 a.m. Hoffmann H. * Jaumann R. Hiesinger H. Claasen F. Spohn T. Mall U. Helbert J. Kappelmann N. Werner K. Wimmer-Schweingruber R. Srama R. Oberst J. Flohrer J. Werner M. Neukum G. van Gasselt S. Schmitz N. Eichentopf K. Knigge T. Kummer U. Langemann M. Mueller H. Haarmann R.
A Dedicated Small Lunar Exploration Orbiter and a Mobile Surface Element **[#2048]**

9:45 a.m. Martin E. * Piedboeuf J.-C. Ouellet A. Picard M. Lange C. Hipkin V.
Toward Canadian Contributions to International Lunar **[#2055]**

10:00 a.m. Ghafoor N. * Dickinson C. McCoubrey R. Chappell L. Barnet M. Dietrich P. Teti F. Sallaberger C.
Preparing for Lunar Exploration — Concepts, Technologies, Partnerships in an Age of Uncertainty **[#2057]**

10:15 a.m. BREAK

10:30 a.m. Hall A. *
Hitching a Ride for Science on Google Lunar X PRIZE

10:45 a.m. Richards R. *
A Lunar Google X-Prize Mission

11:00 a.m. Gump D. P. *
Delivery of Lunar Surface Payloads on a Cost-Shared Commercial Robotic Expedition **[#2045]**

11:15 a.m. Neal C. R. *
Establishing a Lunar Geophysical Network for Exploration and Solar System Science **[#2052]**

11:30 a.m. Robinson M. S. * Lawrence S. J. Speyerer E. J. Stopar J. D.
Intrepid: Lunar Roving Prospector Providing Ground Truth and Enabling Future Exploration **[#2042]**

11:45 a.m. Garrick-Bethell I. * Lin R. Sanchez H. Hemingway D.
Lunar Swirl Impactors: A Low-Cost Mission to Study Lunar Swirls, Magnetism, Water, Space Weathering, Dust, and Plasma Physics **[#2038]**

12:00 p.m. DISCUSSION

ANALYSIS OF LUNAR PYROCLASTIC GLASS DEPOSIT FeO ABUNDANCES BY LRO DIVINER.

Carlton C. Allen[1], Benjamin T. Greenhagen[2], Kerri L. Donaldson Hanna[3], and David A. Paige[4]
[1]NASA Johnson Space Center, Houston, TX 77058 carlton.c.allen@nasa.gov, Jet Propulsion Laboratory, California Institute of Technology, Pasadena, CA 91109 benjamin.t.greenhagen@jpl.nasa.gov, [3]Brown University, Providence, RI 02912 kerri_donaldson_hanna@brown.edu, [4]UCLA, Los Angeles, CA 90024 dap@mars.ucla.edu.

Introduction: Telescopic observations and orbital images of the Moon reveal at least 75 deposits, often tens to hundreds of km across, that mantle mare or highland surfaces [1]. These deposits are interpreted as the products of pyroclastic eruptions and designated herein as lunar pyroclastic deposits (LPD). They are understood to be composed primarily of sub-millimeter beads of basaltic composition, ranging from glassy to partially-crystallized [2]. Delano [3] documented 25 distinct pyroclastic bead compositions in lunar soil samples, though the source deposits for most of these beads have not been identified.

The pyroclastic deposits are important for many reasons. Petrology experiments and modeling have demonstrated that the pyroclastic glasses are the deepest-sourced and most primitive basalts on the Moon [4]. Recent analyses have documented the presence of water in these glasses, demonstrating that the lunar interior is considerably more volatile-rich than previously understood [5]. Experiments have shown that the iron-rich pyroclastic glasses release the highest percentage of oxygen of any Apollo soils, making these deposits promising lunar resources [6].

Taurus Littrow: The Taurus Littrow LPD, located in eastern Mare Serenitatis near the Apollo 17 landing site, is both well characterized from orbital data and represented in the lunar sample collection. The deposit covers an area of several thousand km^2 and is approximately ten meters thick [7]. The LPD extends across the Apollo 17 landing site, and the Shorty Crater orange and black glass beads, with an average diameter of 44 μm [7], are understood to be samples of this deposit. Apollo 17 orange and black glasses are identical in major elemental composition, with the color indicating the degree of ilmenite and olivine crystallization following eruption [8].

Diviner Measurements: The Diviner Lunar Radiometer Experiment on the Lunar Reconnaissance Orbiter [9] includes three thermal infrared channels spanning the wavelength ranges 7.55-8.05 μm, 8.10-8.40 μm, and 8.38-8.68 μm. These "8 μm" bands were specifically selected to measure the emissivity maximum known as the Christiansen feature [10]. The wavelength location of this feature, referred to herein as CF, is particularly sensitive to silicate minerals including plagioclase, pyroxene, and olivine – the major crystalline components of lunar rocks and soils. The general trend is that CF positions at shorter wavelengths are correlated with higher silica content and CF positions at longer wavelengths are correlated with lower silica content. Given the range of lunar mineralogy, a direct correlation between CF positions and FeO content is expected (*i.e.* higher CF indicates higher FeO content and vice versa).

Laboratory Spectra: Laboratory thermal infrared reflectance spectra of fifteen Apollo soil samples, characterized in detail by the Lunar Soils Consortium [11,12], were measured under ambient conditions using the FT-IR spectrometer in the Keck/NASA Reflectance Experiment Laboratory (RELAB) at Brown University [13]. Samples in this study are the 20 - 45 μm splits of bulk soil. In addition, the spectrum of sample 74002 – consisting of nearly pure black pyroclastic glass representative of the Taurus Littrow LPD – was measured. The wavelength of the reflectance minimum in the 8 μm region of each spectrum is equivalent to the emissivity maximum, or CF. These CF values are closely correlated to published FeO concentrations for the 20 – 45 μm splits of these soils [11,12] and the pyroclastic glass [3], with an r^2 value of 0.9.

These laboratory spectra are not directly comparable to orbital data, however. Diviner measures emissivity under vacuum conditions, which create a thermal gradient in the uppermost ~200 microns of the surface. Laboratory measurements of pure minerals in a simulated lunar environment (SLE) demonstrate that CF measurements should be modified according to the relationship: CF(SLE) = (CF(lab)-0.6778)/0.9502 [14]. CF(SLE) values derived from the RELAB measurements of the 15 soils and pyroclastic glass remain closely correlated to FeO, with an r^2 value of 0.9. This correlation between CF(SLE) extends across the full compositional range of lunar soils, from FeO concentrations of 4.62 wt. % (soil 61221) to 22.9 wt. % (pyroclastic glass 74002). These results provide a basis for investigating the correlation between lunar soil FeO abundances and CF values derived from Diviner multispectral measurements, and using this correlation to derive the FeO contents of other lunar pyroclastic deposits.

Correlation of Diviner CF with FeO: Diviner CF values, reduced using the most recent corrections of Greenhagen et al. [15], were derived for 2 x 2 km areas centered on each Apollo landing site, as well as the Taurus Littrow LPD. All data were taken near lunar mid-day. These values were plotted against published FeO abundances for the 20 - 45 μm sieve fraction of a characteristic Apollo soil sample from each site [11,12], along with the FeO content of Apollo 17 pyroclastic glass [3]. The CF and FeO values proved to be closely correlated across the full range of Apollo soil compositions (Fig. 1).

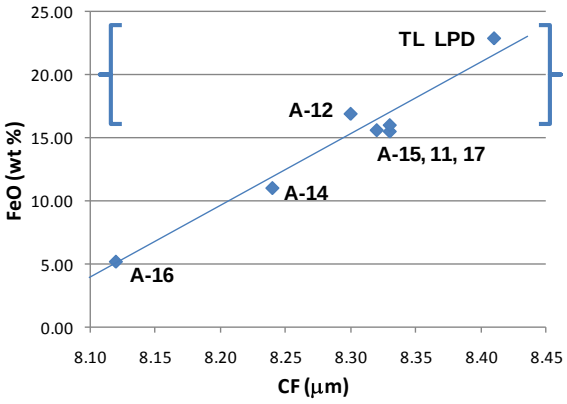

Figure 1. Correlation of Diviner CF values with sample FeO concentrations for the six Apollo sites plus the Taurus Littrow LPD. Brackets denote the full range of pyroclastic glass bead compositions [3].
Regression line: FeO = 61.1 x CF – 492.6 $r^2 = 0.9$

This correlation provides the opportunity to estimate the FeO concentration of other LPD's. These estimates can be compared to the known compositions of pyroclastic glass beads in lunar soils.

Sulpicius Gallus: The Sulpicius Gallus LPD, spanning the mare-highland boundary on the western edge of Mare Serenitatis, contains local concentrations of red and orange material thought to be pyroclastic glass [8]. The Sulpicius Gallus LPD has a higher albedo than the Taurus Littrow LPD, suggesting differing average compositions or differing degrees of crystallization [16,17].

Diviner data, averaged over 2 x 2 km areas on the Sulpicius Gallus LPD, consistently yield maximum CF values of 8.37 μm. This CF value is lower than the value of 8.41 μm that characterizes the Taurus Littrow deposit.

Inserting a CF value of 8.37 μm into the correlation formula shown in Fig. 1 yields an FeO abundance of 18.9 wt. %. This value is significantly below the FeO abundances of orange and black glasses found in the Apollo 11, 14, 15 and 17 soils, but well within the range of the very low titanium and green glasses in soils from the Apollo 14, 15, and 17 sites. [3]. These data indicate that the albedo differences between the Sulpicius Gallus and Taurus Littrow LPD's are due to differing average compositions, rather than to differing degrees of crystallization.

Aristarchus: This LPD spans most of the large Aristarchus plateau, located in Oceanus Procellarum. The deposit displays a range of pyroclastic glass concentrations and spectral signatures, possibly from mixing with underlying material due to cratering [16,17]. The CF value from one of the most glass-rich areas is 8.40 μm, implying an FeO concentration of 20.6 wt. %. This value is close to the FeO concentration of Taurus Littrow glass (22.9 wt. %).

Implications: This work demonstrates that:

- Laboratory CF values, corrected to correspond to a simulated lunar environment, are closely correlated with FeO abundances across the full range of Apollo soils and pyroclastic glasses.
- Diviner CF values are also closely correlated with FeO abundance across the full range of Apollo soils and pyroclastic glasses.
- Diviner CF values have the potential to provide remote analyses of FeO concentrations in previously unsampled lunar pyroclastic deposits.
- Diviner CF values have the potential to provide remote analyses of FeO concentrations across the entire lunar surface.

References: [1] Gaddis, L.R. *et al.* (2003) *Icarus, 161,* 262. [2] Pieters, C.M. *et al.* (1974) *Science, 183,* 1191. [3] Delano, J. (1986), *Proc. Lunar Planet. Sci. Conf., 16th,* D201-D213. [4] Green, D.H. *et al.* (1975) *Proc. Lunar Planet. Sci. Conf., 6th,* 871. [5] Saal, A.E. *et al.* (2008) *Nature, 454,* 192. [6] Allen, C.C. *et al.* (1996) *J. Geophys. Res., 101,* 26,085. [7] Heiken, G. *et al.* (1974) *Geochem. Cosmochim. Acta, 38,* 1703. [8] Weitz, C.M. *et al.* (1999) *Meteorit. Planet. Sci., 34,* 527. [9] Paige, D.A. *et al.* (2009) *Space Sci. Revs,* DOI 10.1007/s11214-009-9529-2. [10] Greenhagen, B.T. *et al.* (2010) *Science, 329,* 1507-1509. [11] Taylor, L.A. *et al.* (2001) *J. Geophys. Res., 106,* 27,985. [12] Taylor, L.A. *et al.* (2010) *J. Geophys. Res., 115,* doi:10.1029/2009JE003427. [13] Pieters, C.M. and Hiroi, T. (2004) RELAB (Reflectance Experiment Laboratory): A NASA Multiuser Spectroscopy Facility, 35th LPSC, Abs # 1720. [14] Donaldson Hanna, K.L. *et al.* (2012) *in press.* [15] Greenhagen, B.T. *et al.* (2012) *in press.* [16] Lucchitta, B.K. and Schmitt, H.H. (1974) *Proc. Lunar Sci. Conf. 5th,* 223. [17] Weitz, C.M. *et al.* (1998) *J. Geophys. Res., 103,* 22,725.

RESULTS OF LEND HIGH-RESOLUTION EPITHERMAL NEUTRON MEASUREMENTS: EVIDENCE FOR TWO HYRODGEN EMPLACEMENT MECHANISMS. W. V. Boynton[1] G.F. Droege[1] K. Harshman[1] I Mitrofanov[2] and the LEND Science team. [1]University of Arizona, Tucson AZ 85718, wboynton@LPL.Arizona.edu, [2]Institute for Space Research of Russian Academy of Science, 117997 Moscow, Russia, mitrofanov@l503.iki.rssi.ru

Introduction: The possibility of volatiles, and particularly ice, being concentrated in permanently shadowed regions (PSRs) was suggested long ago [1,2]. The first evidence of this possibility was found by an analysis of radar reflection data from the Clementine Mission [3], but others have raised questions concerning this result [4,5]. Data from the Lunar Prospector Neutron Spectrometer (LPNS) showed a significant reduction in the flux of epithermal neutrons in the vicinity of both lunar poles [6] indicating an enhancement of hydrogen, but the spatial resolution of the instrument was not sufficient to associate the hydrogen with the PSRs.

More recently, the Lunar Exploration Neutron Detector (LEND) collected data with much better spatial resolution than that of LPNS [7]. With higher resolution, the data showed that the areas of depressed epithermal neutron flux, called neutron suppressed regions (NSRs) were not spatially consistent with the PSRs. In this work we shall show the results of a more detailed analysis of the LEND data that show clear evidence of two distinct populations of hydrogen enrichment in the lunar poles.

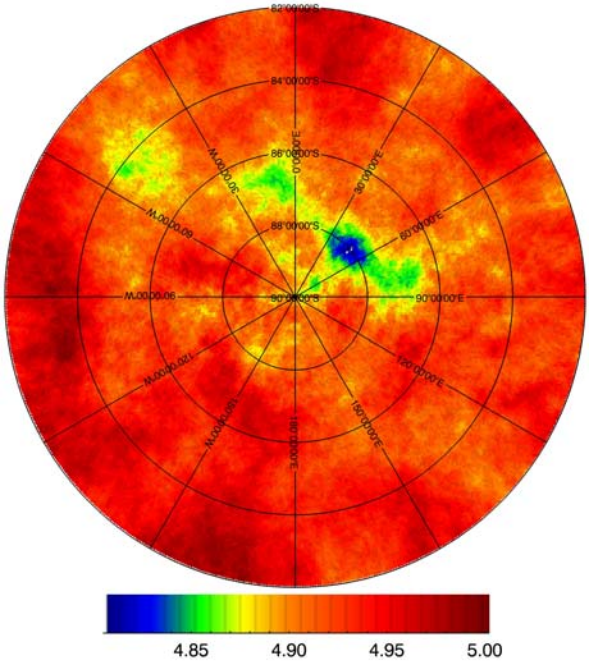

Fig. 1 Map of LEND collimated epithermal count rates in the south polar region south of -82° latitude.

Results: The data from the four collimated sensors are first corrected for changes in efficiency during warm up following each ~14-day on/off cycle and for variations in the cosmic-ray flux with time: cosmic rays are the excitation source for the neutrons. Occassionally one or two sensors were shut off, and the count rates of the working sensors were adjusted upward to the equivalent four-sensor rate with counting uncertainties adjusted appropriately.

Figure 1 shows the counting rates in the South Polar Region. It can be seen that the counting rate is fairly uniform at just less than 5.0 counts/sec, but there are a few areas with significantly lower count rates. The collimated sensors have a field of view (FOV) of 5.6° HWHM [8], which corresponds to 5 km on the surface at 50 km altitude.

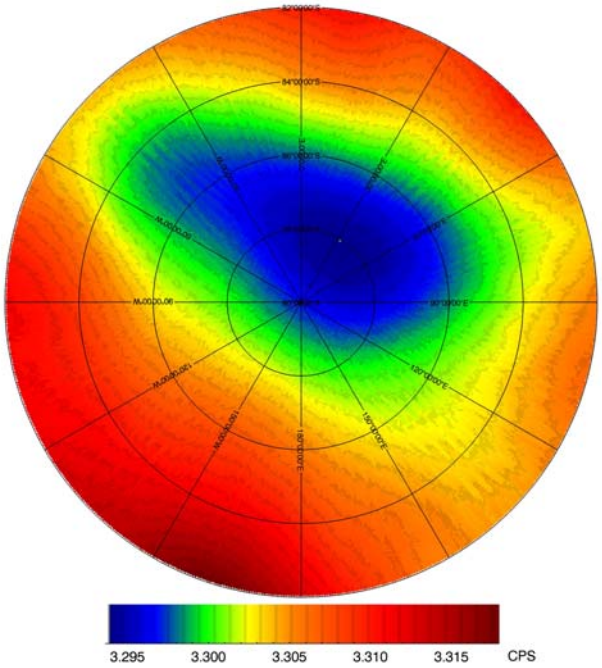

Fig. 2. Background counting rate shows only a very small variation with location.

Some neutrons from outside the FOVare also counted. These neutrons come from three sources: lunar neutrons leaking through the walls of the collimator, lunar neutrons scattered off the spacecraft, and cosmic-ray produced neutrons from the spacecraft. The counting rates from the first two sources depend on the emission of neutrons within view of the spacecraft, but since the spacecraft sees an area so much larger than that of the collimated sensors, the counting rate from this source is averaged over a very large area and does not change much over the polar region. Figure 2 shows a map of the background signal calculated based on the emission rate of neutrons from all regions within

view of the spacecraft. It can be seen that the background counting rate is nearly independent of location within the polar region.

Difference maps. In this work we are interested in finding places of hydrogen enrichement, so we make a map of count rate differences. As will be shown, there are two populations of hydrogen distribution. One is shown by a linear decrease in counting rate with latitude in both polar regions (fig. 3), and the other is due to the NSRs.

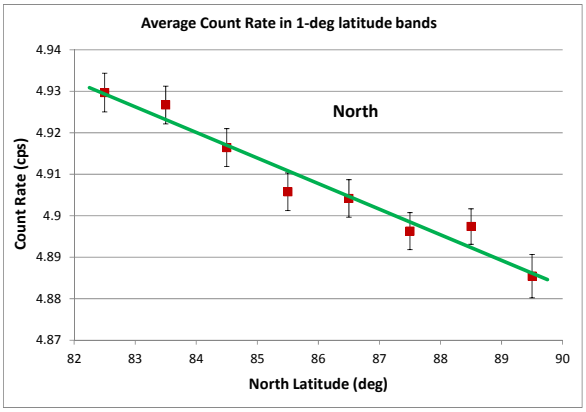

Fig 3. The epithermal count rate (North Pole) decreases linearly with latitude showing an increase in hydrogen concentration. (South is nearly identical.)

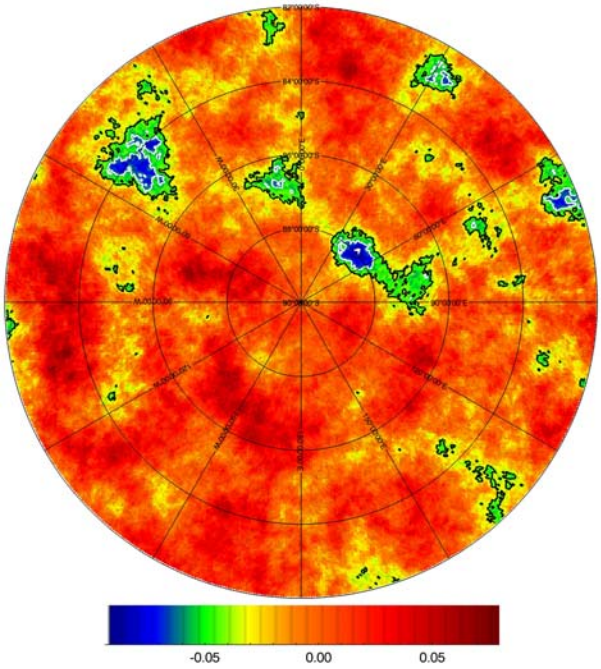

Fig 4. Count-rate difference map in the South Polar Region. Contours are drawn at a difference -0.04 cps.

We make a difference map by subtracting the count rate determined from the linear fit in fig. 3. The difference maps are shown in fig. 4. It is obvious there are some regions with count rates significantly lower than most of the rest of the map. It is not clear just by looking at the map if these regions are just the tail of a normal distribution, or if they represent a different population of hydrogen enrichement.

We examine this question by making a histogram of all of the points (HEALPix bins) in the maps separately for each pole. The results for the South Pole are shown in figure 5. It is very obvious that we have a bimodal distribution of count rates (and thus hydrogen distribution).

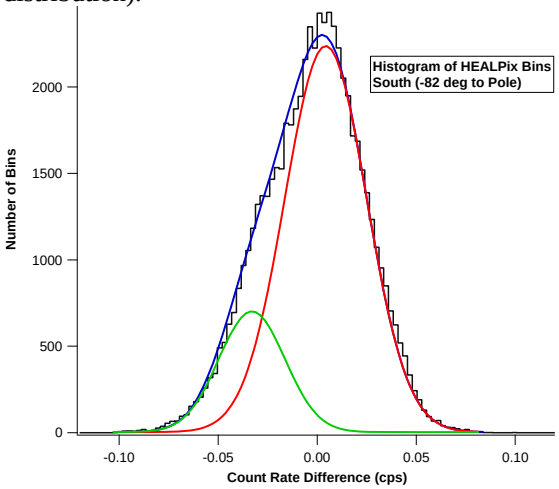

Fig 5. Histogram of HEALPix bins in fig 4 shows a clear bimodal distribution of count rates. The smooth blue line is the sum of the two Gaussian shown in red and green.

Discussion: It is clear from figure 5 that there are two distinct populations of hydrogen distribution, which suggests that two different mechanisms are responsible for the observed distribution. The smaller population has lower count rates and clearly corresponds to the NSRs. It is perhaps not surprising that the NSRs are represent a different mechanism, but prior to obtaining these LEND data, the mechanism was thought to be associated with the PSRs, but we now know that is not the case.

The other distribution is represented by the very regular increase in hydrogen toward the pole. This distribution is not likely to be due to the primary emplacement of hydrogen if it comes from the solar wind because the cosine of the angle would have a higher flux at lower latitudes. This distribution is almost certainly due to average surface temperatures being lower toward the pole, hence volatile migration is suggested.

The implications of these distributions will be discussed in more detail at the meeting.

References: [1] Watson et al. (1961), [2] Arnold (1971), [3] Nozette et al., (1996), [4] Stacey et al. (1997) [5] Simpson and Tyler (1999), [6] Feldman et al. (1998). [7] Mitrofanov et al. (2011), [8] Mitrofanov et al. (2008).

SCIENCE OF AND ON THE MOON WITH THE LUNAR UNIVERSITY NETWORK FOR ASTROPHYSICS RESEARCH. J. Burns[1,3] and J. Lazio[2,3], [1]University of Colorado at Boulder, CASA, 593 UCB, Boulder, CO 80309-0593, USA, [2]Jet Propulsion Laboratory, California Institute of Technology, M/S 138-308, 4800 Oak Grove Dr, Pasadena, CA 91107, USA, [3]NASA Lunar Science Institute.

The Lunar University Network for Astrophysics Research (LUNAR) undertakes investigations across the full spectrum of the science within the mission of the NASA Lunar Science Institute (NLSI), namely science of, on, and from the Moon. The LUNAR team's work on science of and on the Moon is conducted in the broader context of ascertaining the content, origin, and evolution of the solar system. Here we describe the science motivation for instrument packages for a number of future missions.

The **interior structure and composition** of the Moon, particularly of its core, remains poorly constrained. In turn, the size and state of the core (fluid vs. solid) reflect processes that occurred at the time of the formation of the Earth-Moon system, including the likely giant impact responsible for the formation of the Moon, and advancing the state of knowledge of the interior structure was recognized as an important science objective in the *Visions and Voyages for Planetary Science in the Decade 2013–2023* Decadal Survey. Lunar laser ranging provides precision measurements of the Earth-Moon distance at the 10 mm level, and the LUNAR team is developing the technology to advance the precision to the 10 μm level using a next-generation of laser retroreflectors. These retroreflectors could be science packages for a number of future NASA and commercial missions. At these levels of precision, variations in the Moon's librations are easily detectable, and, even at the current 10 mm precision level, using retroreflectors emplaced during the Apollo missions, lunar laser ranging constrains the size of the core to be approximately 400 km in radius, with the specific value depending upon the composition of the core. Other work being undertaken tracks the influence of tides, heat dissipation, and the orbital evolution of the Earth-Moon system.

The **lunar atmosphere** is the exemplar and nearest case of a surface boundary exosphere for an airless body in the solar system. The *Visions and Voyages for Planetary Science in the Decade 2013–2023* Decadal Survey noted that understanding the evolution of exospheres, and particularly their interaction with the space environment, remains both poorly constrained and requires observations at a variety of different bodies. Determining and tracking the properties of the lunar atmosphere both robustly and over time requires a lunar-based methodology by which the atmosphere can be monitored over multiple day-night cycles from a fixed location(s). Relative ionospheric opacity measurements or riometry, measures the amount of power received at different radio frequencies and directly determines the density of the (ionized) atmosphere. The LUNAR team has been developing the technology for a future lunar-based radio telescope, which is also applicable to a lunar riometer that could be deployed on a future lander, either flown by NASA or a commercial entity (e.g., Google X Prize competitor).

The interplanetary medium is pervaded by **dust** from a variety of sources, including small bodies, the inner planets, and interstellar space. Recent work on interplanetary dust by members of the LUNAR team has revealed a substantial population of nanometer size dust, or nanodust, with fluxes hundreds of thousands of times higher than the better understood micron-sized dust grains. This nanodust tends to move with the speed of the solar wind, or at hundreds of kilometers per second, as opposed to more typical Keplerian speeds of tens of kilometers per second. Since impact damage grows faster than the square of the impact speed for high speed dust, nanodust could be an important and previously unrecognized contributor to space weathering. The same technology for a future lunar-based radio telescope would also be applicable for measuring the distribution of dust particles as a function of size in interplanetary space, and ultimately for understanding how dust modifies the surfaces of planets and other objects in the solar system.

Part of this research was carried out at the Jet Propulsion Laboratory, California Institute of Technology, under a contract with the National Aeronautics and Space Administration. The LUNAR consortium is funded by the NASA Lunar Science Institute (via Cooperative Agreement NNA09DB30A) to investigate concepts for astrophysical observatories on the Moon.

LANDING SITE SELECTION BASED ON POLAR ILLUMINATION ANALYSIS. D. B. J. Bussey[1], J.T.S. Cahill[1], J.A McGovern[1], A. Green[2], P.D. Spudis[3], [1]The Johns Hopkins University Applied Physics Laboratory, Laurel MD; [2]University of Maryland, College Park MD; [3]Lunar and Planetary Institute, Houston TX. (ben.bussey@jhuapl.edu).

Introduction: New topographic data returned by the LOLA instrument on NASA's Lunar Reconnaissance Orbiter permit the study of the Moon's polar illumination conditions to a level of detail that was not possible previously. We have used these data, together with LROC images, to analyze the best places to land for different mission scenarios. These may not correspond exactly to the "best pixel" of an illumination map but are a factor of landing error ellipse.

Simulations: Images such as those from LROC provide a very precise snap shot of the illumination conditions for a particular Sun position. However one limitation of images is that they show the lighting conditions at the surface, whereas for mission planning, we need to know illumination conditions at the height of the solar arrays. We have developed a simulation capability called LunarShader which uses a topographic product (e.g. LOLA DEM) and a user-selected Sun position to precisely simulate the lighting conditions.

Different mast heights can be accounted for in the software. A zero mast height obviously corresponds to surface illumination, and these data are used to compare with LROC WAC images as a way to test the fidelity of the simulations. We have found that our simulations precisely match actual images that were acquired with the same illumination conditions (Figure 1).

The usefulness of illumination simulation analyzes is that they permit the study of all possible illumination conditions, something that is not feasible with image analysis alone. One extreme example is the determination of the locations of permanent shadow. With images, one would typically use those acquired during a lunar day in summer. It is reasonable to assume that places that do not see the Sun in summer remain shadowed for the rest of the year. Whilst this is true, these areas of shadow are subtly different from *permanently* shadowed regions. The Sun reaches its highest elevation at a single point in time during a year. Study of ephemeris data covering hundreds of years shows that the subsolar longitude corresponding to this instant of maximum solar elevation varies. Therefore to map permanent shadow, one needs to keep the Sun at this highest elevation for ALL subsolar longitudes. This is the method that we use when mapping the locations of permanent shadow that could contain ice deposits.

Key Parameters: There are several key illumination parameters to be considered when one is planning a surface mission to the lunar poles. Perhaps the two most important are the duration of the single longest shadowed period (this usually occurs near mid winter), and the duration of the longest single period of constant sunlight. Using simulations we are able to fully characterize the illumination conditions at chosen locations on the lunar surface. This allows us to map out the occurrence and duration of all shadowed periods [1]. Analysis of these data also yields information on the key parameters mentioned above.

Single longest shadowed period: The duration of the single longest shadow period is key if one is trying to design a system that can survive for longer than a year. The battery design may be driven by the longest amount of time that the lander will be in shadow. Previous analysis using Kaguya-derived topography indicated that places exist that have maximum shadowed durations of only a few days [1]. We are redoing these analyses using the higher resolution LOLA data.

Maximum length of continuous sunlight: This parameter is key if planning a lander system that is not designed to survive long periods of eclipse. Analysis indicates that places exist that are constantly illuminated for months at a time, nominally centered around mid Summer. Also, using simulations, one can determine a similar parameter, one of quasi-permanent sunlight. This is the amount of time where a lander would not experience an eclipse greater than some selected value, typically a few hours.

Ideal Landing Sites: As mentioned above simulations permit the determination of key parameters that are used to determine ideal landing sites. For each parameter, e.g. areas of maximum mean illumination, there are usually a few "best" pixels. In fact, these locations have been known since we have had Clementine images [2]. What we are now able to do is to conduct detailed illumination analyses on much larger areas. The issue is that these "best pixels" may not actually represent the best landing site selections, due to the ramifications of missing these sites. For example, some of the sites that receive the most illumination are adjacent to pixels that would be catastrophic from a landing operations perspective. We are therefore considering realistic landing error ellipses and determining which areas have the best key parameters. Essentially each landing area is only as good as the worst pixel it contains.

Conclusions: The results from our research will be the identification of the best landing areas near both lunar poles, for a variety of landing error ellipses and mission goals.

References: [1] Bussey D.B.J., J.A. McGovern, P.D. Spudis, C.D. Neish, H. Noda, Y. Ishihara, S.-A. Sørensen (2010) Illumination conditions of the south pole of the Moon derived using Kaguya topography. *Icarus* **208**, 2, 558-564. [2] Bussey, D. B. J. ; Spudis, P. D. ; Robinson, M. S. (1999) Illumination conditions at the lunar south pole. *Geophys. Res. Lett.* **26** , No. 9 , 1187

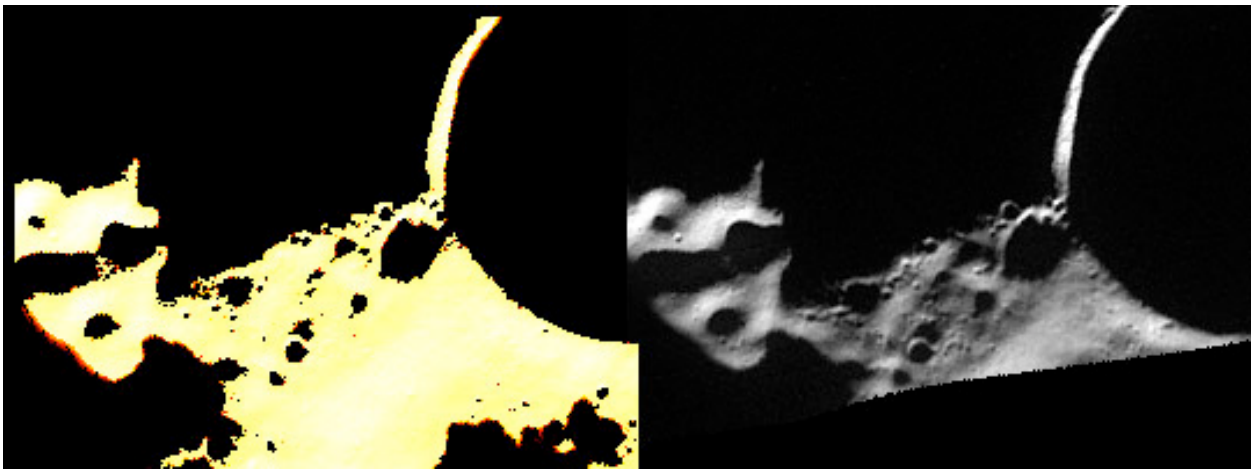

Figure 1. Comparison between the output from LunarShader (left) and a LROC WAC image (right). Our simulations match well with the images.

THE EUROPEAN LUNAR LANDER: A HUMAN EXPLORATION PRECURSOR MISSION. J. D. Carpenter[1], A. Pradier[1], R. Fiackerly[1], B. Houdou[1], D. De Rosa[1], C. Philippe[1] and B. Gardini[1], [1]ESA-ESTEC (Keplerlaan 1, 2201 AZ, Noordwijk, The Netherlands, james.carpenter@esa.int).

Introduction: ESA's Human Space Flight and Operations Directorate is continuing with preparations for its Lunar Lander project. The Lunar Lander is an unmanned precursor mission to future human exploration. This mission will enable the development of technologies, capabilities and scientific knowledge that will allow Europe to participate in future international human exploration activities of the Moon and beyond. The primary objective of the mission is to demonstrate soft precision landing with hazard avoidance and once on the surface it provides an opportunity for payload operations and scientific measurements. The scientific objectives and requirements for the mission have been established to address the major unknowns for future exploration activities.

The Lunar Lander is currently engaged in Phase B1 under lead of the prime contractor Astrium GmbH (Bremen, Germany). Phase B1 includes mission definition, system & sub-system design and technology breadboarding activities. This Phase will be completed in mid 2012. The Phase B1 builds on work carried out in the preceding Phase A studes, following which some important decisions were taken. These include the use of a Soyuz 2-1b launch vehicle, the exclusion of radio-isotope devices (e.g. RHUs/RTGs) from the design, and the targeting of a southern polar landing site.

Mission Architecture: The mission targets a launch in 2018 from Centre Spatial Guyanais, Kourou on a Soyuz launcher. The Lander will then be injected into a transfer orbit to the Moon by the Fregat upper stage and several weeks later will insert its self into a lunar polar orbit.

The precision landing capability will then be applied to ensure a soft precise landing at the Lunar South Pole. The targeted landing sites are located at peaks where the high altitude relative to the surrounding topology, coupled with the slight inclination of the Moon's rotational axis, lead to extended periods of illumination. Landing at these sites potentially allows surface operations to continue for a period of several months using solar power, without the need for radio-isotope based power or thermal control.

Hazards and Illumination: A key factor in ensuring a robust mission design is a complete understanding of the illumination duration at the anticipated landing sites, the areas of the sites and the extent of surface hazards such as boulders, slopes and craters. To this end work is ongoing to fully characterize these aspects of the Lunar surface in the areas around these peaks. For this work we draw heavily on the extensive data sets now available from the LOLA altimeter and LROC cameras on board LRO.

Scientific investigations: The scientific topics that have been defined for the mission emphasise a number of key areas: the integrated dusty plasma environment at the surface of the Moon and its effects on systems; lunar dust as a potential hazard to systems and human explorers; potential resources which can be utilised in the future; and radiation as a potential hazard for human activities. Each of these topics is supported by an independent science Topical Team. These Topical Teams continuously review the science requirements and activities of the mission and are investigating the potential for measurements using existing facilities that can support the objectives of exploration preparation and the activities of the Lunar Lander on the surface of the Moon.

Payload Studies: In addition, a number of payload study activities have been initiated to define candidate payloads for the Lunar Lander. As well as detailing the scientific measurements to be made at the surface of the moon, the payload studies will provide preliminary designs for payloads, identify the major challenges for their development and ensure that the mission study properly accounts for the payload and its interfaces.

Conclusions: We report on the status of the European Lunar Lander mission and the ongoing work on the system design, technology development, characterization of potential landing sites and on science and payload activities in support of the mission.

MG-SPINEL RICH LITHOLOGY AT CRATER COPERNICUS D. Dhingra and C. M. Pieters, Geological Sciences, Brown University, RI 02912 (deepak_dhingra@brown.edu)

Introduction: The diverse mineralogy of the Moon is an indicator of its origin and evolution through time. Mapping the distribution of minerals in the spatial context (both horizontal and vertical) provides us with clues to the history of the planet. Lunar sample analysis and remote sensing studies over the past several decades [e.g. 1-2] have established the dominant mineralogy of the Moon, mainly comprising of minerals like plagioclase, low and high calcium pyroxene and olivine.

Recent remote sensing observations by Moon Mineralogy Mapper (M^3) have added a new lithology to the lunar suite, one dominantly composed of Mg-Spinel. The detections have been made over a small areal extent at only two locations so far, namely, innermost ring of Moscoviense basin on the lunar far side [3] and central peaks of crater Theophilus on the near side [4,5].

Here, we report a new identification of this Mg-spinel lithology at Copernicus crater using M^3 data (the third detection so far) and discuss its implications for the understanding of this lithology.

Mg-Spinel at Copernicus Crater: The spectral signature of Mg-Spinel is characterized by an absence of an absorption band around 1000 nm and a strong absorption around 2000 nm caused by small amounts of Fe^{2+} in the tetrahedral crystallographic site of the mineral [6]. At Copernicus, the Mg-Spinel lithology bears this distinct spectral signature, as is illustrated in Fig. 1 by the magenta spectrum. The surrounding area displays a relatively featureless spectrum (blue spectrum). Spectra from Mg-Spinel rich lithology at Theophilus has been provided for comparison.

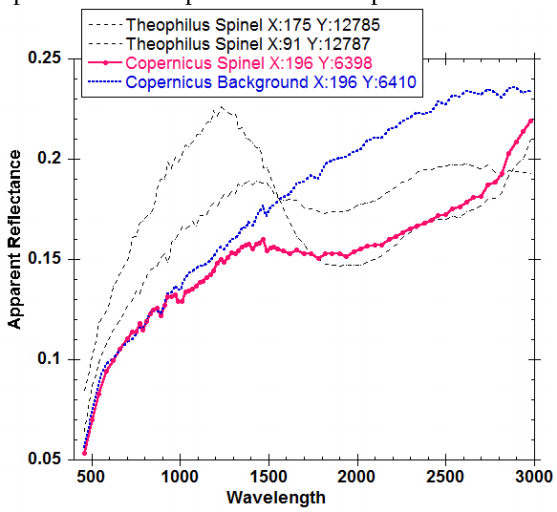

Fig.1 Reflectance Spectrum of the Mg-Spinel lithology at Copernicus Crater (shown in magenta color) with latest M^3 calibration (U2 with RC correction). Mg-Spinel spectra from two locations at Theophilus are shown in black dashed spectra.

Geological Setting: Copernicus is a ~90 km diameter, relatively young, bright rayed-crater on the lunar near side with prominent central peaks. The floor of Copernicus is inundated with impact melts displaying diverse morphologies. The Mg-Spinel bearing lithology occurs as a small hillock on the floor of Copernicus crater, located south of the triplet peak complex. It is not clear based on the available dataset, if this small hillock was originally a part of the central peaks or is just an isolated block exposed by the cratering event. At the same time, it is also noted that the hillock is aligned with the western peak of the crater as can be seen in figure 2(a). Spectrally, on an integrated band strength at 2000 nm (IBD 2000) map – an indicator of the relative strength of the 2000 nm absorption band, the Mg-Spinel rich lithology occurs as a bright spot in an otherwise dark surrounding (Fig. 2b).

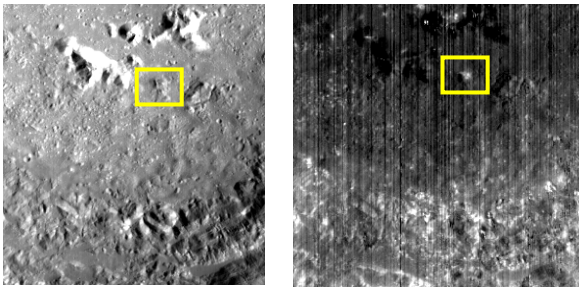

(a) (b)

Fig. 2 (a) M^3 albedo and (b) IBD 2000 map of the Copernicus crater showing the newly identified Mg-Spinel location

High Resolution Studies: The Mg-Spinel rich lithology was examined at higher spatial resolution to better determine the morphological relations. Kaguya Terrain Camera (TC) data [7] and LROC-NAC datasets [8] were used for this study. Figure 3 shows TC and LROC-NAC scenes of the area indicating a boulder strewn region across the slopes of this hillock. These boulders might be the source of the strong 2000 nm absorptions observed in M^3 dataset.

Implications for the Occurrence of Mg-Spinel Lithology: The exposures of Mg-Spinel rich lithology at Moscovience basin and Theophilus crater are located on the innermost rings of Moscoviense and Nectaris basins respectively. This geological setting suggested that the Mg-Spinel rich lithology had a deep seated

origin as the inner rings of the basins are believed to expose material from great depths.

Copernicus crater lies beyond the southern margin of Imbrium basin and is believed to have excavated through the pre-existing Insularum basin [9]. The olivine bearing central peaks at Copernicus crater [e.g. 10] have been interpreted to be of deep seated origin and therefore there is a possibility of the Mg-spinel rich block to have come from deeper source regions and could represent: (a) uplifted part of the central peaks of Copernicus (b) uplifted block from Insularum basin or (c) displaced block from Imbrium basin, although the last possibility is less likely in view of the great distance from Imbrium transient crater rim. In either of the cases, the hypothesis of association of Mg-Spinel rich lithology with deep excavation by large basins seems to be a viable option. Further detailed studies including search for any additional exposures in the area needs to be carried out for better understanding of the geology of Mg-Spinel rich lithology.

Summary: The new identification of Mg-Spinel rich lithology at Copernicus crater provides another set of clues in understanding the occurrence of this new rock type. Pre-liminary analysis of mineralogy and morphology seem to support the suggestion that it may represent a deep seated lithology which is excavated along the inner rings of large basins, either in-situ (as in case of Moscoviense and Theophilus) or as displaced blocks (as might possibly be at Copernicus).

Acknowledgments: This work was supported by NASA M^3 grant NNM05AB26C and NLSI grant NNA09DB34A. Thanks to ISRO for supporting M3 on Chandrayaan-1.

References: [1] McCord T.B. et al. (1972) *JGR, 77,* 1349-1359 [2] Pieters C.M. (1977) *8th PLPSC,* 1037-1048 [3] Pieters C.M. et al. (2011) *JGR,116, doi:10.1029 /2010JE003727* [4] Dhingra D. et al. (2011) *GRL*, doi: 10.1029/2011GL047314 [5] Lal D. et al. (2011) 42nd *LPSC, Abstract#* 1339 [6] Cloutis E.A. et al. (2004) *MAPS, 39,* 545-565 [7] Haruyama J. et al. (2008) *EPS, 60,* 243-255 [8] Robinson M.S. et al. (2010) *Space Sci. Rev., 150,* 81-124 [9] Pieters C.M. and Wilhelms D.E. (1985) *15th PLPSC, JGR, 90,C415-C420* [10] Pieters C.M. (1982) *Science, 215,* 59-61

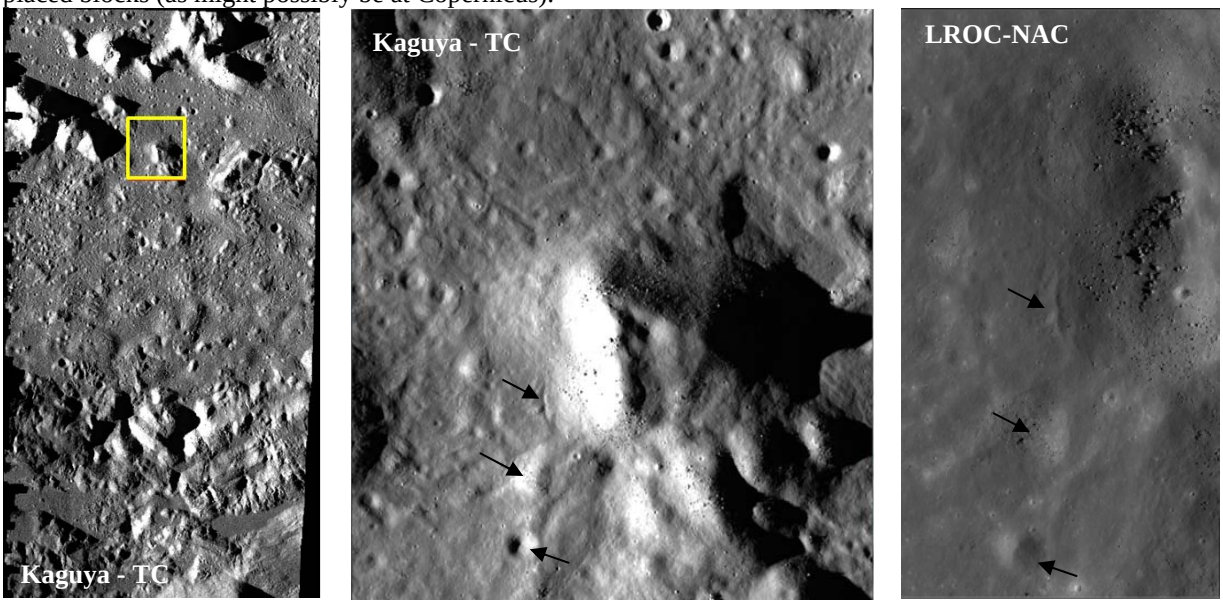

(a) (b) (c)

Fig. 3 High resolution morphological observations of the Mg-Spinel rich lithology. (a) Kaguya TC image with the Mg-Spinel bearing lithology enclosed in the yellow box. (b) The area enclosed in 3(a) at full resolution. (c) The same area in LROC-NAC image. The outcropping boulders can be observed in all the cases. The arrows in 3b and 3c refer to the same locations in the two images.

MINERALOGICAL DIVERSITY OF IMPACT MELTS ON CENTRAL PEAK OF TYCHO AND ITS VICINITY D. Dhingra and C. M. Pieters, Geological Sciences, Brown University, RI 02912, USA (deepak_dhingra@brown.edu)

Introduction: Impact cratering on planetary bodies excavates and re-distributes material from various depths. A sizable amount of energy is commonly partitioned into melting the rocks. The fate of this impact melt in terms of spatial distribution, morphology and mineralogy is varied [e.g. 1-3]. With the availability of high spatial and spectral resolution datasets for the Moon from multiple instruments onboard several missions [e.g. 4-6], a variety of new information is being made available on physical and compositional character of impact melts.

We discuss here the spectral variation in impact melts located on the central peaks of crater Tycho and its vicinity and compare them with unmelted rocks on the peaks. Recent LROC observation of Tycho's peak at Sunrise [7] captured a spectacular scene of a large clast lying over a pool of cracked impact melt providing a context for exploring the relationship between the two entities in space and time. We also attempt to understand this relationship.

Crater Tycho and its Peak: Tycho is a ~85 km diameter Copernican age complex crater located on the southern near-side lunar highlands. It's a bright crater with prominent rays, visible from Earth, even with naked eyes. Impact melt is observed all over the crater: rim, walls, floor and even the peaks, each occurrence displaying a wide diversity of morphologies. Some occur as small smooth melt pools, others have clasts of various sizes. The impact melt also drapes the rocks and is extensively fractured.

Mineralogy and morphology from coordinated high resolution datasets: Datasets from Chandrayaan-1 Moon Mineralogy Mapper (M^3), Kaguya Terrain Camera (TC) and LRO Narrow Angle Camera (NAC) were utilized in conjunction with each other to study the impact melts. The spectral diversity of sampled impact melts is illustrated in Figure 1 along with the spectra of unmelted material. The position of absorption bands around 1 and 2 µm and their relative strengths clearly demonstrate differences not only amongst unmelted material and impact melt but also between impact melts.

The smooth melt patch located north-east of the central peak, near its base, has a featureless spectra with a possibly weak feature around 1 µm and no absorption at 2 µm. The melt does not seem to contain any significant quantity of clasts based on the high resolution Kaguya TC dataset as shown in figure 2(b). A contrasting spectrum is obtained along the crack in the impact melt, possibly rich in clast fragments, located east of the smooth patch. The spectrum shows strong 1 and 2 µm absorption bands and possibly another absorption around 1.2 µm that could be due the to pyroxene or plagioclase. The immediate surroundings too share the same spectral character indicating the presence of a strong mafic composition rich in pyroxene.

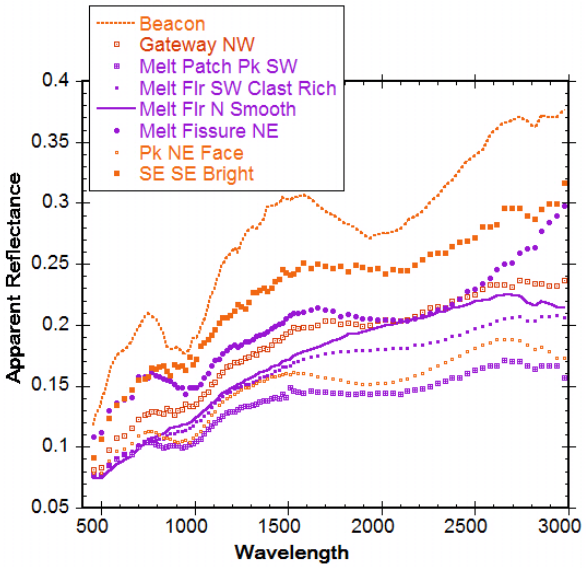

Fig.1 Diversity amongst impact melts (purple) and unmelted rock material (orange) on Tycho central peak and nearby region. Apparent reflectance in latest M^3 calibration (U2 with RC Correction)**.**

The melts on the base of the southwestern region of the peak are clast rich and have been cracked. Spectrum from a homogenous area in M^3 image shows relatively weak absorptions at 1 and 2 µm suggesting presence of high calcium pyroxene. On the central peak, a melt lobe [Fig. 2(d)] shows long wavelength 1 and 2 µm absorptions. In contrast, several unmelted regions on the peak have relatively short wavelength absorptions, especially at 2 µm, possibly hinting that the bulk properties of the melt had a different composition than what we sampled on the peak.

Possible Clast Mineralogy on the Peak: The LROC imaged clast is an interesting find and has been reported to be around ~100 meters. Although it falls below the M^3 spatial resolution of 140 meters, we attempted to locate the clast in M^3 image using 10 m resolution Kaguya TC image obtained under similar illumination conditions. The clast appears to be partially in shadow in M^3 scene. Spectra extracted from the identified pixel

(that presumably contains the clast) and surrounding pixels are shown in Figure 2(a).

The possible clast bearing pixel shows a mafic signature with broad and weak 1 and 2 µm absorption features. The immediate neighboring pixels share similar character suggesting either that the clast has similar composition as the surroundings or the clast comprises of a spectrally neutral material like shocked plagioclase. The two pixels further south do seem to show slight variations in the position of 1 and 2 µm bands as well as strength of the 2 µm band and are likely to be sampling the impact melt based on TC context image. Further detailed analysis is being carried out to validate these differences.

Summary: The spectra of impact melts on Tycho central peak and nearby coupled with their geological context from high spatial resolution data provides important insights into the nature of these prevalent entities on the Moon. The diverse mineralogy and morphology of these melts and their differences from unmelted lithologies on the peak suggests variation in the composition of the melted target material compared to the central peak or variable cooling history. The differences amongst impact melts suggest heterogeneity in melt composition and possibly clast composition and proportion as well.

References: [1] Howard K.A. & Wilshire H.G. (1973) *LPSC* 389-390 [2] Hawke B.R. and Head J.W. (1976) *Impact and Explosion cratering (D.J. Roddy, R.O. Peppin, R.B. Merrill Eds)*, pp 815-844 [3] Smrekar S. and Pieters C.M. (1985) *Icarus, 63*, 442-452 [4] Pieters C.M. et al. (2009) *Curr. Sci., 96*, 500-505 [5] Haruyama et al. (2008) *EPS, 60*, 243-255 [6] Robinson M.S. et al. (2010) *Space Sci. Rev., 150*, 81-124 [7] http://lroc.sese. asu.edu/news/?archives/411-Tycho-Central-Peak-Spectacular!.html

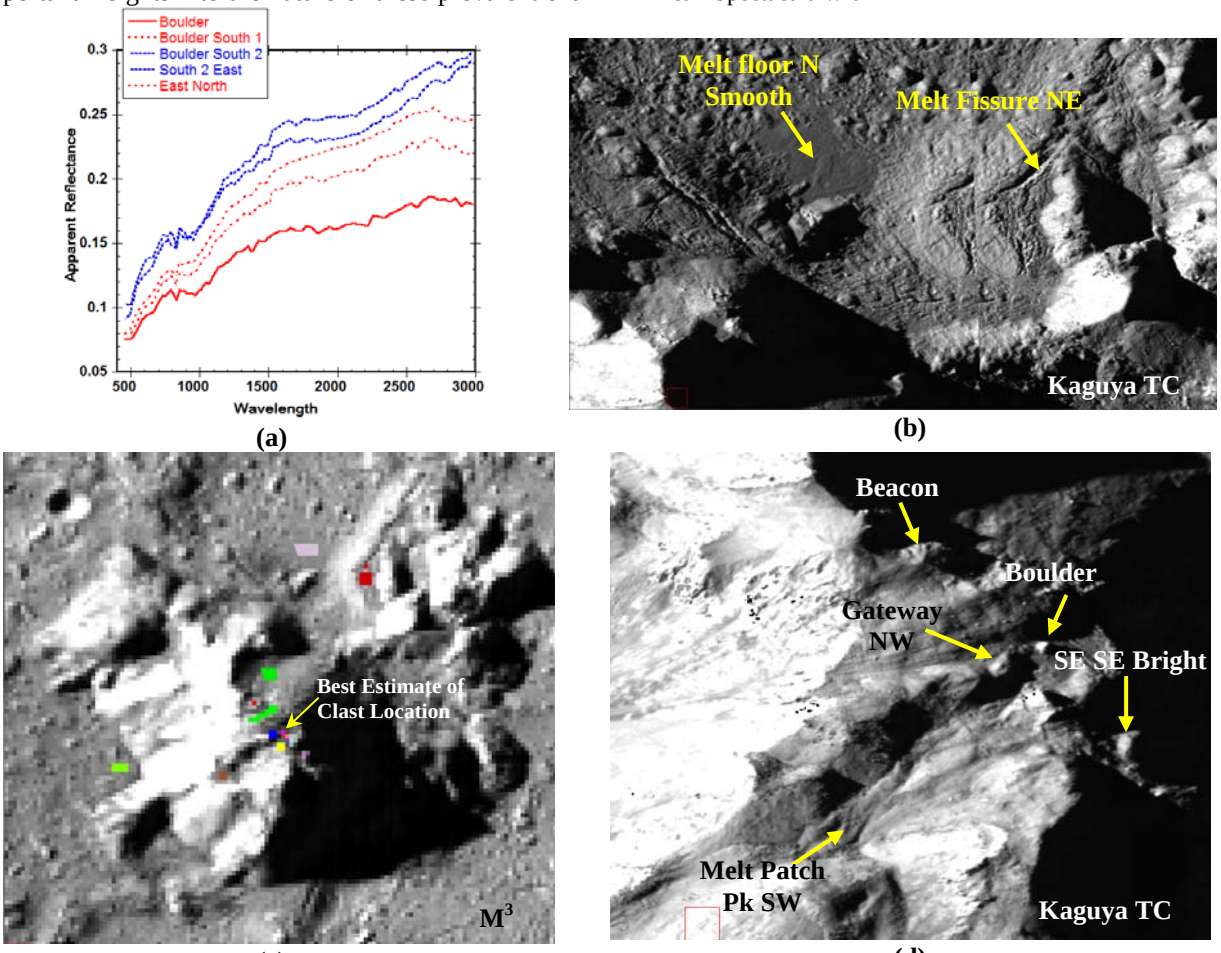

Fig. 2 (a) Spectra of the large clast and surroundings. **(b) & (d)** Kaguya TC Evening context images various parts of the peak and floor which were sampled in M^3 dataset. **(c)** M^3 image with sampled areas marked.

The Science Behind Nasa's Lunar Atmosphere And Dust Environment Explorer. R. C. Elphic[1], G. T. Delory[2], E. J. Grayzeck[3], T. Colaprete[1], M. Horanyi[5], P. Mahaffy[4], B. Hine[1], D. Boroson[6], and J. S. Salute[3], [1]Planetary Systems Branch, NASA Ames Research Center, MS 245-3, Moffett Field, CA, 94035-1000, [2]Space Sciences Laboratory, University of California, Berkeley CA 94720, [3]Planetary Science Division, Science Mission Directorate, NASA, Washington, DC 20546, [4]NASA Goddard Space Flight Center, Greenbelt, MD, 20771, [5]Laboratory for Atmospheric and Space Physics, University of Colorado, Boulder, CO 80309, [6]Lincoln Laboratory, Massachusetts Institute of Technology, Lexington MA 02421

Introduction: Nearly 40 years have passed since the last Apollo missions investigated the mysteries of the lunar atmosphere and the question of levitated lunar dust. The most important questions remain: what is the composition, structure and variability of the tenuous lunar exosphere? What are its origins, transport mechanisms, and loss processes? Is lofted lunar dust the cause of the horizon glow observed by the Surveyor missions and Apollo astronauts? How does such levitated dust arise and move, what is its density, and what is its ultimate fate?

The LADEE Mission: NASA's Lunar Atmosphere and Dust Environment Explorer (LADEE) is currently under development to address these questions. LADEE will determine the composition of the lunar atmosphere and investigate the processes that control its distribution and variability, including sources, sinks, and surface interactions. LADEE will also determine whether dust is present in the lunar exosphere, and reveal its sources and variability. LADEE's results are relevant to surface boundary exospheres and dust processes throughout the solar system, will address questions regarding the origin and evolution of lunar volatiles, and will have implications for future exploration activities.

LADEE's top objectives are:

(1) Determine the composition of the lunar atmosphere and investigate the processes that control its distribution and variability, including sources, sinks, and surface interactions.

(2) Characterize the lunar exospheric dust environment and measure any spatial and temporal variability and impacts on the lunar atmosphere.

LADEE must be capable of measuring a minimum detectable density of 10^{-4} grains/cc, for grain sizes from 100 nm to at least 1 micrometer in radius.

The LADEE Payload: LADEE employs a high heritage instrument payload: a Neutral Mass Spectrometer (NMS), an Ultraviolet/Visible Spectrometer (UVS), and the Lunar Dust Experiment (LDEX). It will also carry a space terminal as part of the Lunar Laser Communication Demonstration (LLCD), which is a technology demonstration. The LADEE NMS will make in situ measurements of exospheric species, and covers a mass range of 2-150. It draws its design from mass spectrometers developed at GSFC for the MSL/SAM, Cassini Orbiter, CONTOUR, and MAVEN missions. The UVS instrument is a next-generation, high-reliability version of the LCROSS UV-Vis spectrometer, spanning 250-800 nm wavelength, with high (<1 nm) spectral resolution. UVS will remotely sense the composition and scale heights of various exospheric species, and the spatial distribution of dust, if it exists. It will also perform dust occultation measurements via a solar viewer optic. LDEX senses dust impacts in situ, at LADEE orbital altitudes of between 20 and 50 km, for a particle size range of between 100 nm and 5 μm. LADEE will be the first mission based on the Ames Common Bus design.

LADEE Science Mission Profile: LADEE's science orbit is driven by the top level science objectives. Whereas the ideal orbit is low-altitude circular over the nominal science mission duration of 100 days, but it is impractical to maintain this within a reasonable fuel budget. The lunar gravity field severely perturbs a low-altitude circular orbit, bringing about mission termination in a matter of days.

LADEE's orbit design is retrograde with low inclination. This permits NMS and LDEX to ram exospheric species and dust over the dawn terminator while shadowed from the sun, minimizing solar UV and outgassing interference. Figure 1 illustrates the altitude-vs-orbit angle sampling for the nominal science mission. The sunrise terminator is at the center.

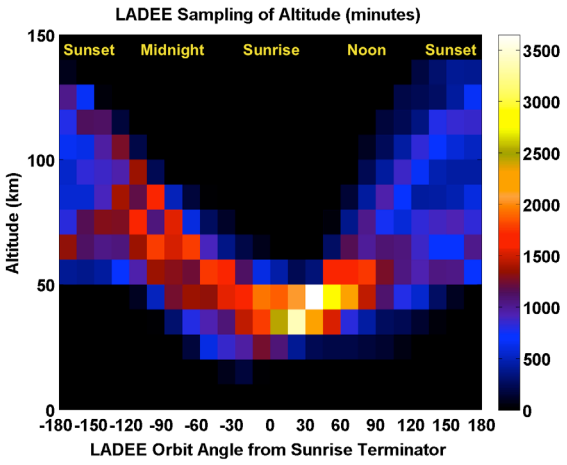

Figure 1. LADEE altitude sampling during the nominal science phase (100 days).

THE 2010 DESERT RATS SCIENCE OPERATIONS TEST: OUTCOMES AND LESSONS LEARNED. D. B. Eppler[1] and the 2010 Desert RATS Science Operations Team[2], 1. Exploration Sciences Office, Astromaterials Research and Exploration Sciences Directorate, Mail Code KX, NASA-Johnson Space Center, 2101 NASA Parkway, Houston, TX 77058, dean.b.eppler@nasa.gov; 2. Full name and affiliation list available from first author.

The Desert RATS 2010 Team tested a variety of science operations management techniques, applying experience gained during the manned Apollo missions and the robotic Mars missions. This test assessed integrated science operations management of human planetary exploration using real-time, tactical science operations to oversee daily crew science activities, and a "night shift" strategic science operations team to conduct strategic level assessment of science data and daily traverse results. In addition, an attempt was made to collect numerical metric data on the outcome of the science operations to assist test evaluation.

The two most important outcomes were 1) the production of significant (almost overwhelming) volume of data produced during daily traverse operations with two rovers, advanced imaging systems and well-trained, scientifically proficient crew-members, and 2) the degree to which the tactical team's interaction with the surface crew enhanced science return. This interaction depended on continuous real-time voice and data communications, and the quality of science return from any human planetary exploration mission will be based strongly on the aggregate interaction between a well trained surface crew and a dedicated science operations support team using voice and imaging data from a planet's surface. In addition, the scientific insight developed by both the science operations team and the crews could not be measurable by simple numerical quantities, and its value will be missed by a purely metric-based evaluation of test outcome. In particular, failure to recognize the critical importance of this qualitative type interaction may result in mission architecture choices that will reduce science return.

There were a number of important lessons that can be applied to future human science operations teams in support of human planetary exploration:

1) Science operations teams need to be led by senior scientists with a range of professional experience in geological sciences. In particular, these teams cannot be made up exclusively of junior scientists with little operational experience. Leadership is critical to providing guidance and varied points of view during operations during complex and often stressful missions.

2) Continuous communications with stable, high fidelity voice and image data gives better science return than conditions where communications have long intervals between contacts. The scientific interaction between the crew and the science operations team that is available during continuous communications resulted in a significant improvement in the understanding of the science of the area explored. Reduced communications would result in a significant decrease in mission science return.

3) A diligent science operations team and a well-trained, scientifically competent astronaut crew can mitigate poor communications conditions, particularly when the communications conditions are anticipated and planned for. This test underscored the need for a science operations team that can adapt to changing conditions.

4) The volume of data coming out of any given day of this mission, particularly when compared to a robotic mission, was enormous. As the mission progressed, it became difficult for the strategic team to assimilate and evaluate the data during a nominal shift due to data management problems and data presentation techniques. In particular, the time consumed in attempting to evaluate recorded verbal data without a written transcript made detailed scientific analysis almost impossible within the given time constraints. The ability to generate written transcripts of verbal observations will be critical to the science analysis of any human exploration mission.

5) When operating with only two daily communications sessions, science analysis and return achieved by a strategic science team was directly related to how well the crew provided both the contextual descriptions of geology and the image data that illustrated the crews' science descriptions. In particular, data retrieval problems or poor image data collected by the crew resulted, not surprisingly, in poor science return.

6) The science metrics collected on Desert RATS 2010 did not provide unambiguous data on the efficacy of particular approaches to science operations management. Although the data suggested some trends, there was not sufficient granularity in the data or specificity in the metrics to allow those trends to be understood on metric data alone.

LADDER: The Development of a Prototype Lunar Space Elevator T.M. Eubanks[1] and M. Laine[2], [1]Liftport Luna, P.O. Box 141, Clifton, Virginia 20124, marshall.eubanks@gmail.com, [2]michael.laine@liftport.com.

Introduction: LADDER is a mission to deploy an operational prototype Lunar Space Elevator (LSE) using currently available technology. The LADDER mission would erect a 264,000 km space elevator from the Lunar surface, past the L1 Lagrange point, to a counterweight deep in cislunar space. The LADDER mission is intended to gain experience with the deployment and operation of a space elevator, deploy scientific instruments and other equipment to the Lunar surface, and return samples of the Lunar surface from Sinus Medii to Earth.

The Prototype Lunar Space Elevator: A space elevator is a structure rising from or near a planetary surface to a sufficient altitude to be held taut by gravity, rotation and orbital dynamics [1]. Typically a space elevator is intended to match its primary body's rotation to allow for an easy transfer of material between some orbit and the surface of its primary. A Terrestrial Space Elevator (TSE) has been considered by the NASA Institute for Advanced Concepts (NAIC), but is a very technically demanding structure, and could not be built using any current material. An LSE, by contrast, is technically much easier and could be built using commercially available string materials such as Zylon or M5. Pearson et al. [2] developed many of the crucial concepts of a LSE, but their proposed mission is much more elaborate than LADDER and would require a functioning Lunar transportation system as a prerequisite. LADDER is intended to achieve both a functioning LSE and to provide a solid scientific return in the same mission, based on one launch from an existing or planned Heavy Lift Launch vehicle. LADDER currently is planned to be executed in a single Discovery class mission, starting with the delivery of 11,000 kg of Zylon HM fiber plus associated equipment to the L1 Lagrange site. While the fiber could be changed if better choices become available, Zylon is sufficient for LADDER [3], and is also commercially available in sufficient quantities for the LADDER LSE.

Figure 1 shows to scale (although with greatly enhanced visibility) the major components of LADDER, the string, the Landing Platform, the supply depot at L1, and the CounterWeight (CW). The CW would use the upper Trans Lunar Injection (TLI) stage for mass, which would provide an important increase in payload mass. In order to lower the delta-V required to insert the TLI upper stage plus fiber into the L1 Lagrange Point, it is planned to use both a lunar gravity assist and solar perturbations with Weak Stability Boundary (WSB) trajectory.

LADDER is being designed with robustness to protect against micrometeorites, and should be able to last for up to a decade assuming the microgram meteorite flux in cislunar space of matches the observed flux of ~ 4 x 10^{-8} m^{-2} sec^{-1} [4].

The Landing Site: LADDER plans to land at or near the zero point of the Lunar coordinate system, at latitude 0, longitude 0 is Sinus Medii. This location is technically the simplest landing point for an LSE, and is a suitable place for a landing station. Figure 2 shows Sinus Medii as observed by Surveyor 6 [5], from ~ 44 km from the proposed landing site.

LADDER Science: The primary science goal of the LADDER technical demonstration mission is the return of the first Lunar samples since 1976. LADDER will both take a core sample upon landing and will deliver one or more microrovers to the Lunar Surface to assist in collecting surface samples. LADDER should have the ability to return up to 10 kg of samples from the first Lift from the Lunar Surface, using a reusable solar-powered lifter. LADDER's ability to return samples from other location

LADDER plans to use Single Cube Retroreflectors (SCR) as Laser ranging targets during deployment of the Landing Platform. Once it reaches the surface, the SCR will remain as a permanent addition to the Lunar Laser Ranging (LLR) retroreflector network, and should improve both the Signal to Noise of the LLR network (the existing Apollo and Lunakhod retroreflectors are both intrinsically less accurate and are also degrading with time) [6].

The LADDER team is actively seeking partners for Lunar science and space science opportunities. Partners should be able to provide autonomous instruments, rovers or other equipment in the 20 kg range or less for delivery to the Lunar surface or to the Counterweight. People interested in discussing these opportunities should contact the authors.

Conclusions: LADDER will provide the core of a new Lunar transportation system for up to a decade after installation, capable of cheaply deploying small payloads to the Lunar surface and lifting samples and other material to L1 and returning them to Earth. With LADDER, sound Lunar surface science can be conducted on a continuing basis for a relatively modest initial investment.

References:

[1] Edwards, B.C. (2003) The Space Elevator, NASA NAIC Phase II Final Report.

[2] Pearson, J., Levin, E., Oldson, J., and Wykes, H. (2005) *Lunar Space Elevators for Cislunar Space Development, Phase I Final Technical Report*, NASA NAIC Research Subaward No.: 07605-003-034, Star Technology and Research, Inc.

[3] *Zylon Fiber PBO Technical Information* (2001) Toyobo Corporation, Ltd, available from http://www.toyobo.co.jp/seihin/kc/pbo/technical.pdf

[4] McDonnell, J. A. M., and Allison, R. J. (1981), LUNAR AND PLANETARY SCIENCE XII, P. 682-684.

[5] *Surveyor Program Results* (1969) NASA SP-184.

[6] Currie, D. G.; Delle Monache, G.; Dell'Agnello, S. (2010) American Geophysical Union, Fall Meeting 2010, abstract #P51C-1467.

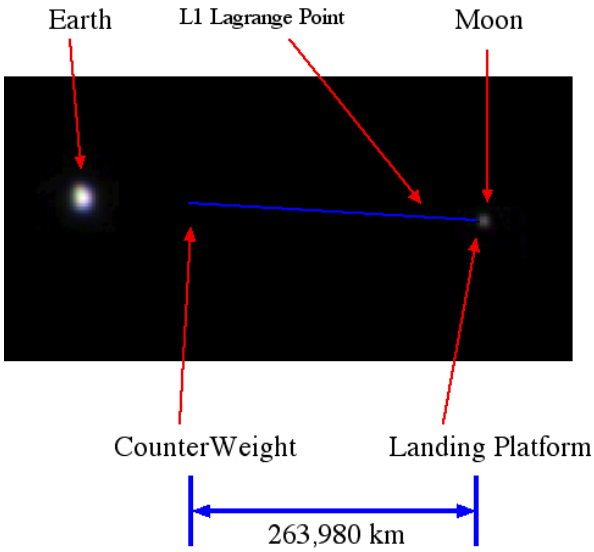

Figure 1. The components of the LADDER LSE, to scale, superimposed on a image of the Earth-Moon system from the Juno spacecraft, taken August 26, 2011 at a distance of 9.66 million km. (Note: the actual LSE would not be visible to the naked eye from such a distance.) Credit-NASA for the original image.

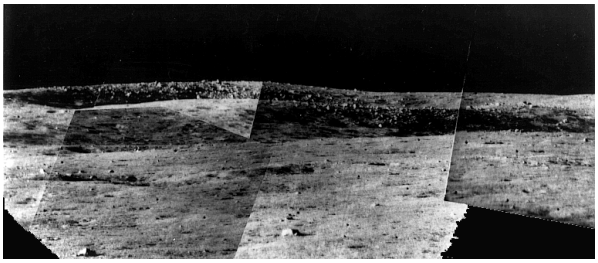

Figure 2. Sinus Medii from Surveyor 6, taken about 44 km from the proposed landing site [Credit – NASA].

SOLAR STORM-LUNAR INTERACTION MODELING: A FOCUS STUDY BY THE DREAM LUNAR SCIENCE INSTITUTE, W. M. Farrell[1,7], R. M. Killen[1,7], G. T. Delory[2,7], L. V. Bleacher[1,7], J. S. Halekas[2,7], D. Krauss-Varben[2,7], P. Travnicek[2,7], M. I. Zimmerman[1,7], D. M. Hurley[3,7], T. J. Stubbs[1,4,7], M. Sarantos[1,4,8], N. Gross[5,7], D. A. Glenar[6,7] A. P. Jordan[7,8], H. E. Spence[7,8], T. L. Jackson[1,7], J. E. Bleacher[1,7], N.E. Petro[1,7], and the DREAM Lunar Science Institute, [1.] NASA/Goddard SFC Greenbelt MD, [2.] Univ. of California at Berkeley, Berkeley, CA, [3.] Johns Hopkins University Applied Physics Laboratory, Laurel, MD, [4.] Univ. of Maryland Baltimore Co., Baltimore, MD, [5.] Boston University, Boston MA, [6.] New Mexico State University, Las Cruces, NM, [7.] NASA's Lunar Science Institute, NASA Ames Research Center, Moffett Field, CA, [8.] Univ of New Hampshire, Durham NH.

Introduction. In June of 2011, team members and collaborators of the DREAM lunar science institute had an intramural workshop on the 'seleno-effectiveness' of solar storms at the Moon.

It is well known in the space weather community that the high energy radiation and intensified plasma from a solar storm has an effect on the terrestrial magnetosphere, including compressing the frontside magnetic field region, elongating the geomagnetic tail, creating intense aurora and forming magnetospheric and ionospheric current systems. These geo-effects all have some level of impact on human systems, the exact nature and intensity still being under investigation.

By analogy, lunar space plasma and surface interaction specialists suspect that solar storms and coronal mass ejections (CME) have an effect at an exposed rocky body like the Moon, but the exact nature of that effect has not been fully investigated. Such an investigation would examine the basic processes occurring on exposed rocky bodies and would feed forward into improvements in design of human systems going to both the Moon and exposed small bodies.

One of the objectives of the DREAM institute is to examine extreme events at the Moon, including the effect of a solar storm and CME at the Moon. This examination would occur by interconnecting available space weather and lunar data sets with the extensive and detailed DREAM exosphere, plasma, and surface interaction models.

Event Selection. The team spent the summer of 2010 identifying an ideal space weather event for study. It was decided by the 'Extreme Event Selection Committee' that an excellent candidate CME passage was the set of events that occurred in early May 1998. These events were ideal because they had been previously studied by the space weather community in regards to their interaction at Earth, and because Lunar Prospector was in lunar orbit with the magnetometer and electron reflectometer systems for direct lunar observations of surface electrical effects.

Model and Data Cross-Connection. The primary challenge of the solar storm-lunar interaction modeling effort was the interconnection or interplay between data and models. All model Curators agreed to start and stop times and also agreed to exchange or interconnect their output products. As such, once one model was run, the output of that model would be used as the input for another model, etc. For example, a model of the expected increase in sputtered ions was produced and this fed forward as an input to 2D and 3D hybrid plasma codes to determine in a self-consistent way the resulting ion trajectories in the larger lunar environment during the solar storm.

Engaging the Public. In parallel with this effort, the DREAM E/PO team included 10 high school student and 2 teachers to participate in the workshop. The schools involved were Eleanor Roosevelt HS in Greenbelt MD and Seton-Keough HS in Baltimore MD. In preparation, the DREAM E/PO team developed a 16-week course that included on-line reading material emphasizing topics such as solar storms, CMEs, solar wind, lunar geology, solar wind plasma perturbations created by the Moon, surface interactions, and lunar exosphere. The syllabus can be found athttp://ssed.gsfc.nasa.gov/dream/DREAM/syllabus1.html. A set of bi-monthly face-to-face and webinar interactions also occurred between the students and DREAM scientists to provide a timely, dynamic exchange of information and ideas.

Results. This presentation will review the major results of DREAM's solar storm-lunar interaction modeling effort to date. A set of surprising results were found including an increase in sputtered components, enhanced near-Moon plasma densities, anomalous surface charging, and a set of expected effects on human systems. Also, the team debated the ideal location for human explorers to hide and remain shielded during a solar extreme event. The primary results of the workshop are now part of an upcoming special topical issue for Journal of Geophysical Research – Planets which is currently open for the acceptance of new papers:

http://www.agu.org/journals/je/callforpapers.shtml.

LUNAR SWIRL IMPACTORS: A LOW-COST MISSION TO STUDY LUNAR SWIRLS, MAGNETISM, WATER, SPACE WEATHERING, DUST, AND PLASMA PHYSICS. I. Garrick-Bethell[1], R. Lin[2], H. Sanchez[3], and D. Hemingway[1]. [1]University of California, Santa Cruz (igarrick@ucsc.edu), [2]University of California, Berkeley. [3]NASA Ames Research Center.

Introduction: Lunar swirls are one of the most enigmatic geologic features in the solar system. Swirls are sinuous high-albedo features correlated with strong crustal magnetic fields (Fig. 1). Swirls are at the intersection of many disciplines, including the origins of lunar magnetism, space weathering, space plasma physics, dust lofting, and most recently, surface hydroxyl formation [1]. Therefore, a mission to swirls would benefit many in the planetary science community.

NASA Ames Research Center, UC Berkeley, and UC Santa Cruz have been designing a low-cost, low-mass mission to swirls that uses cubesat technology. Below we outline how this mission can cost-effectively make first of a kind measurements and inform a number of important problems in lunar science.

Multidisciplinary science at lunar swirls

Swirl formation: The two leading models for swirl formation are the solar wind deflection model [2], and the dust transport model [3]. Under the solar wind deflection model, the brightness of swirls is explained by the local magnetic field deflecting the solar wind (a darkening agent) from portions of the surface. Under the dust transport model, the brightness of swirls is explained by the accumulation of fine, bright dust, due to weak plasma-produced electric fields operating on charged dust lofted during terminator crossings. Measurements of the solar wind flux very near the surface, at bright and dark areas, would determine if the solar wind model is correct. Measurements of lofted dust very near the surface would help determine if dust lofting can contribute to swirl formation.

Lunar magnetism: The origin of lunar magnetism is still unknown, with interpretations suggesting either impact-produced plasma processes [4] or an ancient dynamo [5]. If crustal magnetic anomalies formed in a dynamo field, they should be homogenously magnetized with minimal short-wavelength variability in direction near the surface, except at the scale of small craters. Presently, magnetic field measurements at anomalies have only been taken above ~16 km in altitude, at best. Measurements of the magnetic field near the surface would help determine the strength and coherence of the underlying crustal magnetization, and thereby its formation mechanism. Such measurements would also help explain how the solar wind direction and flux is altered near the surface.

Lunar water: The M3 instrument on Chandrayaan has revealed that high lunar latitudes have higher abundances of hydroxyl molecules [6]. More recently, M3 data were used to show that lunar swirls have relatively low hydroxyl abundances relative to their surroundings [1]. Therefore, swirls are a natural laboratory for understanding water formation on the Moon, and likely on silicate bodies in general. Determining the swirl formation mechanism and quantifying the relevant processes should help elucidate how hydroxyl molecules and water form on the Moon's surface.

Space weathering: A long-standing question in space weathering is the relative importance of micrometeoroid impacts compared to the solar wind [7]. Under the solar wind deflection model for swirl formation, solar wind weathering at swirls is reduced, and the surface is kept brighter. However, because micrometeoroids are undeflected by the magnetic field and reach the surface, swirls may also be a natural laboratory for unraveling and quantifying the relative contributions of these two darkening agents. Improved knowledge of these processes would have applications to the spectral study of asteroids and Mercury.

Lunar dust: Dust lofting during terminator crossings has been inferred from a variety of measurements since the Surveyor missions [8], and may also be important in asteroid geology [9]. However, the amount of dust lofted above the lunar surface, if any, is not fully known. Measurements of the dust flux very near the surface, in particular during terminator crossings, would help constrain how much dust is lofted each day, and possibly the mechanisms behind dust lofting.

Plasma physics: The interaction of the solar wind with weak magnetic anomalies on the Moon presents interesting plasma physics phenomena, such as the development of a mini-magnetosphere [10]. The scale size of the magnetic anomalies ranges from below to above the solar wind proton gyrodiameter; thus, across the transition from kinetic to fluid behavior.

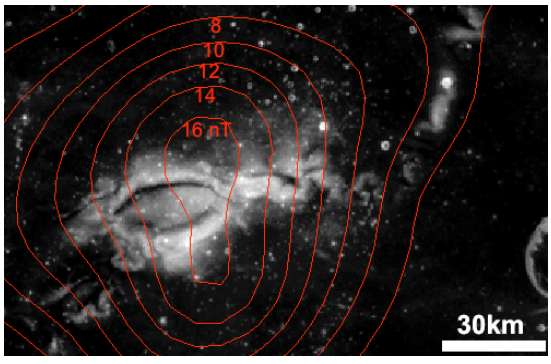

Fig. 1 – Reiner gamma swirl (Clementine 750 nm reflectance) and magnetic field contours at 18 km (Lunar Prospector).

A low-cost mission to lunar swirls

Mission objectives and concept: A mission to swirls that measures very near the surface:

1) Magnetic field strength and direction,
2) Solar wind flux and direction, and
3) Dust density,

would answer the key science questions above. A spacecraft on a very low-angle impact trajectory into the heart of a swirl could perform the necessary measurements at low altitude (Fig. 2), and transmit data in real-time to an orbiting spacecraft, up until the time of impact. Because many of the measurements can be made at high frequency, data from <50 m above the surface is possible, even though the spacecraft is traveling at >2 km/s. After impact, the probe's mission is over, but several probes can be launched to provide multiple transects at one swirl, or at several swirls.

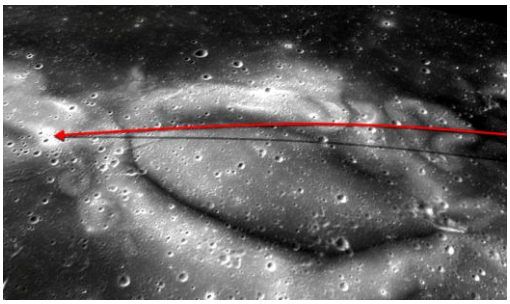

Fig. 2 – Low-angle impact trajectory over Reiner gamma swirl.

Spacecraft and payload: Ames has designed a small mother ship (<200 kg, Fig. 4) capable of orbiting the Moon and releasing two 3u cubesats on impact trajectories. Each of these cubesats is based on the CINEMA spacecraft (Fig. 3), an NSF-funded project built by UC Berkeley and Kyung Hee University (South Korea), and launching in June 2012. The CINEMA spacecraft carries two magnetometers (one inboard and one on a 0.9 m boom) and a particle detector (STEIN). Berkeley is currently designing a modified STEIN particle detector to measure the solar wind flux and direction at high cadence. In addition, Berkeley is designing a very high sensitivity dust detector.

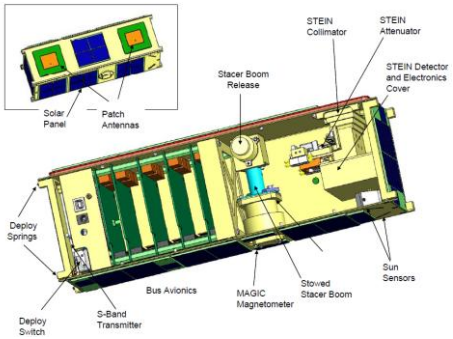

Fig. 3 – The NSF-funded 3u CINEMA cubesat, the basis of the impact probe, scheduled to launch in June 2012.

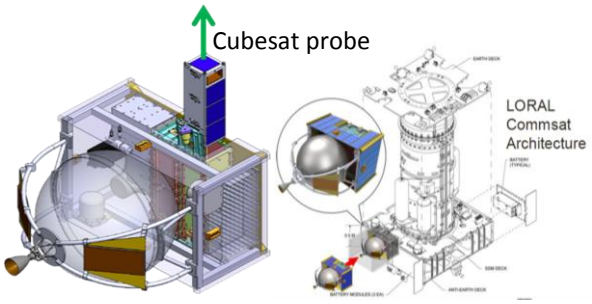

Fig. 4 – Left: Mother ship releasing a 3u cubesat probe. Right: Mothership piggybacking on a LORAL commsat launch.

Trajectory: Launching the spacecraft as a secondary payload greatly reduces the cost of the mission. Therefore, the trajectory to the Moon has been designed based on a drop-off in GTO by a commercial satellite launch (Fig. 5). Once at the Moon, the mother ship enters a highly elliptical orbit, and then conducts a burn to establish an impact trajectory. Then, the mother ship releases the probe, and performs a second burn to reestablish a stable orbit. The mothership flies over the impact site, collects data from the probe, and relays it to Earth. The total mission Δv is 1500 m/s.

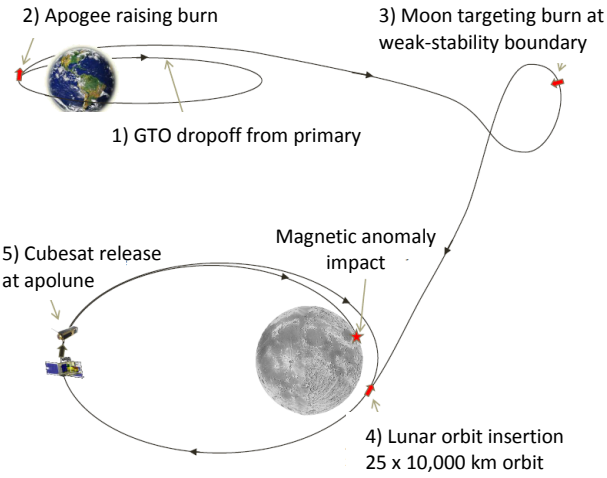

Fig. 5 – Spacecraft and probe trajectory to the Moon.

Conclusions: An impactor mission to lunar swirls could be accomplished for very low cost, while returning science that would benefit many planetary science disciplines. The mission would also demonstrate the first use of cubesats beyond low Earth orbit.

References: [1] Kramer, G. et al. (2011) *JGR*, in revision. [2] Hood, L. L. and Schubert, G. (1980) *Science* 208, 49-51. [3] Garrick-Bethell, I. et al. (2011) *Icarus* 212, 480-292 [4] Hood, L. L. and Artemieva, N. A. (2008) *Icarus* 192, 485-502. [5] Garrick-Bethell, I. et al. (2009) *Science* 323, 356-359. [6] Pieters, C. M. et al. (2009) *Science*, 326, 568-572. [7] Hapke, B. (2001) *JGR* 106, 10039–10073. [8] Colwell, J. E., et al. (2007) *Rev. Geophys.* 45, RG2006. [9] Colwell, J. E. (2005) *Icarus* 175, 159–169. [10]. Kurata, et al. (2008) *GRL* 32, L24205.

"PREPARING FOR LUNAR EXPLORATION - CONCEPTS, TECHNOLOGIES, PARTNERSHIPS IN AN AGE OF UNCERTAINTY" N. Ghafoor[1], C. Dickinson[1], R. McCoubrey[1], L. Chappell[1], M. Barnet[1], P. Dietrich[1], F. Teti[1], and Christian Sallaberger[1], [1]MDA, 9445 Airport Road, Brampton, Ontario, CANADA, nadeem.ghafoor@mdacorporation.com, ryan.mccoubrey@mdacorporation.com, laurie.chappell@mdacorporation.com, mark.barnett@mdacorporation.com, peter.dietrich@mdacorporation.com, cameron.dickinson@mdacorporation.com, christian.sallaberger@mdacorporation, frank.teti@mdacorporation.com

Introduction: The landscape of lunar exploration has changed considerably in recent years, owing to both changes in near-term objectives by international space agencies, and the current state of the world economy. Throughout this challenging period, the Canadian Space Agency (CSA) has embarked on a clear path towards delivering surface mobility for potential use on future Lunar and Martian missions. Of particular note are those facing Canada's largest space manufacturer, MDA, in a variety of tasks including: several Phase 0 studies for a variety of Lunar vehicle classes; Terrestrial rover prototypes; and Analogue Science deployments employing these prototypes. The present work will provide an overview of these developments within the international lunar framework, as well as provide future possibilities for their deployment.

Phase 0 Studies: Commencing in 2007, MDA was funded by CSA to conduct a trio of surface mobility concepts. The first was the **T**errainable, **R**econfigurable **A**utonomy-**C**apable **T**ool-using **E**xploration and **U**tility **R**over (TRACTEUR), which was to assess a large, modular "work-horse" rover chassis. The chassis was to be configurable for autonomous activities as well as movement of payloads via trailers, modular tools, or additional interfaces. The main operation of the vehicle was: to support unmanned operations and exploration; cargo and habitation relocation; site preparation and base construction (including regolith handling); and finally pressurized and unpressurized manned operations and exploration (including ISRU).

The second such study was the **L**unar **E**xploration **M**anned **U**tility **R**over or LEMUR. Several key technical innovations were investigated including human-rated safety, autonomy & telerobotic operation, multi-configuration rover traction & terrainability, architecture expansion options, power and telecommunications.

Finally, the **R**obotic **A**ssistant and **P**recursor **I**nvestigation **E**xploration **R**over (RAPIER) was identified to advanced key technology requirements for lunar exploration, most notably autonomous surface mobility. This dexterous vehicles would nominally navigate tens of kilometres of difficult terrain carrying sensitive analytical instruments, transmit results and images, drop-off instrument packages and collect samples for detail analysis. All three concepts are shown in Figure 1.

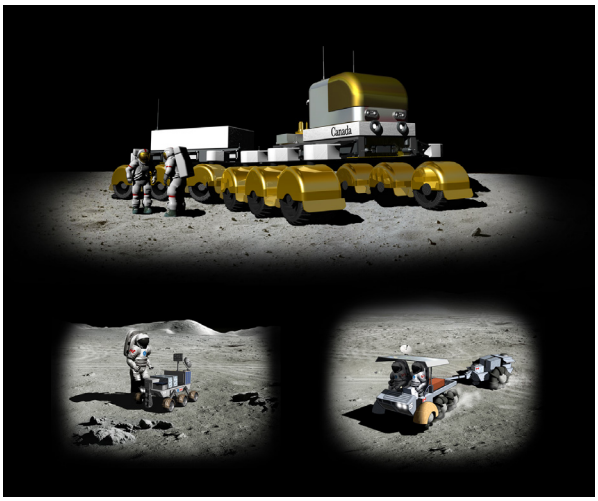

Figure 1 – TRACTEUR (top), LEMUR (bottom right) and RAPIER (bottom left)

MDA conducted two additional Phase 0 mission studies beginning in 2008, building on previous concepts and successes. The first was a concept for a Canadian rover as part of NASA's proposed Constellation framework known as **M**anned **L**unar **M**ission (MLM) that, much like TRACTEUR and LEMUR, would provide a modular chassis system and configurable control systems for transport of crew, pressurized modules, or even a crane, known as CRADLE (**C**anadian **R**econfigurable **A**dapter for the **D**eployment of **L**arge **E**lements). CRADLE would be capable of moving up to 9000 kgs of payload such as a habitation modules for a lunar base.

The second study during this period was the development of a Canadian node of the **I**nternational **L**unar **N**etwork (ILN). ILN provided the necessary architecture for a Lunar Landed system, tailored specifically to objectives derived from it's Canadian science team.

Additional studies have been conducted focusing on rover payloads including a novel Ground Penetrating Radar, as well as studies looking at the optimal architecture of robotic manipulator systems (i.e. robotic arms) for planetary exploration. Such systems are the signature technology of MDA, makers of the shuttle Canadarm, Space Station Canadarm 2 & Dextrous Manipulator systems.

Prototyping: MDA is currently developing or co-developing several Lunar prototypes for CSA, including an analogue rover, advanced navigational vision system, and a suite of scientific instruments such as ground penetrating radar, as part of CSA's **E**xploration **S**urface **M**obility (ESM) program. The rover system, known as **L**unar **E**xploration **L**ight **R**over (LELR, shown in Figure 2), builds upon the advancements made during the MLM program, and has configurable design to accommodate scientific exploration, **I**n **S**itu **R**esource **U**tilization (ISRU) activities, or be upgraded to facilitate crew transport within it's 300 kg payload capacity.

Figure 2 – Concepts illustrating the uses of LELR

In support of science and ISRU type investigations, a **L**unar **G**round **P**enetrating Radar (GPR) prototype is also currently under development. Based upon niche Canadian technology, the LGPR project promises to deliver a state of the art instrument.

Finally, an intelligent sensor system prototype is being developed that will integrate the strengths of lidar in providing highly precise short- to long-range 3D imaging with the strengths of stereoscopic cameras in allowing high-resolution texture mapping and scene modeling. The resulting product will be an innovative compact system for navigation, path planning, hazard mapping and scientific use.

Analogue Deployments: MDA has been involved in an increasing number of analogue deployments to field test their technologies. Most recently (2010) a sample return deployment to SP and Meteor craters was undertaken to demonstrate the capabilities of the CSA's **C**anadian **B**readboard **R**over (CBR), built by MDA. The rover, in conjunction with a suite of autonomous navigational sensors and camera systems, robotically explored the surrounding terrain, while being teleoperated from CSA headquarters in St. Hubert, Canada (see figure 3).

Figure 3 – CBR rover at SP Crater in Arizona

In addition to testing the technical aspects, several scientific studies were also carried out, most notably through US partnerships that provided a robotic arm and mini-corer. Decisions affecting the operational tasks of the rover were made by a Science Team stationed at CSA, thus testing a variety of operational scenarios, and providing a wealth of information for future missions planning.

Future Activities: Given the current uncertainty surrounding Lunar exploration, it is more important then ever to harness international partnerships in both science exploration and technology development in the development of future missions. The technologies, and more importantly the lessons learned, lay the framework for future development that is capable of covering a variety of future Lunar robotic exploration missions.

Constraints from Diviner Lunar Radiometer Data for Future Lunar Landing Sites B. T. Greenhagen[1], D. A. Paige[2], and the Diviner Science Team, [1]Jet Propulsion Laboratory, California Institute of Technology, Pasadena, CA, USA; [2]University of California, Los Angeles, CA, USA. Email: Benjamin.T.Greenhagen@jpl.nasa.gov

Introduction: The Diviner Lunar Radiometer is the first multispectral thermal instrument to globally map the surface of the Moon. This unprecedented and growing dataset is revealing the extreme nature of the lunar thermal environment, thermophysical properties , and surface composition. Diviner data provide new constraints for future landing site selection.

Diviner Lunar Radiometer: Launched onboard LRO in June 2009, the Diviner Lunar Radiometer is a nine channel pushbroom mapping radiometer designed to measure broadband reflected solar radiation (two channels) and emitted thermal infrared radiation (seven channels) between 0.3 and 400 μm at spatial resolutions ranging from 0.2 to 1.3 km [1]. The two solar reflectance channels both span 0.3 to 3 μm and are used to characterize the photometric properties of the lunar surface. The three shortest wavelength thermal infrared channels (ch 3: 7.55-8.05 μm; ch 4: 8.10-8.40 μm; ch 5: 8.38-8.68 μm) were specifically designed to characterize the mid-infrared Christiansen Feature [2]. Diviner's longer wavelength thermal infrared channels span the mid- to far-infrared between 13 and 400 μm and are used to characterize the lunar thermal environment, including thermophysical properties such as rock abundance and surface roughness. [1]

After more than two years of nearly continuous mapping, Diviner has now acquired observations over four complete diurnal cycles and two complete seasonal cycles. Diviner daytime and nighttime observations cover approximately 80% and 90% of the surface area of the moon, respectively. Calibrated Diviner data and global maps of visible brightness, brightness temperature, bolometric temperature, rock abundance, nighttime soil temperature, and silicate mineralogy from the first year of the LRO Mapping Orbit are available through the PDS Geosciences Node [3,4].

Thermal Environment: The complex and extreme lunar thermal environment posses challenges for future landed missions, but it also provides opportunities. Surface temperatures in equatorial regions such as the Apollo landing sites are close to 400K at noon, and less then 100K at night, with annual average temperatures at depth of approximately 250K [5]. Diviner has mapped the entire Moon over a full year and has located areas that have subsurface temperatures that are significantly hotter and colder than latitudinal averages. These thermally atypical regions are of interest to future mission planners to extend the range of latitudes and the range of lunar environments that can be accessed, explored and sampled [5].

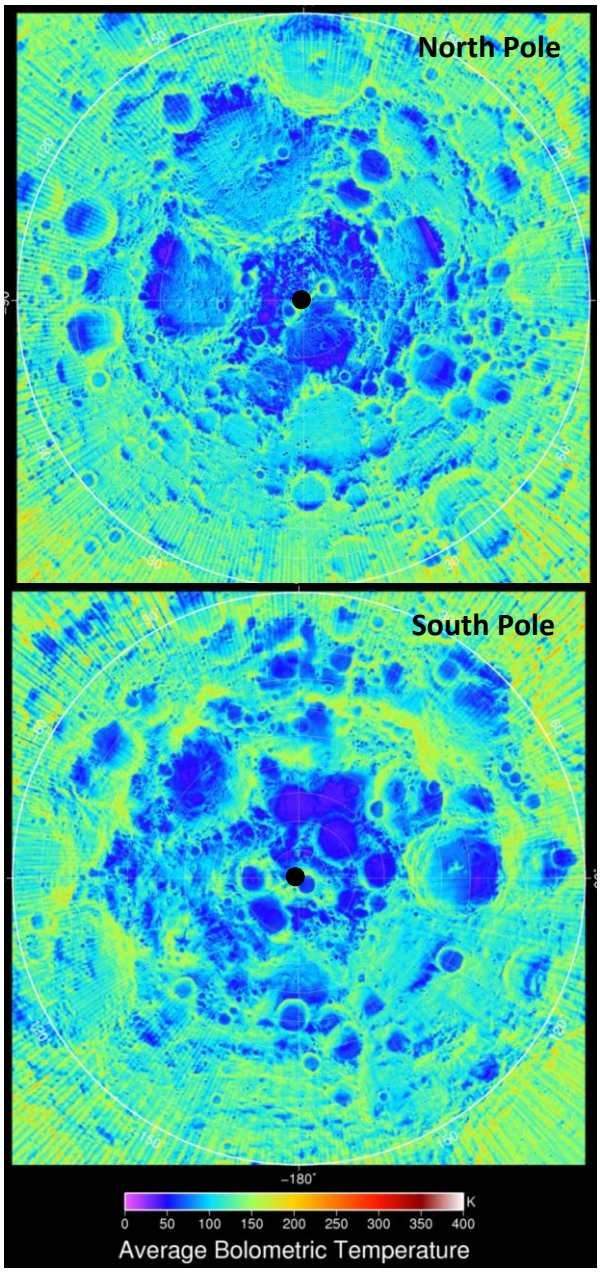

Figure 1: Maps of average bolometric temperature for the North (top) and South (bottom) Poles. Outer latitude ring is 80 degrees. Data stripping at lower latitudes is caused by a lack of overlapping coverage at all local times.

Polar Volatiles. Diviner's thermal mapping results place strong constraints on the thermal stability of polar volatiles. In the lunar polar regions there are large areas within permanently shadowed craters with annual average temperatures of less than 50K (Fig. 1). These regions are cold enough to permit the stability of water ice, as well as a range of more volatile and less volatile compounds. Frozen volatiles are thermally stable below the surface in large regions surrounding permanently shadowed areas within ~10 cm of the surface. [6]

Silicate Mineralogy: Diviner was designed to characterize the Christiansen Feature (CF) and constrain lunar silicate mineralogy [2]. The CF is tied to the fundamental vibrational band and shifts to shorter wavelengths with increasing polymerization of the SiO_4 tetrahedra (e.g. quartz and plagioclase feldspar exhibit CFs at shorter wavelengths than less polymerized pyroxene and olivine) [e.g. 7]. Also, given the relatively restricted geochemistry of the lunar surface (plagioclase feldspars have little Fe and higher Al and Ca; pyroxenes and olivines have high Fe and/or Mg and essentially no Al), Diviner measurements of CF position can be use to infer some geochemical abundances such as FeO [8].

South Pole Aitken Basin. Diviner data provide an important constraint on plagioclase abundance that can be used to infer the amount of country rock mixing [2]. This is a critical quantity for evaluating high value SPA Basin targets that have been identified using near-infrared spectroscopy. The use of near-infrared datasets with Diviner data reveal more than either dataset individually.

Silica-rich Sites. Diviner data have been used to confirm the presence of high silica minerals such as quartz or alkali feldspar for several lunar "red spots" and the Compton Belkovich anomaly on the lunar farside [9,2]. This class of landing site offers a unique opportunity to study evolved lunar crust and siliceous lunar magmatic processes.

Rock Abundance and Surface Roughness: Surface hazards for future landing sites include rock abundance and surface roughness. Both the presence of rocks in a predominately particulate surface and surface roughness induce variable temperatures or anisothermality within a given Diviner pixel. Anisothermality causes a wavelength difference in apparent brightness temperature. By using multispectral Diviner observations, it is possible to assess the magnitude of anisothermality and quantify the surface coverage of rocks, the temperature of the rock-free regolith, or the approximate RMS roughness of the surface. [10]

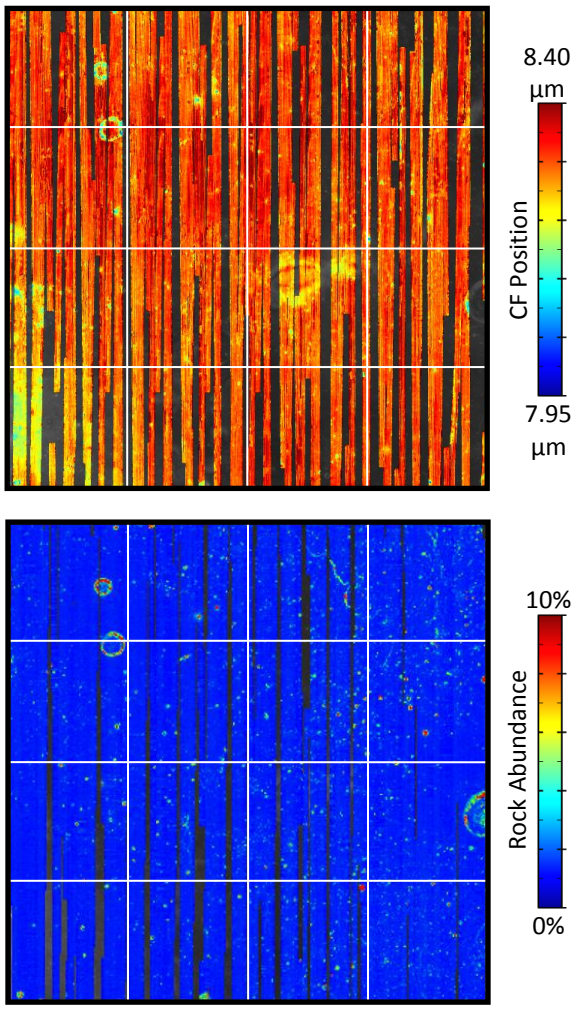

Figure 2: Examples of Diviner composition and rock abundance data products for the Rainer Gamma region. The map of CF position (top) shows variations in composition and space weathering across the scene. The rock abudance map highlights small fresh craters and the walls of larger, older craters. Latitude and longitude lines are drawn at 2.5 degree increments around -60E / 8N. Diviner data are overlain on the Clementine v2 basemap.

References: [1] Paige D.A. *et al.* (2010) *SSR, 150*, 125. [2] Greenhagen B.T. *et al.* (2010) *Science*, *329*, 1507. [3] Paige D.A. *et al.* (2011) LPSC XLII, #2544. [4] Greenhagen B.T. *et al.* (2011) LPSC XLII, #2679. [5] Paige D.A. *et al.* (2011) *JGR*, submitted. [6] Paige D.A. *et al.* (2010) *Science*, *330*, 479. [7] Logan L.M. *et al.* (1973) *JGR*, *78*, 4983. [8] Allen C.C. *et al.* (2011) LEAG (this mtg). [9] Glotch T.D. *et al.* (2010) *Science*, *329*, 1510. [10] Bandfield J.L. *et al.* (2011) *JGR*, in press.

DELIVERY OF LUNAR SURFACE PAYLOADS ON A COST-SHARED COMMERCIAL ROBOTIC EXPEDITION. D. P. Gump, Astrobotic Technology Inc. 4551 Forbes Avenue, Suite 300, Pittsburgh, PA 15213, david.gump@astrobotictech.com

Introduction: The agenda for robotic activity on the moon is sufficiently broad and the expense of mounting a commercial mission is now sufficiently affordable to close the business case for repeated private-sector expeditions that sell payload accommodations on a per-kg basis to all interested parties.

Astrobotic Technology Inc., a spin-off from Carnegie Mellon University's Field Robotics Center, is exploiting both the University's deep technical expertise and its tradition of internally fabricating advanced robots for hazardous and challenging environments using modest budgets.

In addition, Astrobotic Technology has signed a launch contract with SpaceX to use the economical Falcon 9 to inject its single-stage spacecraft/lander into trans lunar trajectory. This will be the first mission of the Falcon 9 for beyond-Earth destinations.

The mission will be able to deliver up to 110 kg of payload for space agencies, academic researchers, and the media/marketing industries. Both lander and rover provide power and communications to payloads. Payloads on both have access to the regolith less than a half-meter away from their mounting locations.

The initial mission will launch in the April-July 2014 period, with the date and lunar desintation dependant primarily on customer preferences.

Mission design. A Falcon 9 launches and injects the spacecraft through TLI with second stage re-ignition. The single-stage lander cruises for four days, orbits, descends and lands. Pinpoint landing near a feature of interest is achieved by optical registration of images captured during orbit and descent to stored images from LROC. The lander detects hazards during approach of the final landing site and diverts to safely land within 200 meters of the target. The rover departs for a 12-day trek until local sunset, when it enters hibernation until the next dawn..

Ground Operations: Launch ops occur at SpaceX's Cape Canaveral facility. Surface operations are centered in Pittsburgh at CMU. To maintain continuous 24/14 surface operation, operators are rotated every six hours.

Cruise, Orbit and Landing: Mission trajectory has been designed through Satellite Toolkit through partnership with AGI. Control of descent and in-flight attitude maneuvers will be evolved from autonomous vehicle control systems developed at CMU.

Lander design: The lander is a pallet structure, which delivers the rover and stationary payload to the lunar surface. The lander hosts payload and provides 500W of persistent solar power during daylight. It is solar powered with rechargeable batteries for storage and surge power. Baseline communication is a pointed antenna with omnis as backup.

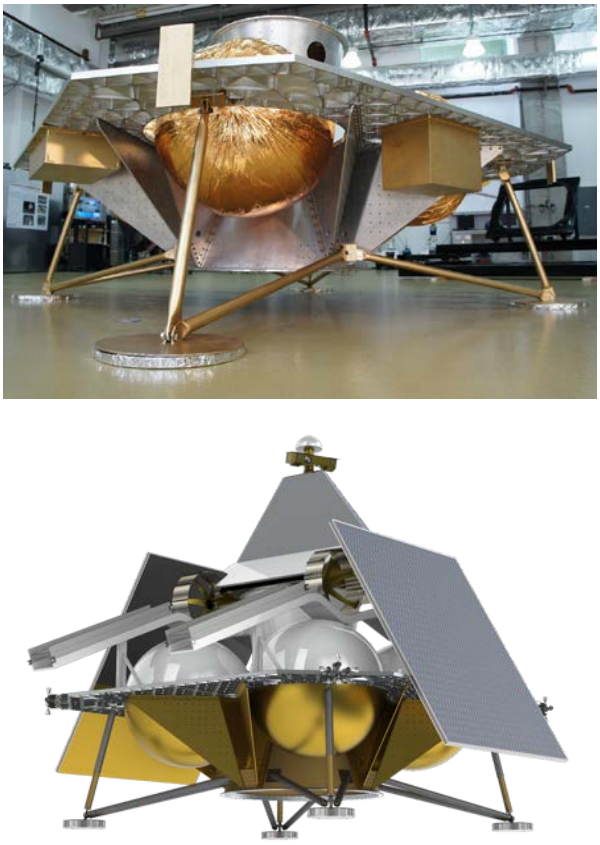

Figure 1. Top photo is lander primary structure after shake table testing; bottom image is full lander with rover mounted on top.

Lander solar arrays generate 500 watts average power. The 28V 54Ahr battery incorporates lithium iron phosphate cells. Battery packs have been developed, prototyped and tested for power draw and thermal.

Rover Design: Three rover prototypes already have been fabricated and field tested. Rover structure is primarily composite. Structure components are manufactured at Carnegie Mellon's Advanced Composites Lab and critical components have been manufactured and tested to verify process and quality. Rover structural analysis has been performed for loads from launch and roving.

The rover is a skid-steered vehicle with passive suspension. Two actuators propel and steer the rover. Roller chain transmits torque from shoulder actuators to the wheels; chain

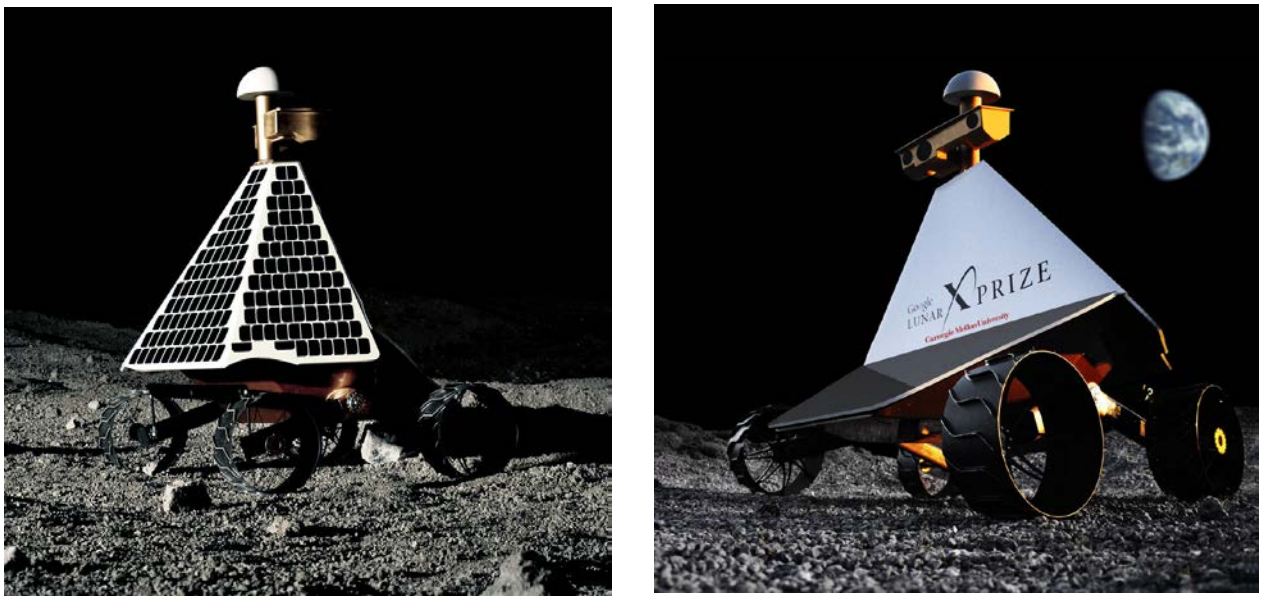

Figure 2. Prototype lunar rovers shown above have been field-tested in lunar-like slag heaps near Pittsburgh, demonstrating an ability to surmount steep obstacles during teleoperation. The camera head rotates 180 so that the rover can move toward or away from the sun while keeping its solar panels fully illuminated and its slanted radiator pointed to black sky to dump excess heat.

enables high torques with minimal mass and complexity. Placement in the shoulders insulates actuators from lunar dust and extreme temperatures of the lunar surface and eliminates wire flexure or steering through the suspension. Each shoulder actuator transmits torque to both wheels on one side. Extensive testing on mobility prototypes has validated system performance under thermal and mechanical load.

Alliances with Harmonic Drive and International Rectifier provides robust space actuation. Actuation stacks are developed by CMU and Harmonic Drive are driven by OM9373 motor drivers from International Rectifier. All actuation stacks have been detailed, prototyped and tested including functional field testing and thermal vacuum tests.

The rover is powered by a fixed faceted conical solar array avoiding complex, mass intensive deployments. The rover operates much like a sailboat tacking to keep the sun on the solar array and off the radiator. Full motion is achieved with a bidirectional drive train and rotatable camera head. The power system electronics mimic that of the spacecraft. A battery identical to the spacecraft battery provides surge power for drive actuators and payloads.

An asymmetric, composite structure with dual structural and thermal function, achieves passive thermal regulation for the hot lunar equatorial day. Critical robot components are thermally isolated from the solar panels and chassis with MLI. Motors, avionics, batteries, and other electronics which generate heat are connected to a radiator which faces away from the sun either directly or through high conductivity thermal pathways. The result is a robot that absorbs little heat from its surroundings and efficiently dumps self-generated heat.

Planetary dynamics of the Moon surface I.E.Harris 536 Crescent, St Lambert Quebec Canada J4P 1Z2 ieharris_374@sympatico.ca

The hydroxyl radical has been found recently in sample of rock o the Apollo 15 mission .The sites lies in the Mare Imbrium 30.391 longitude degrees east : 26..06 degrees north near the Archimedes crater it thus has large mountain ranges to the north and east being in a flood plain of basalt rock at this place. .The detection of the OH radical in a fluorapatite from this region is significant . Equally significant is the binding of the OH detected, which was in the order of 4600 ppm + or - 2000 ppm - using TOF-SIMS ..[1] The fluorapatite Ca 4 (PO 2) is in a chemistry of stress, in other words the material has been stressed. In the quantity of OH detected from the time of flight ion spectrometry it would seem that it is bound in anion sites, or roughly the OH is bound in place of the O anions

The basalt of the Moon is examined under somewhat different categories than that on the earth due to perceived differences The definition or description of basalts on the earth would be feldspathic plagioclase (calcic plagioclase) and pyroxene with or without olivine and as accessories iron -often magnetite – with quartz and and an amphibole such as hornblende or hyperstene. Two other differences in distinguishing the Moon from the earth may be common in origin from a possible process , a surface process.

The rock which has not been found on the surface of the Moon which we would expect would be the clays , micas , amphiboles and some phosphates contained on earth for the latter . One other difference that has been noticed is that very magnetic nano – iron has been picked up in these areas of lunar night and daylight, which is magnetic, and is not seen on the surface of the earth.

The atomic elements with thermodynamics of detection or testing more easily picks up the cations ,nevertheless we are able increasingly to see their anion counterparts packed in their temperature and pressure movement in positions, In the detecting of this OH radical or indeed water in the rock as HOH or OH , these movements and position are shown , as indeed the methods of detection are showing , and the most logical position for a small amount of OH is seen as substituting in the anions in the O's process OH additions. Thus in the manner of detection in thermodynamics or stress they are an attenuation of phase and electric transitions. The attenuation may be a reason why the OH is retained

Therefore from where we should find the OH hydroxyl radical because it somewhat operates in temperature and pressure thermodynamic events as an in and out mechanism or some sort of safety valve for retaining the molecule, and by a quick reaction the OH can either come back in or go out , but the molecule is able to obtain some sort of integrity .

In that event through confirmation of process by this lunar sample of a phosphate we may be able to explain the differences of the Moon in our inability to find much surface rock with the OH in it , and the nano-iron magnetism making one assumption of the earth material hematite. The assumption is from something recently noted.

---

[1] Francis McCubbin et al, ,Detection of structurally bound hydroxyl in fluorapatite from Apollo Mare basalt 15038.128 using TOF-SIMS, Am.. Min . Vol . 95 No 8-9 August –September 2010 at pg 1141

The said lunar sample with the OH bound in it is surface and as all lunar samples are, exposed to the to the direct radiation of the Sun and for this for fourteen days at a time and to the chilling through the equally long night. . The samples largely consisting of breccia and as the sample from the Apollo missions would be drawn from these lunar day and night surface and the breccia as almost always coming apart in cataclysmic events or staying together as the case may be but in a stressed condition.

The temperature differences in the parts of the surface of the Moon where they occur can explain both the absence of the OH bearing rocks in the samples per se and the nano-iron .

On the earth we have both terrain which uses processes of accepting temperature rises and controlling temperature rises. sand dunes for instance , or soils. From a study the soils retain their a constant temperature by using an OH process. Soils will maintain constant temperature by process that is to say that whatever the temperature above the soil , the soil maintains a temperature and that temperature is constant meaning that some energy is being used. So that this is similar to the situation of the sands of the desert which are infertile and whose temperature is permitted to fluctuate while the soil is not.

Attention is brought to the study on a natural titanium bearing hematite . A 30 degree tilt out of basal plane axis of spin orientation was found using time of flight diffraction . The material was seen as ilmenite lamellae (titanium process) acting as a hard magnetic stage and hematite acting as a soft magnetic phase .[2] . The magnetite form of iron would of course be the magnetic hard stage. What has happened is that the thermodynamic process has been attenuated with the moving of the hysteresis, that is to say it does not occur as quickly with a few other molecular effects. The assumption is that hematite in which the OH is found in this case retains a small amount of it for exactly such purpose . It may be what causes the c axis anisotropy. That with the temperature may be the cause of the nano-iron on the Moon.

The problem of the cooling off over several hundred degrees in the surface sample area of the Moon can also be visited in another paper [3] The paper shows how the OH radical could be retained in the lunar night The feldspathoid which would be a common melt rock observed down to cryrogenic temperatures at 100 degrees K. The crystal becomes squatter and there is some rotation ,only that.

We have in a particular area subject to certain conditions on the Moon found samples which do not contain such a process however in considering the regolith upper and lower the process which would be used ,say on earth soils ,- that which one might find in the lower regolith leaving the upper regolith to ambient In fact it makes likely our finding of water ice or water near the poles which is not subject to such conditions: what also has to be considered in light of work which has been done recently on earth in connection with soils[4] which seems to prove behaving as such.

---

[2] Richard Harrison et al , Spin Orientation in natural Ti- bearing hematite Evidence for out of plane component , Am Min Vol. 95 No 7 July 2010 at pg 974

[3] G Diego Gatta et al , Low Temperature behavior of natural kalsinite with P 31 symmetry : An in situ single X ray diffraction study, Am Min, Vol. 95No 7 July 2010 pg 1027

[4] Micrometeorology 2010 of the author. The constant temperature of the soil over a large area was found. It was found in the OH HOH water transformations of the clay in the soil, the silica and humus operation as the neutral components. . It was in the face of earth solar radiation and other radiation type energy sources of normal and ever present nature.

A DEDICATED SMALL LUNAR EXPLORATION ORBITER AND A MOBILE SURFACE ELEMENT.

H. Hoffmann[1], R. Jaumann[1], H. Hiesinger[2], F. Claasen[3], T. Spohn[1], U. Mall[4], J. Helbert[1], N. Kappelmann[5], K. Werner[5], R. Wimmer-Schweingruber[6], R. Srama[7], J. Oberst[1], J. Flohrer[1], M. Werner[8], G. Neukum[9], S. van Gasselt[9], N. Schmitz[1], K. Eichentopf[1], T. Knigge[10], U. Kummer[10], M. Langemann[10], H. Müller[11], R. Haarmann[12], [1]German Aerospace Center (DLR) Berlin, Institute of Planetary Research, Rutherfordstrasse 2, 12489 Berlin, Germany (ralf.jaumann@dlr.de, harald.hoffmann@dlr.de), [2]Westfalische Wilhelms-Universitat, Münster, Germany, [3]DLR, Raumfahrtmanagement, Königswinterer Strasse 522-524, 53227 Bonn, Germany, [4]Max-Planck-Institut für Sonnensystemforschung, Max-Planck-Strasse 2, 37191 Katlenburg-Lindau, Germany, [5]Universität Tübingen, Institut für Astronomie und Astrophysik, Sand 1, 72076 Tübingen, Germany, [6]Christian-Albrechts-Universität, Institut für experimentelle und angewandte Physik, Kiel, Germany, [7]Max-Planck-Institut für Kernphysik Heidelberg, 69029 Heidelberg, Germany, [8]DLR Oberpfaffenhofen, Institut für Hochfrequenztechnik und Radarsysteme, 82234 Wessling, Germany, [9]Institute of Geological Sciences, Freie Universität, Berlin, Germany, [10]EADS, Astrium Friedrichshafen, 88039 Friedrichshafen, Germany, [11]DLR Institut für Raumfahrtsysteme, Robert Hooke Str. 7, 28359 Bremen, Germany, [12]Kayser-Threde GmbH, Perchtinger Str. 5, 81379 München, Germany.

The Moon is an integral part of the Earth-Moon system, it is a witness to more than 4.5 b. y. of solar system history, and it is the only planetary body except Earth for which we have samples from known locations. The Moon is thus a key object to understand our Solar System. The Moon is our closest companion and can easily be reached from Earth at any time, even with a relatively modest financial budget. Consequently, the Moon was the first logical step in the exploration of our solar system before we pursued more distant targets such as Mars and beyond. The vast amount of knowledge gained from the Apollo and other lunar missions of the late 1960's and early 1970's demonstrates how valuable the Moon is for the understanding of our planetary system (e.g. [1], [2]). Even today, the Moon remains an extremely interesting target scientifically and technologically. New data have helped to address some of our questions about the Earth-Moon system, but many remain and new questions arose. In particular, the discovery of water at the lunar poles, and water and hydroxyl bearing surface materials and volatiles, as well as the discovery of young volcanism have changed our view of the Moon. Therefore, returning to the Moon is the critical stepping-stone to further exploring our immediate planetary neighborhood. Here, we present scientific and technological arguments for a Small Lunar Explorations Orbiter (S-LEO) dedicated to investigate so far unsolved questions and processes. Numerous space-faring nations have realized and identified the unique opportunities related to lunar exploration and have planned missions to the Moon within the next few years. Among these missions, S-LEO will be unique, because of its unprecedented spatial and spectral resolutions. S-LEO will significantly improve our understanding of the lunar environment in terms of composition, surface ages, mineralogy, physical properties, and volatile and regolith processes. S-LEO will carry an entire suite of innovative, complementary technologies, including high-resolution camera systems, several spectrometers that cover previously unexplored parts of the electromagnetic spectrum over a broad range of wavelengths, and a communication system to interact with landed equipment on the farside. The Small Lunar Explorations Orbiter concept is technologically challenging but feasible, and will gather unique, integrated, interdisciplinary data sets that are of high scientific interest and will provide an unprecedented new context for all other international lunar missions.

The most visible mission goal of S-LEO will be the identification and mapping of lunar volatiles and investigating their origin and evolution with high spatial as well as spectral resolution. Therefore, in addition to mapping the geological context in the sub-meter range, a screening of the electromagnetic spectrum within a very broad range will be performed. In particular, spectral mapping in the ultraviolet and mid-infrared will provide insight into mineralogical and thermal properties so far unexplored in these wavelength ranges. The determination of the dust distribution in the lunar orbit will provide information about processes between the lunar surface and exosphere supported by direct observations of lunar flashes. Measuring of the radiation environment will finally complete the exosphere investigations. Combined observations based on simultaneous instrument adjustment and correlated data processing will provide an integrated geological, geochemical and geophysical database that enables:

- the exploration and utilization of the Moon in the 21st century;
- the solution of fundamental problems of planetology concerning the origin and evolution of terrestrial bodies;
- understanding the uniqueness of the Earth-Moon System and its formation and evolution;

- the absolute calibration of the impact chronology for the dating of solar system processes;
- deciphering the lunar regolith as record for space environmental conditions;
- mapping lunar resources.

S-LEO is featuring a set of unique scientific capabilities w.r.t. other planned missions including: (1) dedicated observation of volatiles (mainly H_2O and OH), their formation and evolution in direct context with the geological and mineralogical surface with high spectral and spatial resolution (< 1m/px); (2) besides the VIS-NIR spectral range so far uncovered wavelengths in the ultraviolet (0.2 – 0.4 µm) and mid-infrared (7 - 14 µm) will be mapped to provide mineralogical context for volatile processes (e.g. sources of oxygen); (3) detection of rock-forming elements by means of x-ray fluorescence in the spectral range of .5-10 keV in order to constrain the composition of key elements of lunar surface materials; (4) monitoring of dust and radiation in the lunar environment and its interaction with the surface; and (5) monitoring of present-day meteoroitic impacts.

In 2009 ESA commissioned a Mobile Payload Element (MPE) to assist the ESA Lunar Lander mission. The MPE, currently under study in Germany, is designed to be a small, autonomous, innovative vehicle of roughly 10-12 kg for scouting the environment in the vicinity of the lunar landing site. The novel capability of the MPE will be to acquire samples of lunar soil in an area of >100m around the lander and to bring them back to the spacecraft for analysis by on-board instruments. This will enable access to soils that are less contaminated by the descent propulsion system plumes to increase the chances of detection of any indigenous lunar volatiles. The MPE shall acquire samples of regolith with landing-induced contamination being below the detection limit of the associated volatile-seeking instruments. Subsurface regolith sampling is preferable to understand the concentration of volatiles as a function of depth. Additional benefits for the overall science accomplished by a Lunar Lander mission could be obtained if the MPE were to conduct 'field geology' type observations and measurements along its traverses, such as geochemical and mineralogical in situ investigations with dedicated instruments on rocks, boulders and regolith. This would dramatically expand the effective area studied by the ESA Lunar Lander mission. Based on technology trades the baseline concept for the MPE system is composed by a 4-wheel active chassis with wheels, a power supply with fixed solar generators plus a secondary battery, a thermal system with active heating and passive insulation, a sensor package for autonomous operations and a VHF/UHF communication system between MPE and the Lander. One unique scientific aspect of the MPE could be the in situ study of rocks, boulders and lithic (rock) fragments which otherwise would only be amenable to measurements using any instrument heads mounted on the lander robotic arm (provided any rocks were within reach of the arm). To fulfill the science objectives, the MPE will be equipped with a stereo camera, the PLUTO mole subsurface regolith sampling system (as flown on Beagle 2) as well as a close-up imager. This instrument package allows acquisition of regolith samples from both illuminated and locally shaded terrain, sampling from the subsurface and from underneath large boulders and documentation of the samples acquired by close-up imaging of the sample site, ideally before and after sample acquisition. A suite of terrain temperature sensors is implicitly included to provide context for the samples acquired from permanently shadowed locations or below the surface, but also to contribute to landing site general science. As an option for the in-situ characterization of the sample material with respect to mineralogy and possibly volatile content, spectrometer experiments or a color capability of the camera could be added.

Further, a laboratory environment is currently being established at Freie Universität Berlin in order to allow sample-based geochemical measurements of key rock-forming elements in the soft X-Ray domain (.5-10 keV). The laboratory is used for the hardware development of X-Ray spectrometer experiments to be employed on lunar orbiter and on lunar lander missions.

References:

[1] H. Hiesinger, J.W. Head, New Views of Lunar Geoscience: An Introduction and Overview, In: Ne Views of the Moon (B.L. Jolliff et al. eds.) Rev. Min. Geochem., 60, 1-81 (2006).

[2] R. Jaumann, The Moon, In: Encyclopedia of Astrobiology, M. Gargaud et al. (eds.), Vol. 2, Springer, 280-282 (2011).

NASA LUNAR SCIENCE INSTITUTE: COLORADO CENTER FOR LUNAR DUST AND ATMOSPHERIC STUDIES (CCLDAS) M. Horanyi, T. Munsat, Z. Sternovsky, S. Kempf, E. Gruen, A. Colette, Xu Wang, A. Mocker, S. Robertson, and the CCLDAS Team (CCLDAS, U. of Colorado, Boulder, CO 80309-0392; Ph: (303) 492 - 6903, E-mail: horanyi@colorado.edu)

Introduction: The Colorado Center for Lunar Dust and Atmospheric Studies (CCLDAS) is one of the seven US teams of NASA's Lunar Science Institute. CCLDAS is focused on experimental investigations of the lunar surface, including dusty plasma and impact processes, the origins of the lunar atmosphere, and the development of new instrument concepts with a complementary program of education and community development. This presentation will show our most recent results: **a)** the completion of a 3 MV dust accelerator; **b)** the status of the Lunar Dust Experiment (LDEX) instrument development for the LADEE mission; **c)** small-scale supporting laboratory experiments; and **d)** the development of new instrument concepts for surface exploration of airless bodies.

The dust accelerator facility: A 3 MV Pelletron has been installed that contains a dust source, feeding positively charged particles into the large accelerator (Figure 1). The facility is used for impact experiments to study the production of secondary particles, plasma and neutrals, crater formation, and for the testing and calibration of dedicated dust instruments, for example. We will present the technical details of the facility and its capabilities, as well as the results of our initial experiments for damage assessment of optical devices, and penetration studies of thin films. We will also report on the use of this facility for the testing and calibrating the LDEX instrument. We also discuss the opportunities to use this facility by the lunar, planetary, space and plasma physics communities.

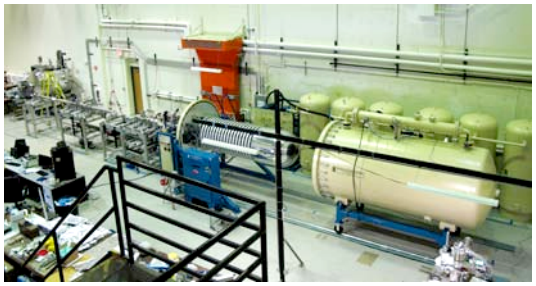

Figure 1. The 3 MV dust accelerator installed in the CCLDAS Lunar Environment and Impact Laboratory. The accelerator is used to simulate the effects of dust impacts with speeds >> 10 km/s for micron sized projectiles. The facility will be also used to test and calibrate plasma and dust instruments, including the Lunar Dust Experiment (LDEX) for the LADEE mission. The facility is now operational and available for the lunar community for impact studies.

The Lunar Dust Experiment (LDEX): LDEX) is a dust detector instrument designed and built for the LADEE (Lunar Atmosphere and Dust Environment Explorer) mission (Figure 2). The goal of LDEX is to map the dust environment of the Moon from a ~ 50 km altitude orbit.

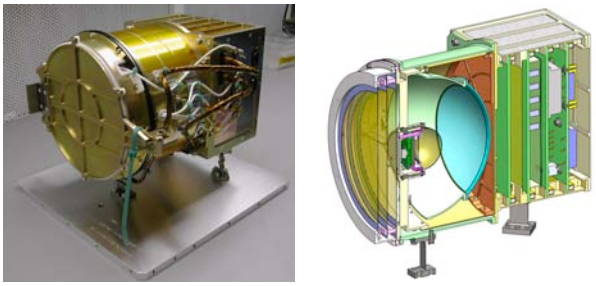

Figure 2. The LDEX engineering model (left), and its schematic diagram (right).

LDEX will measure the density and mass of dust particles. It is sensitive to individual impacts by particles > 0.25 micron in radius. Smaller particles can be detected in a cumulative mode, if present in sufficient quantities. LDEX is the first dust detector instrument optimized for operation while exposed to the UV environment above the sunlit lunar surface. The engineering model (EM) has been constructed and calibrated. The flight unit is currently under construction.

Small-scale laboratory experiments: These experiments are dedicated to the investigations of charging and mobilization of dust on surfaces. The effects of UV radiation, and the solar wind plasma flow. The most recent results address the effects of surface magnetic fields on the generation of intense, localized electric fields that are likely to play an important role in dust transport.

The Moon does not have a global magnetic field, unlike the Earth, rather it has strong crustal magnetic anomalies. Data from Lunar Prospector (LP) and SELENE (Kaguya) observed strong interactions between the solar wind and these localized magnetic fields. We use a horseshoe permanent magnet as an analogue to create a magnetic dipole field above an insulating surface in plasma. A complex potential distribution above the surface is observed. In our experiments, electrons are magnetized with gyro-radii r smaller than the distances from the surface d ($r < d$) and ions are un-magnetized with $r > d$. A non-

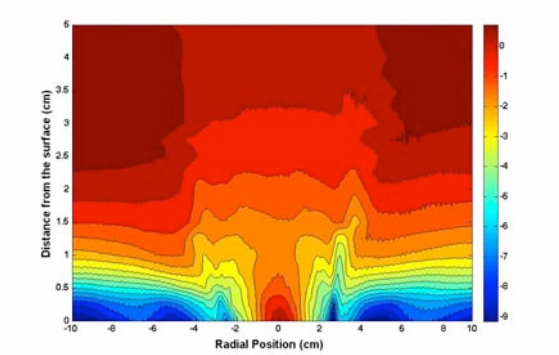

Figure 3. The potential distribution above a surface magnetic 'anomaly'. The color-code shows the measured values of plasma potential in Volts.

monotonic sheath is shown above the surface in the central magnetic dipole. Unlike negative charging on surfaces by electrons with higher mobility, potential on the surface in the central dipole is found slightly more positive than the bulk plasma potential because the surface charging is dominated by the cold unmagnetized ions while the electrons are magnetically shielded away. A potential minimum is found in the shielding region between the surface and the bulk plasma, most likely caused by the electrons that access the region due to the collision and are mirror-trapped between the two magnetic cusps. The value of the potential minimum with respect to the bulk plasma potential decreases with increases in the plasma density and the neutral pressure due to a spreading spatial density distribution in the sheath caused by the collisions. Potential on the surface fluctuates in the radial direction along the central dipole field line.

New instrument concepts: The observations of the inward transport of interstellar dust and the outflow of near-solar dust provide a unique opportunity to explore the dynamics and transport of small charged particles throughout the heliosphere. The flux, direction and size-distribution of interstellar dust can be used to test our models about the large-scale structure of the heliospheric magnetic field, and its temporal variability with solar cycle. The measurements of the speed, composition and size distribution of the recently discovered, solar wind-entrained nano-dust particles hold the key to understand their effects on the dynamics and composition of the solar wind plasma. Both the inflowing interstellar grains and the out-flowing nano-dust particles can be measured onboard a near Earth spacecraft at 1 AU, using modern dust detection techniques. The recently developed Dust Telescope (DT) instrument will be discussed, including its capabilities to measure the mass, charge, velocity vector, chemical and isotopic composition of the impacting dust particles, enabling the unambiguous identification of interstellar and interplanetary particles of various origin.

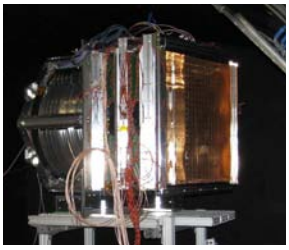

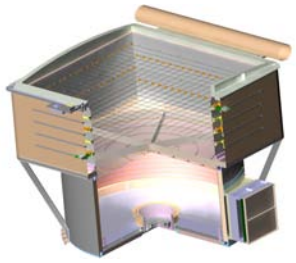

Figure 4. Laboratory model of a dust telescope (left) combining a trajectory sensor, and an impact dust detector the measure the mass, velocity, chemical and isotopic composition of interplanetary and interstellar dust. The schematic drawing of this instruments (right).

These measurements will provide an unexplored opportunity to link the heliospheric, space, planetary and astrophysics communities. We will also discuss the science requirements, instrumentation, and implementation options of this mission that could be achieved either by a small spacecraft orbiting the Moon, or by landing a payload on the lunar surface. As part of a landing package DT could be used as a modern version of the Lunar Ejecta and Meteorite experiment (LEAM) of the Apollo 17. DT could be used to detect the putative population of the slow-moving highly charged lunar dust particles, in addition to the flux and composition of interplanetary and interstellar dust bombarding the lunar surface.

References: http://lasp.colorado.edu/ccldas

COMPTON-BELKOVICH VOLCANIC COMPLEX: NONMARE VOLCANISM ON THE MOON'S FAR SIDE. B. L. Jolliff,[1] S. J. Lawrence,[2] M. S. Robinson,[2] F. Scholten,[3] B. R. Hawke,[4] B. T. Greenhagen,[5] T. D. Glotch[6], H. Hiesinger[7], and C. H. van der Bogert[7], [1]Dept. Earth & Planetary Sciences & McDonnell Center for the Space Sciences, Washington University, One Brookings Drive, St. Louis, MO 63130; [2]School of Earth & Space Exploration, Arizona State University, Tempe, AZ 85287; [3]German Aerospace Center (DLR), Institute of Planetary Research, Berlin; [4]SOEST, University of Hawaii, Honolulu, HI 96822; [5]Jet Propulsion Laboratory, Pasadena, CA 91109; [6]Dept. of Geosciences, Stony Brook University, Stony Brook, NY 11794; [7]Institut für Planetologie, Westfälische Wilhelms Universität Münster, Germany; <blj@wustl.edu>

Introduction: Images from the Lunar Reconnaissance Orbiter Cameras (LROC), including digital terrain models derived from the LROC Wide and Narrow Angle Cameras, and mineralogical data from the Diviner Lunar Radiometer provide evidence that a small silicic volcanic complex lies at the center of the Compton-Belkovich "thorium anomaly," known from Lunar Prospector gamma-ray data [1,2,3,4]. The Compton-Belkovich volcanic complex forms a low, broad dome about 25×35 km across and ~1 km in elevation, although the central part of the dome is depressed (Fig. 1 and [1]).

Superposed on the broad dome are a range of volcanic constructs, from small, circular domes and "bulges" with ~500 m base diameters to intermediate-size, irregular domes up to several km in maximum dimension, to larger volcanic features, with up to 6 km basal diameter, with summit depressions and flank slopes to over 20 degrees (Fig. 2). Within central parts of the Compton-Belkovich volcanic complex are irregular depressions, which we interpret to have resulted from collapse of a near-surface magma chambers following flank eruptions.

The Compton-Belkovich volcanic complex is the only silicic, nonmare volcanic feature known on the Moon's farside, and it is located ~900 km distant from the Procellarum KREEP Terrane where all of the Moon's other known silicic volcanics occur.

Compositional and mineralogic data: Diviner data in the region of the Christiansen Feature show that the broad Compton-Belkovich volcanic complex corresponds to an area of relatively silicic composition [5,6]. Lunar Prospector gamma-ray thorium data, after accounting for the broad compositional response function of the gamma-ray spectrometer [2], are consistent with Th concentrations as high as those seen in small samples of lunar granite and felsite, known from Apollo samples [e.g., 7-13], i.e., 40-55 ppm.

Origin: We hypothesize that the volcanic complex formed by intrusion of a magma with a KREEP-like composition that was generated deep in the crust. The intrusion ponded near the surface, likely within megaregolith. A deep origin is indicated by the observation that large impact craters in the region did not excavate KREEP- or Th-rich material. Generation of a silicic lava, e.g., 65-75 wt% SiO_2, deep in the crust and transportation directly to the surface seems implausible owing to the high viscosity of dry (or even slightly wet) silicic lava compositions. The broad, low-relief topography of the Compton-Belkovich volcanic complex and the low slopes along the apparently constructional east and west flanks are more consistent with a

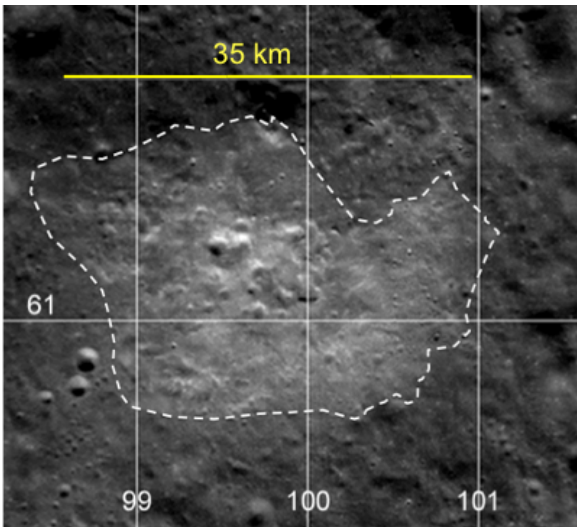

Fig. 1a. Wide-angle Camera (WAC) 604 nm [14].

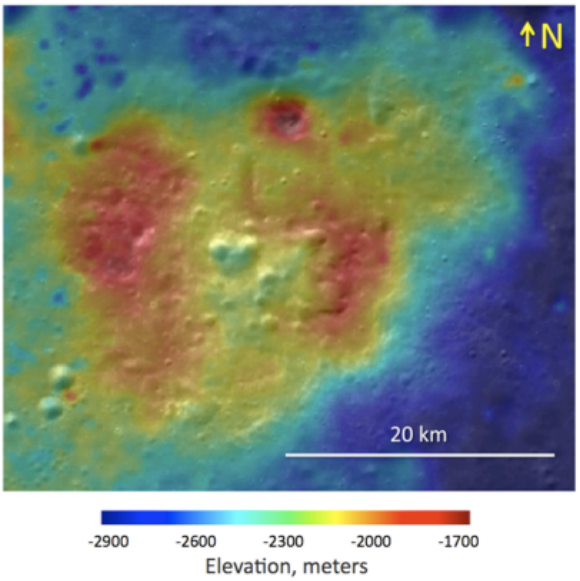

Fig. 1b. WAC digital terrain model (DTM) [15,16] draped over WAC image, 100 m/pixel.

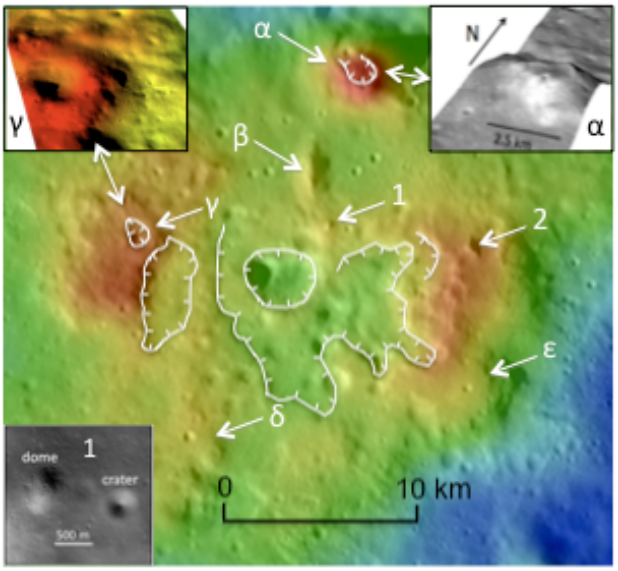

Fig. 2. Volcanic features in the Compton-Belkovich volcanic complex. Large cumulo-volcano structures, alpha and gamma, and small dome 1 shown in the corner insets.

lava of KREEP-basalt composition, i.e., SiO_2 ~50-52 wt% and viscosity some 3-5 orders of magnitude lower than rhyolite, even if it contained a small fraction of water [17].

We consider the emplacement to have occurred in four stages: (1) Melt generated deep in the crust or at the crust-mantle boundary intruded and ponded at the base of the megaregolith where there is a substantial density contrast with the anorthositic upper crust (Fig. 3). (2) The magma body inflated to form a broad, low dome, causing arcuate structural weaknesses in the uplifted megaregolith. (3) Lava exploited structural weaknesses and initially erupted at the surface, prior to extensive differentiation, producing volcanic constructs along the east and west sides of the complex, possibly concurrent with initial collapse in the central region. (4) Late-stage silicic derivative melts then extruded to form domes with a range of morphologies, including the large alpha dome to the north and smaller domes and bulges in the central region, especially along the flanks of the collapse scarps. The offset (or extension) of the Compton-Belkovich volcanic complex reflectance feature to the east-southeast of the topographic expression (as well as the asymmetric Th distribution in that direction) could result from pyroclastic dispersal preferentially on the eastern side of the complex. A combination of upward-enrichment of late-stage silicic differentiates and pyroclastic dispersal of silicic (rhyolitic) residual melt would have produced a veneer of silica and Th-rich material at the surface, masking the underlying megaregolith or KREEP-basalt/basaltic andesite intrusive.

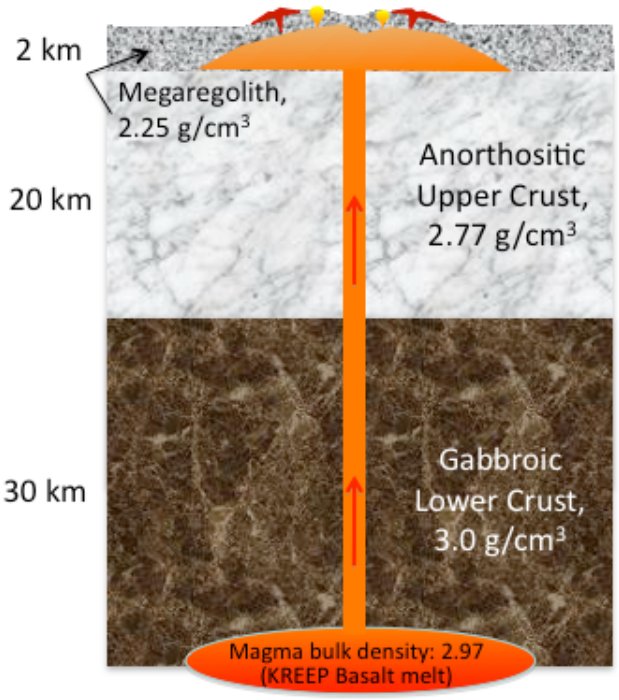

Fig. 3. Model for the origin of the Compton-Belkovich volcanic complex. Rise of magma in response to lithostatic pressure resulting from layered crust as shown (using methods in [18]). Assumed density of silicic melt (yellow, at surface) is 2.4-2.5 g/cm^3.

Acknowledgements: We thank the LROC science operations team and the Diviner and LRO Ops teams for their excellent work, and NASA for support of the LRO project.

References: [1] Jolliff B. et al. (2011) *Nature Geoscience* **4**, 566-571. [2] Lawrence D. et al. (2003) *J. Geophys. Res* **108**, 6-1-6-25. [3] Lawrence D. et al. (1999) *Geophys. Res. Lett.* **26**, 2681-2684. [4] Gillis J. et al. (2002) *Lunar Planet. Sci.* **33**, Abstract #1934. [5] Greenhagen B. et al. (2010) *Science*, **329**, 1507-1509. [6] Glotch T. et al. (2010) *Science*, **329**, 1510-1513. [7] Ryder, G. (1976) *Earth Planet. Sci. Lett.* **29**, 255-268. [8] Warren, P. et al. (1987) *Proc. Lunar. Planet. Sci. Conf. 17th* in *J. Geophys. Res.* **92**, E303-E313. [9] Marvin U. et al. (1991) *Proc. Lunar Planet. Sci.* **21**, 119-135. [10] Jolliff B. (1991) *Proc. Lunar Planet. Sci.* **21**, 101-118. [11] Jolliff B. (1998) *Int. Geol. Rev.* **40**, 916-935. [12] Seddio S. et al. (2009) *Lunar Planet. Sci.* **40**, Abstract #2285. [13] Seddio S. et al. (2010) *Lunar Planet. Sci.* **41**, Abstract #2688. [14] Robinson M. et al. (2010) *Space Sci. Rev.* **150**, 81-124. [15] Scholten, F. et al. (2010) *Lunar Planet. Sci.* **41**, #2111. [16] Scholten F., et al. (2011) *Lunar Planet. Sci.* **42**, #2046. [17] Bottinga Y. and Weill D. (1972) *Am. J. Sci.* **272**, 438-475. [18] Parfitt L. & Wilson L. (2008) *Fundamentals of Physical Volcanology*, Blackwell Publishing, Malden, MA, 230 p.

PROJECTILE FRAGMENTS IN ANCIENT LUNAR REGOLITH BRECCIAS: EXPLORING THE SOURCES AND TEMPORAL RECORD OF LUNAR IMPACTS. K. H. Joy[1,2], D. A. Kring[1,2], M. E. Zolensky[2,3], D. K. Ross[3,4], D. S. McKay[2,3]. [1]CLSE, LPI/USRA, 3600 Bay Area Blvd., Houston, Texas 77058, USA (joy@lpi.usra.edu). [2]NASA Lunar Science Institute. [3]ARES, NASA Johnson Space Center, Houston, TX 77058, USA. [4]ESCG-Jacobs Technology, 2224 Bay Area Blvd. Houston TX 77058, USA.

Introduction: A key lunar and planetary science goal is to understand the sources of projectiles that formed the large (>300 km) lunar basins. Resolving the sources of these basin-forming impactors will help to provide constraints for models of Solar System dynamics, understand the delivery of volatiles to the early Earth-Moon system, and to explain the causes of possible spikes in the ancient impact record [1].

A direct geochemical record of impactor origin is recorded by several meteorites that survived collision with the lunar surface. For example, a carbonaceous-chondrite (Bench Crater meteorite [2]) and an enstatite-chondrite (Hadley Rille meteorite [3]), have been previously reported in lunar soils. However, it is not known exactly at what time these meteorites impacted the lunar surface, and if they were involved in crater-forming events; so these samples provide only a limited perspective on the sources of impactors striking the Moon through time.

Regolith breccia time-capsules: Regolith breccias, which are consolidated samples of the lunar regolith (soil), were closed to further impact processing at the time they were assembled into rocks [4]. They are, therefore, time capsules of impact bombardment at different times through lunar history.

Here, we present a study of regolith breccias collected by the Apollo 16 mission from the Cayley Plains Formation.We used a revised calibration (after [5]) of the ratio of trapped $^{40}Ar/^{36}Ar$ ('parentless' ^{40}Ar derived from radioactive decay of ^{40}K, ratioed to solar wind derived ^{36}Ar) to semi-quantitatively calculate the timing of the assembly of the Apollo 16 regolith breccias (see Joy et al. [6] for more details, where the Apollo 16 $^{40}Ar/^{36}Ar_{Tr}$ values were taken from McKay et al. [4]). Our revised calibration indicates that the Apollo 16 ancient regolith breccia population was assembled between 3.8 and 3.4 Ga, consistent with regoliths developed and closed after the Imbrium basin-forming event (~3.85 Ga), during the time of declining basin-forming impacts.

Methods: We have used optical microscope and FEG-SEM techniques to identify non-lunar compositionally 'exotic' rock and mineral fragments within thin sections of these samples (see Joy et al., this meeting [7] for details, and Fig. 1a here). Samples are then analysed using the NASA JSC Cameca SX100 electron microprobe (EMP) to derive mineral (1 µm beam) and bulk fragment (10-20 µm beam) compositions.

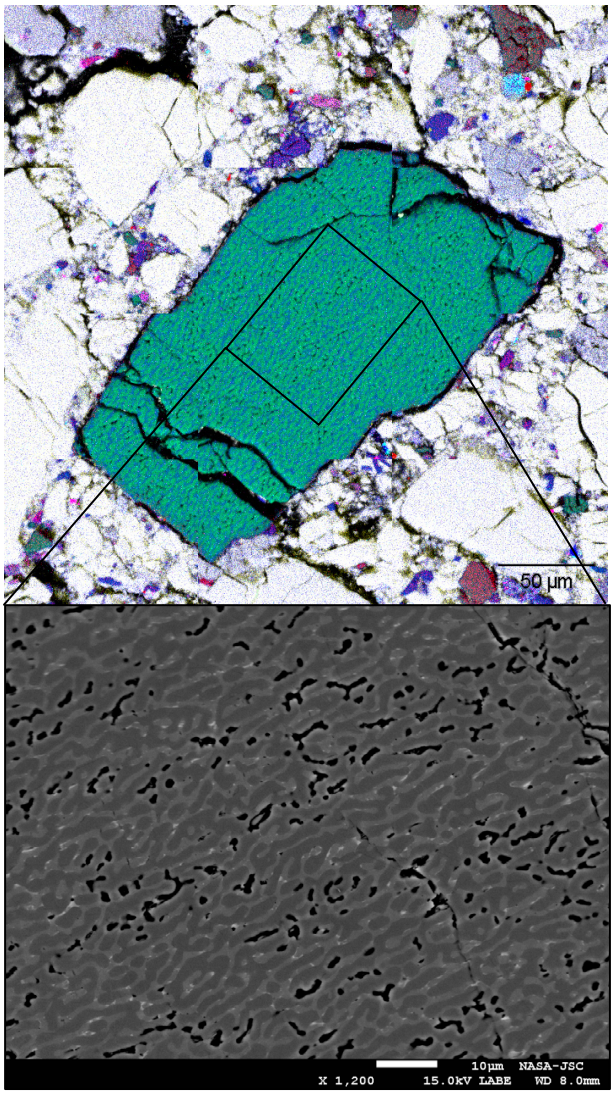

Figure 1. (a) Top: False-colour image (where Al=white, Mg=green, Si=blue, Fe=red, Ti=pink, Ca=yellow, K=cyan [7]) of large (~475 × 325 µm) cryptocrystalline UMMF fragment in 66035,13 (see also [13]). (b) Bottom: Close-up BSE image of UMMF with ultrafine grained intergrowth of forsteritic olivine (dark grey) and enstatitic pyroxene (medium grey). Porous texture is clearly seen.

Results: In ancient (~3.8-3.5 Ga) regolith breccias 60016, 60019, 61135, 66035 we have identified a suite of ultra-magnesian mafic fragments (UMMFs). These fragments contribute 0.02 to 0.25 % to the surface area of the fine fraction (<2 mm) regolith component in each thin section.

The UMMFS have different textures: (1) Microcrystalline fragments are formed of forsteritic olivine grains (Fo_{95-98} Fig. 2a), sometimes enclosing near end-member enstatitic pyroxene ($En_{90-96}Fs_2Wo_{2-8}$). MnO concentrations in the forsteritic olivine are variable, with FeO/MnO ratios of 40-70 in some grains and up to 122-190 in others (Fig. 2a). The clasts sometimes also contain small (<5 μm) irregular interstitial phases (glass?), including an Al, Ca, Na, P and K component. (2) Cryptocrystalline fragments are fine grained clasts consisting of intergrowths between forsteritic olivines and enstatitic pyroxenes (<3 μm too fine grained to be compositionally determined by EMP). They are frequently porous, with small (<5 μm) pores often aligned throughout a fragment to give a mottled texture (Fig. 1). They also include microcrsyts (<1 μm) of an Al-richer phase (Fig. 1). (3) Barred fragments and (4) amorphous fragments exhibit poor or no crystal habit, and are formed of material with a composition intermediate to magnesian olivine and pyroxenes.

Interpretation: The olivine and pyroxene phases in the UMMFs are more magnesian than any lunar indigenous mafic minerals previously analysed (Mg-Suite lithologies typically have olivine with Fo_{80-93}, whilst some are magnesian dunites that extend those compositions to Fo_{95} [8]: Fig. 2a). The mafic phases are also compositionally distinct from experimentally produced and theoretically calculated minerals from the early mantle cumulates of the lunar magma ocean [9,10]. The bulk composition of all of the UMMFS are highly magnesian (bulk Mg# 93-99: Fig. 2b) compared with known lunar rocktypes (Fig. 2).

The bulk composition and olivine compositions of the UMMFS are as magnesian (Fig. 2a) as chondrules [11] and chondrule olivines from carbonacous chondrite groups. This compositional evidence suggests that the UMMF are non-lunar, and possibly originate from a primitive chondritic meteoritic source. In comparison with primitive carbonaceous chondrite chondrules [11], the UMMFs have similar Al_2O_3, Na_2O and Mg# compositions, but lower Cr_2O_3 and MnO (higher FeO/MnO ratios: Fig. 2b), and are typically TiO_2-richer.

Summary: In ancient (~3.8-3.4 Ga) regolith breccias 60016, 60019, 61135 and 66035 we have identified a suite of ultra-magnesian fragments that are consistent with material delivered to the Moon by primitive (carbonaceous) projectiles during the last stages of the basin-forming epoch.

Our investigation demonstrates how detailed analytical studies can be employed to search the lunar regolith for meteoritic material; helping to address several key scientific objectives for the exploration of the Moon [1].

References: [1] NRC (2007) The Scientific Context for the Exploration of the Moon. ISBN: 0-309-10920-5, [2] Zolensky M.E.(1996) *Meteoritics and Planetary Science* 32, 15-18 [3] Rubin A.E. (1997) *Meteoritics and Planetary Science* 32, 135-141 [4] McKay D. S. et al. (1985) *JGR, 91,* D277–303 [5] Eugster O. et al. (2001) *Meteoritics and Planetary Science* 36, 1097-1115. [6] Joy K. H. et al. (In Press) *Geochimica et Cosmochimica Acta.* [7] Joy K.H. et al. (2011) LEAG 2011 Abstract #2007. [8] Papike J. J. et al. (1998) Planetary Materials. *Reviews in Mineralogy 36.* [9] Elardo S. M. et al. (2011) *Geochimica et Cosmochimica Acta* 75 (2011) 3024–3045 [10] Longhi J. (2010) *Geochimica et Cosmochimica Acta 74,* 784-798. [11] Hazel D. C. and Palme H. (2010) *Earth and Planetary Science Letters* 294, 85–93 [12] Jones R. H. (1990) *Geochimica et Cosmochimica Acta,* 54, 1785-1802. [13] Warren P. H., and Wasson J. T. (1979) *LPS X*, 583-610.

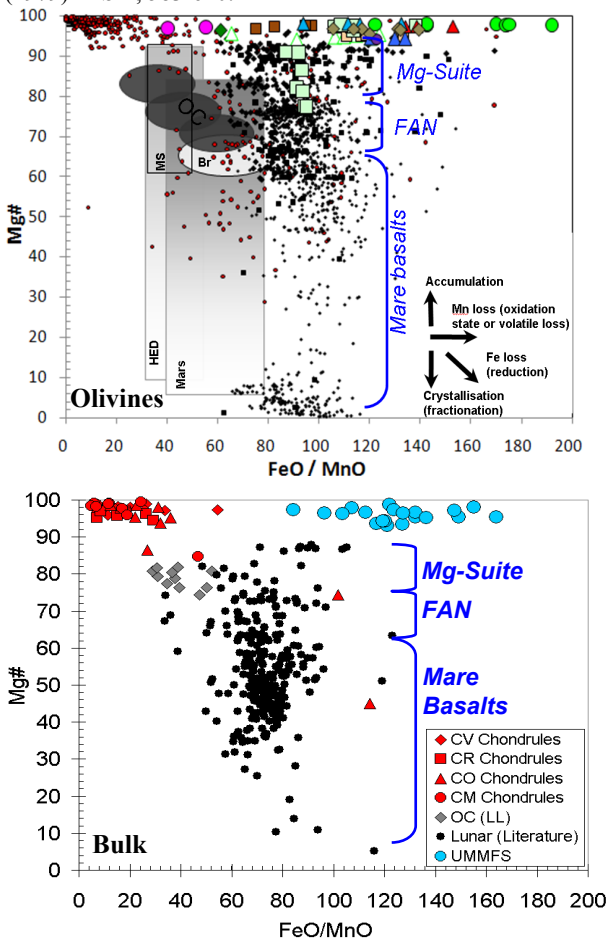

Figure 2. (a) Top: Olivine compositions in UMMFS analysed in our study (large coloured symbols) compared with lunar olivines (black symbols), carbonaceous chondrite olivines (small red symbols) and other groups of meteorites (martian, HED, mesosiderite, ordinary chondrite and bracinite). Data compiled from many sources. (b) Lower: Average bulk composition of UMMF fragments in 60016,83, 60016,93, 60016,95, 60019,176, 61135,36 and 66035,13 compared with lunar bulk rock compositions (taken from various literature sources) where the main lunar rock suites are shown,

RECONNAISSANCE ELEMENT MAPPING OF LUNAR REGOLITH BRECCIAS. K. H. Joy[1,2], D. K. Ross[3,4], M. E. Zolensky[2,3], D. A. Kring[1,2]. [1]CLSE, LPI/USRA, 3600 Bay Area Blvd., Houston, Texas 77058, USA (joy@lpi.usra.edu). [2]NASA Lunar Science Institute. [3]ARES, NASA Johnson Space Center, Houston, TX 77058, USA. [4]ESCG-Jacobs Technology, 2224 Bay Area Blvd. Houston TX 77058, USA.

Introduction: The lunar surface is covered with a regolith produced by impact comminution of underlying rock [1,2]. This boundary layer with space preserves a record both of the Moon's geological history and its collisional evolution with impacting asteroids and comets (*e.g.,* [3]). Regolith breccias are lithified samples of regolith that has been fused together by impact shock and thermal metamorphism. These complex samples, and the rock fragments they contain, can be used to investigate a range of geological processes.

We are studying Apollo and lunar meteorite regolith breccias. These samples include the Apollo 16 regolith breccias that formed across 4 billion years of lunar history [4,5]. We have also been studying the Dhofar 925 and 961 stones that have been postulated to originate from the South Pole-Aitken Basin [6].

With these samples we aim to (1) identify and classify meteorite fragments to temporally constrain the sources of projectiles hitting the Moon, with the aim to better understand the lunar impact record and provide constraints for models of Solar System evolution; (2) identify phases in impact melts and melt breccias that can be age dated using *in situ* U-Pb age dating techniques, with the aim to investigate the lunar impact flux; (3) Petrographically characterise the samples, and identify unusual or unique lunar rock types to constrain the heterogeneity and geological history of the lunar crust.

We have employed innovative analytical element mapping techniques to chemically fingerprint rock-types and phases of interest.

Method: We studied 30 µm thin sections of several Apollo 16 regolith breccia samples, and 100 µm thick sections of the Dhofar 925 and 961 stones. Each section was carbon coated and mapped completely, or in part, using the NASA JSC JEOL 7600f Field Emission Gun Scanning Electron Microscope (FEG-SEM) using a beam current of 15 nA, and an accelerating voltage of 25 to 30 nA. Our instrument has a faraday cup, so we can set the sample current at a known value, and check at the end of runs to gauge beam stability.

Images were collected at a magnification of ×150. The system was coupled to a Thermo Scientific EDS (electron dispersive spectrometer) with NSS software to derive <1 µm per pixel back-scatter electron (BSE) images (Fig. 1b) and spatially resolved element data (~2-3 µm per pixel). Each pixel of data that is collected retains a complete 0-20 KeV energy spectrum and, therefore, we were able to extract maps of C, O, Na, Mg, Al, Si, P, S, Cl, K, Ca, Ti, Cr, Mn, Fe, Co and Ni data.

Element distribution and concentration maps were then processed using the ImageJ software package to normalise each element to the same brightness scale, assign each element a colour, and recombine the colourised images to make qualitative false-colour element maps. These typically have large file sizes on the order of 10s to 100s mb of data, and contain a wealth of compositional information.

Identification of lunar lithologies and meteorite fragments: To investigate the distribution of rock-forming elements we use a colour scheme where Mg=green, Al=white, Si=blue, K=cyan, Ca = yellow, Ti = pink and Fe = red (modified from [7-10]). This colour scheme (Fig. 1c) is useful for initial reconnaissance petrographic characterisation and rapid identification of different lunar rock types: for example, (i) evolved lithologies, like granites, stand out in blue and cyan colours; (ii) lunar Mg-Suite lithologies (dunites, troctolites etc.) and magnesian (primitive) projectile fragments appear in green colours; (iii) mare basaltic material appears in red, purple and pink colours, (iv) lunar and meteoritic metal and sulphides appear bright red; (v) anorthositic fragments are dominated by white; (vi) impact melt breccias, which are composed of a mixture of mineral and glass phases, typically range from greenish-white to reddish white.

Identification of mineral phases suitable for in situ dating: To locate phases of interest for U-Pb dating studies (*i.e.,* phosphate and Zr-rich phases), we used a colour scheme of P = green, Ca = blue and Fe = red. These three elements were selected because there are EDS peak overlaps between P (K-α 2.015 keV), Zr (L-α 2.042 keV) and S (K-α 2.308 keV) that make it challenging to distinguish between phosphate, Zr-bearing, and sulphide phases. In this colour scheme, however, phosphate minerals will appear cyan as they contain P and Ca; sulphide minerals will appear yellow as they contain S and Fe; and zircon will appear green as it is not associated with either Ca or Fe (Fig. 1d).

Summary: These element maps are a valuable time-saving resource when studying complex brecciated samples. Examples are shown in Figure 1. We study these maps in detail and combine these data with optical and BSE images, electron microprobe and ion microprobe studies. So far we have used these techniques to identify potential extralunar material in

Apollo 16 regolith breccias [11], and characterise the petrography of lunar meteorites Dhofar 925 and 961 [12]; locating apatites, merrillites and zircons for U-Pb age dating (analysis in progress).

When we have finished studying the Apollo samples, we plan to make these element maps available to other lunar researchers who may be interested in investigating a particular phase or clast type to address their own lunar science goals. The maps will be a data resource that can be mined repeatedly to reveal new insights about the geological history of the Moon.

References: [1] Hörz F. et al. (1991) Chapter 4. *The Lunar Sourcebook.* pp. 61-120. [2] McKay D. D. et al. (1991) Chapter 7. *The Lunar Sourcebook.* pp. 265-356. [3] Lucey P. et al. (2006) Chapter 2. *Reviews in Mineralogy & Geochemistry*. 60, 83-219. [4] McKay D. D. et al. (1986) *LPS XVI*, D277-D30.3 [5] Joy K. H. et al. (In Press) *Geochimica et Cosmochimica Acta.* [6] Jolliff B. A. et al. (2008) *LPS XXXIX,* Abstract #2519. [7] Joy K. H. et al. (2008) *Geochimica et Cosmochimica Acta.* 72, 3822 - 3844 [8] Joy K. H. et al. (2011) *Geochimica et Cosmochimica Acta.* 75, 2420-2452. [9] Kearsley A. T. et al. *74th Annual Meeting of the Meteoritical Society*, Abstract #5280. [10] Snape et al. (2011) *Meteoritics and Planetary Science* doi: 10.1111/j.1945-5100.2011.01230.x. [11] Joy K. H. et al. (2011) *LPS XXII*, Abstract #2103. [12] Joy K. H. et al. (2011) *74th Annual Meeting of the Meteoritical Society*, Abstract #5100.

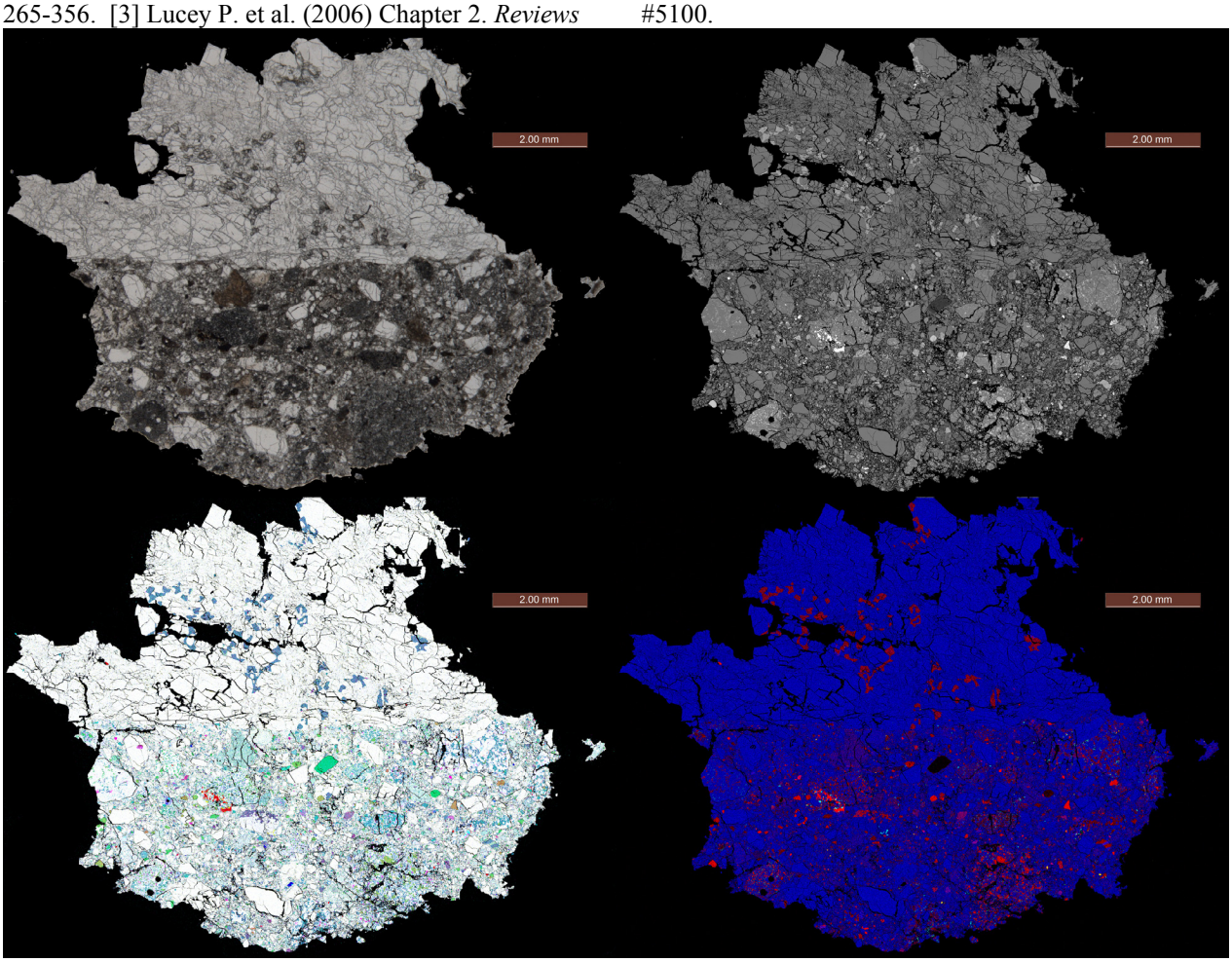

Figure 1. Surface area maps of Apollo 16 regolith breccia 66035,13. The sample is composed of a large ferroan anorthosite clast (top of sample) and a regolith breccia portion (base) of sample with many clasts including impact melts, mineral fragments and igneous lithics. (a) Top left: Optical image scan of the thick section surface. (b) Top right: Montaged area back scatter electron map. (c) Lower left: False colour element map where Al=white, Ca=yellow, Fe=red, Si=blue, Mg=green, Ti = pink and K=cyan (see text for details). The large bright green clast in this image is an ultra-mafic magnesian fragment (UMMF [11]), which is potentially non-lunar (primitive asteroid debris) in origin) (d) Lower right: False colour element map where Ca=blue, Fe=red and P=green. Apatites appear cyan colour, zircons green colour and sulphides are yellow (see text for details). Small apatite grains can be seen to a clast to the lower left of the sample centre.

DEVELOPING AN INTEGRATED, MULTI-INSTITUTIONAL APPROACH FOR STUDIES OF FUNDAMENTAL PLANETARY PROCESSES ON THE MOON: THE GIANT IMPACT, LUNAR MAGMA OCEAN, AND LUNAR CATACLYSM HYPOTHESES. David A. Kring[1] and the Center for Lunar Science and Exploration Team, [1]Lunar and Planetary Institute, Universities Space Research Association, 3600 Bay Area Blvd., Houston, TX 77058 (kring@lpi.usra.edu).

Introduction: The LPI-JSC Center for Lunar Science and Exploration, along with its collaborators at the University of Arizona, University of Houston, University of Maryland, University of Notre Dame, Rice University, and its international partners, is a founding member of the NASA Lunar Science Institute (NLSI). The NLSI has created an opportunity for the Center to (i) develop a core, multi-institutional lunar science program that addresses the highest science priorities identified by the National Research Council for NASA (2007); (ii) provide scientific and technical expertise to NASA that will infuse its lunar research programs, including developing investigations that influence current and future space missions; (iii) support the development of a lunar science community that both captures the surviving Apollo experience and trains the next generation of lunar science researchers; and (iv) to use that core lunar science to develop education and public outreach programs that will energize and capture the imagination of K-14 audiences and the general public.

Science Objectives: At the core of the Center's activities is a series of studies to test the giant impact hypothesis for the Moon's origin; the lunar magma ocean hypothesis and its implications for differentiation of all terrestrial planets; and the lunar cataclysm hypothesis, which has become a critical measure of events involved in the accretion and orbital evolution of planetary bodies in both the inner and outer solar system. To illustrate our integrated approach, we outline here a subset of the results obtained thus far regarding our investigation of the earliest collisions to have affected the Moon.

We begin with the discovery of a surviving fragment of a collision among planetesimals that occurred during the accretion of Earth and prior to the origin of the Moon [e.g., 1]. After the Moon accreted, collisions continued to modify its crust and upper mantle. Hydrocode modeling of the formation of the oldest and largest basin on the Moon, the South Pole-Aitken Basin, indicates a significant amount of mantle material was melted and incorporated into a central melt zone [2], thus providing a compositional parameter for the identification of impact melts associated with that event and its age. Similar modeling of other basins is underway [3], which is providing the input needed to evaluate post-basin evolution of the lunar crust [e.g., 4]. Interestingly, the integration of hydrocode and thermal evolution models can test the cadence of impacts during the basin-forming epoch while also providing new tools for evaluating lunar topography and gravity and their implications for the evolution of the lunar crust. We have found that basins may have influenced stresses in the lithosphere and the eventual eruption of basalts on the lunar surface [5]. In parallel, we are testing models of basin-formation, with a specific structural study of the Orientale Basin, which is the youngest and best preserved basin on the Moon. That study suggests the formation of the outer rings of the basin formed along normal faults [6] and, thus, in a manner similar to that seen at the Chicxulub impact crater on Earth.

During the basin-forming epoch, the Moon's crust and upper mantle were repeatedly affected by impacting asteroids and, to a lesser extent, comets [e.g., 7, 8]. We had previously developed a tool to evaluate the sources of projectiles using the size distribution of lunar craters [8]. We used that tool to probe the most ancient lunar terrains in more detail and discovered a shift in the size distribution of craters that implies a shift in the impact velocities of impacting asteroids [9]. At some point between the formation of the South Pole-Aitken and Nectaris basins, impact velocities appear to have roughly doubled. This is consistent with a shift in the orbits of Jupiter and other outer solar system planets that has previously been implied [e.g., 10, 8]. It is also consistent with the Apollo-era view that all Nectarian and Early Imbrian basins were produced during a cataclysmic surge of impactors. It also implies, however, that some of the pre-Nectarian basins, including the South Pole-Aitken Basin, were produced independently through other collisional mechanisms.

We are continuing to probe the source of debris hitting the Moon during the basin-forming epoch and compare it to more recent times using newly developed techniques to measure highly siderophile elements and Os-isotopes. Applying that approach to mantle-derived samples has revealed new evidence [11] of the late accretion of siderophiles to the Earth-Moon system. Applying that approach to individual Apollo impact melt samples has also been used to detect the chemical signatures of the impactors in specific impact events [12, 13]. While some of the impact melts con-

tain the remnants of known meteoritic sources, others contain the remnants of projectiles that are not represented in the current inventory of meteorite analogues, although they still seem to have an asteroidal, rather than cometary, origin.

The lunar regolith contains a complementary record of impacting debris and has the potential of revealing how that flux of material has changed with time. Thus, we began an examination of ancient regolith breccias from the Apollo 16 landing site and recalibrated an existing technique for determining their ages [14]. We then studied a subset of the breccias for remnant impactors. In a series of exciting discoveries [e.g., 15; and this conference), relic grains of impactors have been found in breccias ranging from 3.8 to 3.4 Ga, spanning the final phase of the basin-forming epoch. These impactor relics confirm a contribution of chondritic material to the Moon, although, interestingly, it has affinities to carbonaceous chondrites rather than ordinary and enstatite chondrites.

We also continue to test the lunar cataclysm hypothesis with a series of geochronologic studies of lunar samples. This includes traditional Ar-Ar analyses [e.g., 16] and the development and application of detailed U-Pb analyses of single zircon crystals and associated phosphates in impact melt breccias and related impact lithologies [e.g., 17, 18].

It is critical for those geochronologic studies to be integrated with updated geologic assessments of the Apollo landing sites and the geologic context of the samples. In a new photogeologic assessment of the Apollo 17 landing site on the margin of the Serenitatis Basin, significant deposits of Imbrium ejecta have been mapped [19]. Thus, we are now sorting through the chemistry and ages of impact melts from the Apollo 17 site to determine which are associated with Imbrium and which are associated with Serenitatis.

Crucial to the success of our assessment of the early collisional evolution of the Earth-Moon system has been the multi-disciplinary and multi-institutional integration that a program like NLSI can produce. That program also provides a platform for integrating lunar science with exploration.

Exploration Objectives: As the community develops the architecture and hardware to return to the lunar surface, our team has developed a series of studies to determine where on the lunar surface the NRC's highest science objectives can be achieved. For example, we have determined that one of the best sites for testing the lunar cataclysm hypothesis is Schrödinger Basin [e.g., 20, 21]. At that one locality, we should be able to determine the age of the oldest basin (South Pole-Aitken) and that of the second youngest (Schrödinger), thus bracketing nearly the entire basin-forming epoch. Interestingly, Schrödinger also contains volcanic deposits of Eratosthenian and Copernican age, thus providing two additional benchmarks in the evolutionary stratigraphy of the Moon. Because the collection of impact melts during and after the basin-forming epoch will be needed to evaluate the collisional flux throughout lunar history, we are also mapping the locations where those impact melts are accessible to robotic and human exploration assets [e.g., 22].

Training Objectives: Our Center and the NLSI are committed to developing a healthy lunar science community. For that reason, our Center sponsors the (a) Lunar Exploration Summer Intern Program, which provides an opportunity for teams of students to identify lunar landing sites where the NRC (2007) objectives can be accomplished; the (b) Field Training and Research Program at Meteor Crater, which provides an opportunity for students to study impact cratering processes and how they modified the Moon; and (c) the development of material that teachers and university faculty anywhere in the world can use to incorporate lunar science into their classrooms. The latter material is accessible through the Lunar Science and Exploration portal (http://www.lpi.usra.edu/lunar/) and the Center's web site http://www.lpi.usra.edu/nlsi/.

Acknowledgements: I thank the Chair of LEAG, Dr. Charles Shearer, for inviting this summary. I also thank the entire Center's team for its contributions to a re-invigorated lunar program. A complete list of the researchers, teachers, and students involved in the Center is posted at http://www.lpi.usra.edu/nlsi/teamMembers/.

References: [1] Weirich J. R. et al. (2010) *Meteoritics & Planet. Sci., 45,* 1868–1888. [2] Potter R.W.K. et al. (2010) *LPS XXXXI,* Abstract #1700. [3] Potter R.W.K. et al. (2010) *LPS XXXXII,* Abstract #1452. [4] Kiefer W. S. et al. (2011) *LPS XXXXII,* Abstract #2349. [5] McGovern P. J. and Litherland M. M. (2011) *LPS XXXXII,* Abstract #2587. [6] Nahm A. L. and Kring D. A. (2011) *LPS XXXXII,* Abstract #1172. [7] Kring D. A. and Cohen B. A. (2002) *JGR, 107,* doi: 10.1029/2001JE001529. [8] Strom R. G. et al. (2005) *Science, 309,* 1847–1850. [9] Marchi S. et al. (2011) *LPS XXXXII,* Abstract #1192. [10] Gomes R. et al. (2005) *Nature, 435,* 466. [11] Bottke W. F. et al. (2010) Science, 330, 1527–1530. [12] Puchtel I. S. et al. (2008) *GCA, 72,* 3022–3042. [13] Galenas M. G. et al. (2011) *LPS XXXXII,* Abstract #1413. [14] Joy K. et al. (in press) *GCA.* [15] Joy K. (2011) *LPS XXXXII,* Abstract #2103. [16] Norman M. D. et al. (2009) *GCA, 74,* 763–783. [17] Nemchin A. A. et al. (2009) *Meteoritics & Planet. Sci., 11,* 1717–1734. [18] Grange M.L. et al. (2011) *GCA, 75,* 2213–2232. [19] Spudis P. D. et al. (2011) *LPS XXXXII,* Abstract #1365. [20] O'Sullivan K. M. et al. (2011) *GSA Special Paper, 477,* 117–128. [21] Kramer G. Y. et al. (2011) *LPS XXXXII,* Abstract #1545. [22] Öhman T. and Kring D. A. (2011) *LPS XXXXII,* Abstract #1177.

ON-ORBIT CONTROL OF LUNAR SURFACE TELEROBOTS FROM EARTH-MOON LAGRANGE POINTS. D. F. Lester[1], K. V. Hodges[2], and M. L. Raftery[3] [1]Dept. of Astronomy, University of Texas, Austin TX 78712 (dfl@astro.as.utexas.edu), [2]School of Earth and Space Exploration, Arizona State University, Tempe AZ 85287 (kvhodges@asu.edu), [3]Boeing Space Exploration Division, League City TX 77573 (michael.l.raftery@boeing.com).

Introduction: We propose a novel approach to operation of future lunar surface telerobots at least as a precursor to return of humans to the lunar surface. This approach builds on current interest in the human space flight community (e.g. HDU/DSH, HEFT, HAT) for a habitat facility at an Earth-Moon Lagrange point (EM L1 or L2), perhaps in the very near-term, and ideally using technologies validated on the International Space Station [1].

The Latency Advantage: These locations, about 50000-60000 km over the near- and far-sides of the Moon, provide light-time two-way control latencies to the lunar surface of order 400 ms, *six times smaller than the control latency from the Earth*. Such small latencies allow for near-telepresence in command and control of surface assets. This allows for a high degree of cognitive coupling with lunar surface activities and likely enables complex tasks that would otherwise require in situ humans [2]. The approach has potential value for lunar science, resource assessment, and site development. In the former case, with an appropriately capable telerobot, an astronaut-scientist at EM L1/2 could do high-productivity field geology without actually being on the surface, where he or she would be operationally limited by a constraining space suit. While some of this work could be done from a Multi-purpose Crew Vehicle (MPCV) crew transport, we consider a long-duration habitat as offering more potential for longer-duration exploration sorties by the telerobot.

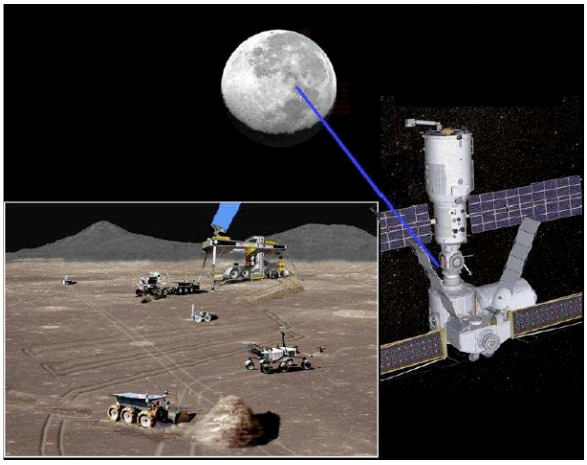

EM L1 and L2 as Enabling Destinations for Lunar Science: Such an L1/L2 habitat promises many advantages as a base station for science operations on the lunar surface. For projects that require long-distance or long-duration surface operations, such habitats can also be used as depot facilities, with equal opportunity access to and from anywhere on the lunar surface. Many exploration architectures have envisioned EM L1/2 as "high-camps" for human travels to the lunar surface, where reusable landers could be based on-orbit. These locations offer significant advantages for travels outside of cis-lunar space as well. Both because of the "interplanetary superhighway" that connects such solar system Lagrange points with economical trajectories, and the prospect of using lunar ISRU for such deep space travels, EM L1 and L2 have been proposed as jumping off points for voyages to Mars and beyond [3], [4]. These same economical trajectories connect these Earth-Moon Lagrange points with much more distant Earth-Sun Lagrange points that are of increasing value to astronomy and heliophysics. Servicing of science spacecraft that normally operate at those much further locations can thus be achieved at a more convenient job-site in the Earth-Moon system.

Orbital Trades: Orbits around EM L1 and L2 are optimal for such telerobotic control operations. While low lunar orbits offer smaller time delays, those orbits are not highly stable, and even in stability optimized orbits (e.g., for LRO), a habitat would require several hundred m/s of propulsion per year for stationkeeping. In such orbits, target sites would regularly rise and set, such that telerobotic control would be frequently be asynchronous. In both of these respects, EM L1/ L2 orbits provide distinct advantages. Stationkeeping strategies for such orbits require only about 100 m/s/yr propulsion, and much of one entire lunar hemisphere is continuously in the line-of-sight. This would offer telerobotic control to sunlit sites on the lunar surface at all times [5]. The recently successful Artemis mission demonstrates that orbital maintenance at these Lagrange points is straightforward. A habitat at EM L1/2 is in almost continuous sunlight, greatly simplifying power management and, even for EM L2 over the far-side, a halo orbit can assure continuous communication line-of-sight with the Earth. It should be understood that shifting the habitat between EM L1 (for near side access) and L2 (for far-side access) is a relatively low propulsion proposition, as shown with Artemis. Thus, the same habitat could be used for tasks on different sides at different times.

Low Latency Functionality: Controlling a rover that has more dexterous capabilities – and more intuitive user interfaces – than current robotic reconnaissance rover designs, astronauts at EM L1/2 could approach complicated lunar surface tasks with a much higher degree of cognition, awareness, and control than could operators on the Earth. Low-latency teleoperations with cutting-edge technologies could revolutionize our approach to lunar field geology, providing virtual experiences that closely approximate "boots on the ground" field geology while retiring considerable human risk that would normally accompany astronaut sorties. As we invent a new era of planetary field geology that involve coordinated astronaut and robotic activities [6], telepresence could play an important role in the development of sustainable, multi-year research programs on the lunar surface.

Heritage and Extensibility: Terrestrial commercial telerobots are in rapidly increasing use for mining and undersea science, as well as for oil/gas and cable operations. Transcontinental surgery, and military surveillance and munitions (drones) as well. These all use control latencies of a few hundred milliseconds, so on-orbit telerobotic control can take advantage of terrestrial technology investment and operations expertise. On-orbit telerobotic control is also highly extensible, offering huge advantages in latency mitigation to work in other settings, such as Martian moons, asteroids, Mars (e.g. Human Exploration using Real-time Robotic Operations - HERRO [7]), and even at exploration destinations that pose special environmental risks for human exploration (e.g. Venus). Of course, such telerobotic control is also of high value in minimizing the need for EVA for near Earth asteroid visits, and for servicing/depoting/construction projects in the locale of the habitat itself. In many respects, on-orbit control of surface telerobots is not much different from local control of those robots from a surface habitat.

Telerobotic capability has been identified as an important policy mandate, and telepresence capabilities are considered by the agency to be one of several "grand challenges" for space technology [8]. We invite the lunar science community to consider the priority scientific tasks that such on-orbit operations might enable. While human visits to the lunar surface provide optimal opportunities for field geologic research, on-orbit telerobotics may provide attractive alternatives at lower cost and with less human risk in the short term. Telerobotic geology of this sort would be especially valuable precursor activities in advance of human exploration campaigns.

References: [1] Lester, D. and Thronson, H. 116-RSA-7, AIAA Space 2011 Conference. [2] Lester, D., and Thronson, H. 2011, *Space Policy 27, 89-93.* [3] Decadal Planning Team archives, http://history.nasa.gov/DPT/DPT.htm, [4] Lo, M. and Ross, S. AIAA Space 2001 Conference. [5] Farquhar, R. 1972, *Astronautics & Aeronautics* 10, 59–63. [6] Hodges, K.V. and Schmitt, H.H. in press, Geological Society of America Special Paper 483 "Analogs for Planetary Exploration". [7] Schmidt, G., Landis, G., Oleson, S., Borowski, S., and Krasowski, M., AIAA-2010-0629, AIAA Aerospace Sciences Meeting. [8] http://www.nasa.gov/pdf/503466main_space_tech_grand_challenges_12_02_10.pdf.

LUNAR ASTRONAUT NAVIGATION USING LASOIS: PERFORMANCE OF A SIMULATED APOLLO-14 TRAVERSE AT HALEAKALA NATIONAL PARK, HAWAII

R. Li[1], S. He[1], B. Skopljak[1], X. Meng[1], A. Yilmaz[2], J. Jiang[2], M. S. Banks[3], S. Kim[3], C. Oman[4]. [1]Mapping and GIS Laboratory, CEEGS, The Ohio State University, 470 Hitchcock Hall, 2070 Neil Avenue, Columbus, OH 43210-1275, li.282@osu.edu; [2]Photogrammetric Computer Vision Laboratory, CEEGS, The Ohio State University; [3]Visual Space Perception Laboratory, University of California Berkeley; [4]Man Vehicle Laboratory, Massachusetts Institute of Technology.

Introduction: The different environmental conditions found on the moon can significantly affect spatial orientation as experienced by landed lunar astronauts. During the Apollo 14 mission, astronauts successfully completed a traverse of about 1.4 km. However, disorientation due to a lack of spatial cues, altered gravity, and other factors prevented them from reaching their goal, Cone Crater, before they had to return to base to prevent their resources from running out [1, 2]. To help overcome these challenges on the lunar surface an astronaut navigation system, the Lunar Astronaut Spatial and Orientation Information System (LASOIS), has been designed and implemented to incorporate data from lunar orbital, ground, and suit-mounted (on-suit) sensors. This system has been tested multiple times in lunar-like environments, most lately at Haleakala National Park, Hawaii.

Methodology:

Components of LASOIS. The LASOIS system includes hardware for data acquisition along with software for the integration of multiple algorithms for data processing, integration, and display [3]. Orbital sensors incorporated into the network include the LROC (Lunar Reconnaissance Orbiter Camera) and the LOLA (Lunar Orbiter Laser Altimeter) altimeter. Sensors mounted on the astronaut suit include an IMU (Inertial Measurement Unit) mounted on one boot heel (right or left), a step sensor mounted on the bottom of the same boot, and a stereovision system (a pair of digital imagers) mounted on the chest (see Figure 1). The integrated IMU and step sensor data captures the distance of each astronaut stride, and 3D attitude. By tracking and matching ground features on the lunar surface, data from the stereovision system provides heading as well as positioning information.

Localization at the beginning of an Extra-Vehicular Activity (EVA) traverse. A panorama is taken at the beginning of an EVA traverse. Landmark matching (or DEM matching) is employed to register the panorama to orbital data [3] based on terrain features surrounding the starting point. Position and orientation are calculated from the computation of rotation and translation between the panorama and the orbital images through the landmarks (or DEMs).

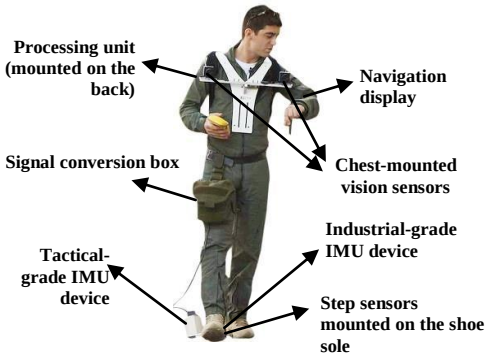

Figure 1. Suit-mounted sensors.

Continuous localization on an EVA traverse. During the EVA traverse, an Extended Kalman Filter is used to integrate signals from the IMU, the step sensor and the stereovision imagers in order to obtain in real time the changing positions and orientations of an astronaut. A boot-mounted IMU measures acceleration and the angular rate of change of the heel of the astronaut at a high frequency (up to 100 Hz). The step sensor records periods when the astronaut boot is not moving (a zero velocity phase). An algorithm of zero velocity updates (ZUPTs) is used to remove bias in the IMU whenever the step sensor detects a zero velocity phase for the astronaut. As a result, velocity and distance can be accurately reconstructed. Since the stereovision imagers usually provide better heading determination data, they can be used to further compensate for any bias in the heading direction found in the IMU signal. After sensor integration, astronauts can retrieve precise localization information concerning spatial position and orientation from a wrist-mounted interface display.

Figure 2. Designed Traverse in Experiment

Experimental Design: In the Apollo 14 mission, one of the important scientific target was Cone Crater, which was 340 m in diameter. The two astronauts had to walk approximately 1.4 km northeast of the landing spot in one and half hours while relying on a map and their own experience to locate this target of interest [2].

A traverse was designed for the field test at Haleakala National Park to simulate this Apollo 14 EVA traverse and to test the developed system. This simulated traverse is illustrated in Figure 2 as a white line. The human subject started at point A, then headed toward a crater named Halali'i that was 2 km to the northeast of the starting point. A looped traverse was performed after reaching Halali'i. The subject walked back to the starting point A. The distance of the round trip was 6.1 km.

During this traverse, the human subject was able to obtain real-time position information through the system's wrist-mounted display. It took 6500 seconds to finish the 6 km traverse at an average speed of 1 m/s. Along the traverse, 7800 images were taken. The sampling frequency of the IMU was 100 Hz.

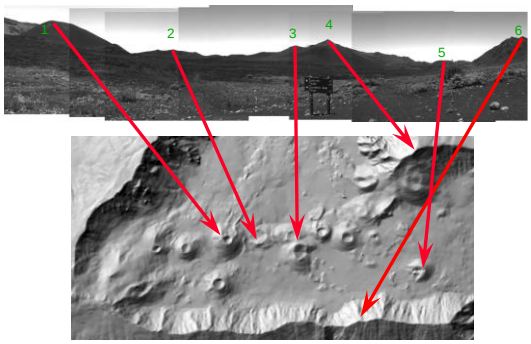

Figure 3. Landmarks matched on the panorama and the DEM.

Experimental Results and Conclusions: Six significant landmarks were selected on the images obtained by the chest-mounted vision system and registered with landmarks found on the global DEM derived from orbital data (See Figure 3). Localization accuracy at the starting point through this orbit-ground matching technique was 21 m. The traverse reconstructed by the LASOIS on-suit sensors is displayed as a blue line in Figure 4, compared with the ground truth obtained by GPS (red line). The LASOIS-derived end point of the traverse deviated from the starting point (A in Figure 2) of the ground truth by 150 m, making a disclosure error of

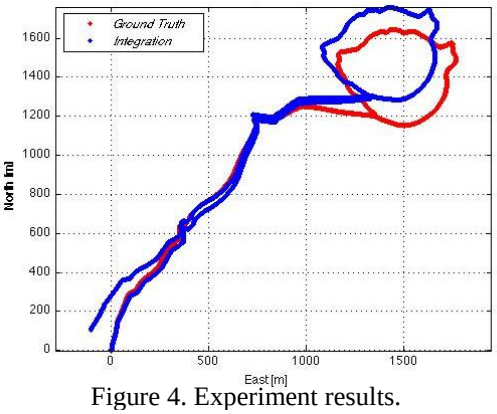

Figure 4. Experiment results.

2.42% over 6.1 km. The maximum error of 200 m was found in about half way, about 3 km from the starting point. We conclude that LASOIS is capable of providing precise navigation information to enable lunar astronauts to safely navigate on the lunar surface, locate science targets, and return safely to the lander or vehicle.

References: [1] Jones E.M. (1995) Apollo 14 Lunar Surface Journal, http://www.hq.nasa.gov/alsj/a14/a14j.html. [2] Manned Spacecraft Center, (1971). Apollo 14 Mission Report. http://www.hq.nasa.gov/alsj/a14/A14MRntrs.pdf. [3] Li R. et al. (2011) LPSC, Abstract #2100.

Acknowledgements: This research has been supported by the National Space Biomedical Research Institute through NASA NCC 9-5.

Recent Progress in Lunar Topographic Mapping using OrbiterMapper and LROC NAC Stereo Images. Ron Li[1], Liwen Lin[1], Wei Wang[1], Justin Crawford[1], Xuelian Meng[1], Shaojun He[1], Mark Robinson[2], and the LROC Science Team. [1]Mapping and GIS Laboratory, CEEGS, The Ohio State University, 470 Hitchcock Hall, 2070 Neil Avenue, Columbus, OH 43210-1275, [li.282, lin.1128]@osu.edu. [2]Arizona State University.

Introduction: As one of seven remote-sensing instruments carried onboard the Lunar Reconnaissance Orbiter (LRO), the Lunar Reconnaissance Orbiter Camera (LROC) system has two NAC (Narrow Angle Camera) cameras that acquire high-resolution imagery for the assessment of meter-scale features on the lunar surface [1, 2]. Stereo pairs for 3D topographic mapping are formed by combining images from two or more adjacent orbits (cross-track stereo). The Ohio State University (Ohio State) has developed an OrbiterMapper software package to generate topographic products using LROC NAC data in support of the science goals of the LRO mission.

Development of OrbiterMapper: OrbiterMapper is a software application package that photogrammetrically processes lunar and Martian orbital imagery for 3D topographic generation. The entire process can be divided into two major sections: (1) image processing that primarily involves image preprocessing and a hierarchical coarse-to-fine hierarchical matching process [3] for the extraction of accurate dense matching; and (2) geometric processing that mainly includes boresight calibration and bundle adjustment to remove the geometric inconsistencies in the Exterior Orientation (EO) parameters among stereo orbits [4]. With dense matching points from image processing and bundle-adjusted EO parameters from geometric processing, highly accurate 3D terrain models can be constructed.

The current version of OrbiterMapper includes several significant improvements over previous versions. These improvements include two rounds of grid matching for more reliable matching and three-fold matching along seam lines in order to decrease seam inconsistency in the DEM overlapping area.

Two rounds of grid matching are used to overcome the problem of small artificial bumps (1 m ~ 2 m) due to mismatching. These bumps usually are located in smooth areas having steep slopes, areas that have large image distortion between stereo images caused by a large slew angles. When performing grid matching in these areas, matching points from previous levels have difficulties in providing accurate prediction of matched points for least-squares matching, which would cause mismatching and, in turn, bumps in the terrain if grid matching is performed only once. Therefore, the grid-matching step is performed twice. The result of the first round of grid matching provides information for eliminating mismatching points, consequently, is capable of offering good predictions and dense points for the second round. Figure 1 shows an example of the improvement from two rounds of grid matching on the Tsiolkovskiy Crater DEM.

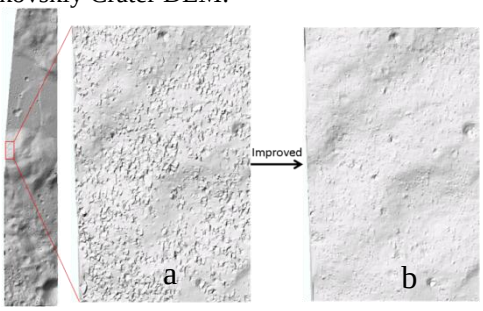

Figure 1. Tsiolkovskiy Crater DEM: a) result from 1 round of grid matching compared with b) the improvement made by 2 rounds of grid matching.

Another reason for the occurrence of small bumps on the DEM could be a narrow range of pixel values over an image area. A small range of pixel values means low contrast and obscure features in the image, which could cause a slight disturbance of accuracy in least-squares matching and, thus, lead to small artificial bumps. These artificial bumps probably would mislead scientific observations and analysis of the lunar surface. We find that performing suitable image stretching and enhancement in a local area to increase the image contrast and distinctness of features can effectively remove these artificial bumps (0.1 ~ 0.4 m). This is illustrated in Figure 2, which shows a sample region from the DEM of stereo pair images M161252379 and M161245596.

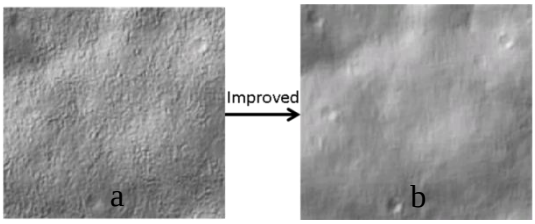

Figure 2. One Sample Region showing improvement from image stretching and enhancement for bump removal: a) before and b) after local stretching and enhancement.

Although the geometric inconsistencies among EOs of stereo orbits could be improved by geometric processing, conspicuous seam lines may exist along the DEM overlapping area of two NAC CCDs. In a previous version of OrbiterMapper, the 3D coordinates

of the points along the seam lines, like other points in the DEM, were derived through the intersection of two matching points in two-orbit images. However, the points in the seam lines can actually have triple matching points: two inter-strip points located in the overlapping area of two CCDs in one orbit, and a third one in the other orbit's CCD. If all of these three matching points can be used for intersection of the ground point, then it is possible to distribute the remaining geometric inconsistencies (about a half pixel) to several pixels across the seam line, which would lead to the further alleviation of the seam line. Figure 3 shows an example of this improvement for the Compton Crater site: an almost invisible seam line due to the employment of all three matching points.

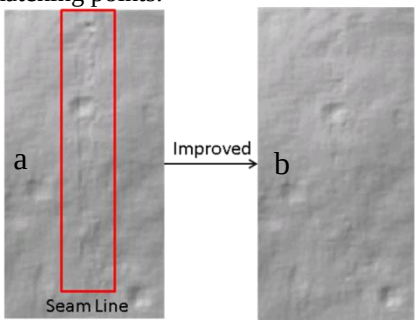

Figure 3. Example of the improvement of seam lines at the Compton Crater site: a) the original result with visible seam line, and b) improved result.

In addition to these improvements to OrbiterMapper, efforts also are being made for boresight calibration and jitter analysis. Boresight calibration is designed to obtain highly-accurate boresight parameters that describe the relative alignment between two NAC cameras [4]. Currently, we are conducting experiments using two methods for boresight calibration to improve boresight parameters. The first method is to combine the boresight calibration and bundle adjustment together to jointly solve both boresight parameters and EO polynomial parameters. The other method is to consecutively perform bundle adjustment and boresight calibration to separately compute EO polynomial parameters and boresight parameters. In addition, it has been found that some DEMs from NAC stereo imagery are subject to geometric distortions due to spacecraft jitters [3, 5, 6]. This jitter effect is represented as artificial horizontal ripples in the cross-track direction. We are currently working on detecting and modeling the jitter effect in order to eliminate artificial terrains on DEM products.

Topographic Products for Scientific Applications: Since June 2010, OrbiterMapper has been evaluated through a DEM comparison using data covering the Apollo 15 landing site and Tsiolkovskiy Crater. OrbiterMapper has been applied successfully to the generation of 3D lunar terrain for different scientific objectives. To date, we have generated topographic products for more than ten sites, including Compton, Compton-Belkovich, and King Crater. Our products have been used by LRO science team members to study the formation of lunar features such as craters and lunar lobate scarps and to analyze topographic characteristics of targets of interest. Among these products, a considerable number of requests have been for the research of lunar lobate scarps, which are relatively small-scale, discontinuous, linear or curvilinear tectonic landforms with relatively steep scarp faces. The study of lunar lobate scarps, one of the youngest landforms on the moon, can shed light on mechanical clues about the lunar regolith and lithosphere [7, 8]. Recently, we are generating a DEM product of the lobate scarps near Mandel'shtam Crater, a group of scarps that can be viewed as the surface expression of splay faults [9]. Figure 4 shows one sample region of the lobate scarps in this DEM and several elevation profiles across the scarps.

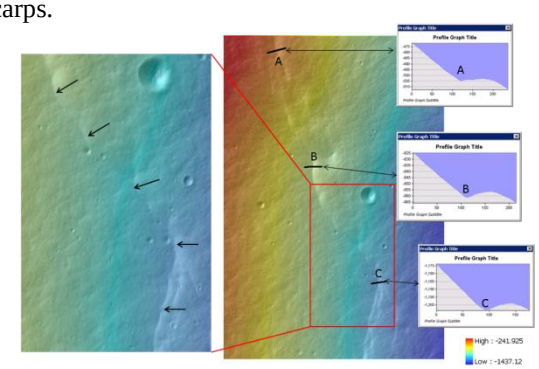

Figure 4. Lobate scarp near Mandel'shtam Crater [stereo pair: M161252379 and M161245596]. A, B, and C are 3 examples of elevation profiles across the scarps.

Acknowledgements: This research is supported by the National Aeronautics and Space Administration under Agreement No. NNX08AR29G issued through the Science Mission Directorate.

References: [1] Robinson, M. S. et al. (2005) *LPSC XXXVI*, Abstract #1576. [2] Robinson, M. S. et al. (2010) *Space Science Reviews*, 150:81-124. [3] Li, R. et al. (2011) *IEEE Transitions on Geoscience and Remote Sensing*, 49(7):2558-2572. [4] Li, R. et al. (2010) *Annual Meeting of LEAG*, Abstract #1595. [5] Mattson, S. et al. (2010) *LPSC XLI*, #1871. [6] Mattson, S. et al. (2011) *LPSC XLII*, Abstract #2756. [7] Banks, M. E. et al. (2011) *LPSC XLII*, Abstract #2779. [8] Watters, T. R. and C. L. Johnson. (2010) in Planetary Tectonics, Cambridge Univ. Press, 121-182. [9] Watters. T.R. et al. (2010) *Science*, 329(5994):936-940.

Global mapping of neutrons from the Moon by LEND instrument onboard LRO M.L. Litvak[1], I. G. Mitrofanov[1], A. B. Sanin[1], W. V. Boynton[2], G. Chin[3], J. B. Garvin[3], D. Golovin[1], G. Droege[2], L. G. Evans[4], K. Harshman[2], A.S. Kozyrev[1], A. Malakhov[1], T. McClanahan[3], G. Milikh[5], M. Mokrousov[1], R. Sagdeev[5], R. Starr[6], J. Trombka[5], [1]**Space Research Institute, RAS, Moscow, 117997, Russia, litvak@mx.iki.rssi.ru,** [2]University of Arizona, Tucson, AZ USA **,** [3]NASA Goddard Space Flight Center, Greenbelt, MD USA, [4]Computer Science Corporation, Greenbelt, MD USA, [5]University of Maryland, College Park, MD USA, [6]Catholic University, Washington DC, USA,

Introduction: The Lunar Exploaration Neutron Detector (LEND) was flown onboard Lunar Reconainsane Orbiter (LRO) to provide global mapping of Moon neutron albedo in different energy ranges and to derive the distribution of hydrogen at the polar regions of the Moon with spatial resolution ~ 10 km [1,2,3].

The observation of the neutron leakage spectrum may provide details about the Moon itself as well as about the space environment. Regional variations of neutron flux in the thermal energy range correlate with concentrations of major and minor soil forming elements (like Fe, Ti, K, Gd, Sm) having large macroscopic absorption cross sections. The intensity of epithermal (neutrons with energies from 0.4 eV up to 100 keV) neutron flux is sensitive to the abundance of hydrogen. Even a small amount (~100 ppm) of H causes significant depression of epithermal neutron flux. Fast neutrons (neutrons with energies from 100 keV up to 15 MeV) can be used to analyze the average composition of lunar regolith via correlation of intensity of fast neutron flux and average atomic mass of the lunar soil.

More than 10 years ago, the first global remote sensing observations were accomplished by Lunar Prospector Neutron Spectrometer (LPNS). LPNS was able to create global maps of lunar thermal, epithermal and fast neutrons [4,5]. LPNS revealed vast polar regions of extended neutron suppression (4-5% lower in comparison with low latitude areas) of epithermal neutrons at both the north and south poles (interpreted presumably as water ice rich areas, [6]). The best spatial resolution of LPNS (~45 km at altitude of 30 km) was too poor to resolve local areas with highest H abundance leaving open the question whether the hydrogen was uniformly distributed within extended suppression territory or localized in permanently shadowed regions. LPNS global maps of thermal and fast neutrons also have shown significant regional variations of neutron flux across the surface closely related with non-homogeneity of soil composition (caused by enhanced abundance of Fe-oxides in mares and South Polar Atkin basin, see for example [4,5]).

LEND is similar to LPNS in the global monitoring of thermal, epithermal and fast neutrons by omni-directional neutron detectors with spatial resolution strongly defined by the altitude but also having the significant additional advantage of being able to measure epithermal neutron flux with much better spatial resolution (at least 5 times better) than was done before [1,2,3]. At an altitude of 50 km LEND's resolution is comparable with the size of large Permanently Shadowed Regions (PSR) providing the possibility to reanalyze polar areas to better localize regions of neutron suppression and hydrogen abundance inside them. LEND latest observations during the more then 1 year of mapping phase allowed to create global maps of Moon neutron flux in different energy ranges with various spatial resolution.

In our analysis we have created LEND global maps showing regional variations of thermal, epithermal and fast neutron fluxes and have compared it with variances of soil elemental composition. The second task of investigation was analysis of signals from different LEND detectors to estimate amplitude of neutron signal measured by LEND collimated sensors and compare it with spacecraft background. Finally, the third task was to compare LEND global mapping with previous results accomplished by Lunar Prospector Neutron Spectrometer (LPNS).

Results: We have presented the latest results of data reduction and analysis of lunar neutron flux measured by the LEND instrument onboard LRO mission. Three energy ranges, thermal (<0.015 eV), epithermal (0.4-100 eV) and fast (>0.7 MeV) have been studied in our analysis.

The largest regional variations of factors of 3-4 are seen in the LEND thermal neutrons map between the mare basaltic terrains on the nearside and highlands on the farside of the Moon. This coincides with results from LPNS data analysis and is explained by significantly higher abundance of iron within the maria (Figure 1).

The variation of epithermal neutron flux across the lunar surface is much smaller (~10%) and most evident in the extended neutron suppression poleward of 70S and 70N, clearly visible in both LEND and LPNS data (Figure 2). In addition to the analysis of global maps based on comparison of data from omni-directional detectors, LEND can map epithermal neutrons with significantly higher spatial resolution than previously reported using counting collimated sensors. The data reduction procedures may be used to remove the fast neutron component of background in the collimated sensors, leaving only the epithermal neutrons recorded in the collimator field of view. The last one was esti-

mated as 1.7 counts per second (from the total counting rate about 5 counts per second). The resulting map reveals new local neutron suppression areas not visible before, associated both with partially sunlit and permanently shadowed areas [7,8].

The fast neutron flux changes by 25% across the lunar surface from maria to the highlands, with the largest value of fast neutron flux observed in mare terrains. This result is consistent with the LPNS argument that mare basalts are rich in iron thus producing more fast neutrons in comparison with Al-rich highlands (Figure 3). The latitude band profile of fast neutron flux does not show significant polar extended neutron suppression effect as observed in the epithermal neutron range. One may distinguish only small areas around poles with neutron suppression less than 1%. This may lead to a model where the hydrogen distribution at the lunar poles, on average is depth dependent with higher weight fraction of H beneath a relatively hydrogen poor regolith.

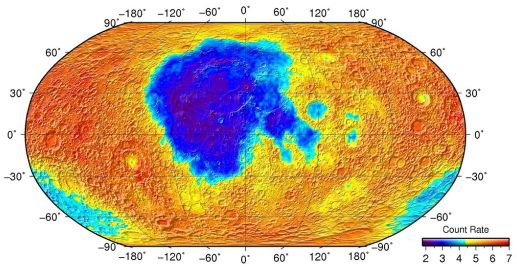

Figure 1. Smoothed map 1°x1° of thermal neutron flux from lunar surface measured as a difference in counting rate between the pair of LEND Doppler detectors.

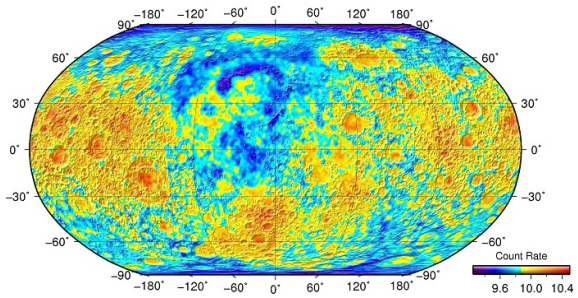

Figure 2. Smoothed map 1°x1° of epithermal neutron counting rate measured by LEND detectors.

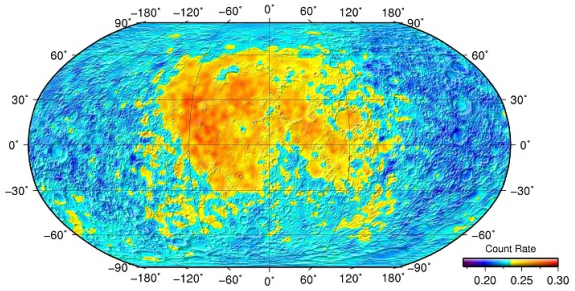

Figure 3. Smoothed map 1°x1° of fast neutron flux from the lunar surface measured by LEND fast neutron sensor.

References:

[1] Mitrofanov I.G. et al. (2008) Astrobiology, Volume 8, 4, 793-804. [2] Mitrofanov I.G. et al. (2010), Space Science Reviews, Volume 150, Issue 1-4, 183-207. [3] Mitrofanov I.G. et al. (2010), Science, Volume 330, Issue 6003, 483. [4] Feldman, W. C., et al (1998) Science, 281, 1489–1493. [5] Feldman, W. C., et al, (1998), Science, 281, 1496– 1500. [6] Feldman, W. C., et al., (2001), J. Geophys. Res., 106(E10), 23,231–23,252. [7] Mitrofanov I.G. et al., (2011), J. Geophys. Res in press. [8] Sanin A.B. et al., (2011), J. Geophys. Res, in press.

USE OF ROBOTIC PRECURSOR MISSION FOR FOLLOW-ON HUMAN EXPLORATION: CASE STUDY LUNAR ANALOGUE MISSION AT THE MISASTIN LAKE IMPACT STRUCTURE

M. M. Mader[1], G. R. Osinski[1], I. Antonenko[1], T. Barfoot[2], M. Battler[1], M. Beauchamp[1], A. Chanou[1], E. Cloutis[3], M. Daly[4], R-D. Capitan[1], R. Francis[1], N. Ghafoor[5], R. A. F. Grieve[1], K. Hodges[6], B. L. Jolliff[7], M. Kerrigan[1], E. McCullough[1], J. Moores[1], C. Otto[8], A. Pickersgill[1], A. Pontefact[1], L. Preston[1], D. Redman[9], H. Sapers[1], B. Shankar[1], A. Singleton[1], P. Sylvester[10], L. L. Tornabene[1], T. Unrau[1], K. Young[6], and M. Zanetti[7].[1]Centre for Planetary Science and Exploration/Canadian Lunar Research Network, Depts. Earth Sciences/Physics and Astronomy, University of Western Ontario, London, ON, Canada, [2]Institute for Aerospace Studies, Univerisity of Toronto, ON, Canada, [3]Dept. of Geography, University of Winnipeg, MB, Canada, [4]Dept. Earth and Space Science & Engineering, York University, ON, Canada, [5]MDA Space Robotics, Brampton, ON, Canada, [6]School of Earth and Space Exploration, Arizona State University, AZ, USA, [7]Dept. Earth & Planetary Science, Washington University, MO, USA, [8]NASA Johnson Space Center, TX, USA, [9]Sensors & Software, Toronon, ON, Canada, [10]Dept. of Earth Sciences, Memorial University, NL, Canada. (marianne.mader@gmail.com, gosinski@uwo.ca).

Introduction: Sample return from the Moon and Mars is a high priority for the international scientific community, in order to ground truth theories of planetary formation and surface processes. Robotic missions followed by human exploration missions have been proposed as an effective strategy for surface exploration (e.g., [1, 2]).

In order to prepare and test protocols for future lunar sample return missions, our team carried out two analogue missions at the Mistastin Lake impact structure, Canada, funded by the Canadian Space Agency. The first mission took place over three weeks in August and September 2010 and involved robotic surveying of proposed "landing sites". This was followed by a second, two-week mission, at the same location in 2011, which included simulated astronaut surface operations.

For each deployment a mission control team was based at the University of Western Ontario located in London, Ontario, over 1900 km away; communication was via satellite terminal in the field, with daily data budgets of ~100 MB. Neither the mission control team nor the 'astronauts' had *a priori* knowledge of the site.

To determine how to optimize a robotic precursor mission for field reconnaissance for augmentation of a follow-on human mission, several important questions were addressed by our study:

- What key instruments and scientific data are needed from a robotic precursor mission to support human operations/sample return?
- How do we adapt robotic precursor mission to the science needs of a specific landing site?
- What surface mobility system is best-suited for a robotic precursor mission with a human follow-on/samle return?

Our analogue mission campaign was driven by the paradigm that the operational and technical objectives are conducted while conducting new science and addressing real overarching scientific objectives. Without such scientific focus, operational and technical lessons learned may have been applied out of context.

Lunar Analogue Site: The Mistastin Lake impact structure, in northern Labrador, Canada (55°53'N; 63°18'W), was chosen because it represents an exceptional analogue for an a lunar highland crater [3]. This site includes both an anorthositic target and preserved ejecta deposits (including melt and breccias) [4]. The intermediate-size crater formed by a meteorite impact ~36 million years ago. The original crater has been differentially eroded; however, a subdued rim (diameter ~ 28 km) and distinct central uplift are still observed [5]. The inner portion of the Mistastin Lake impact structure is covered by the Mistastin Lake and the surrounding area is locally covered by soil/glacial deposits and vegetation. The topography directly surrounding the lake is slightly elevated in plateaus extending up to 5 km away from the shoreline (Fig. 1).

The overarching mission objectives for the analogue mission were to further our understanding of impact chronology, shock processes, impact ejecta and potential mineral resources.

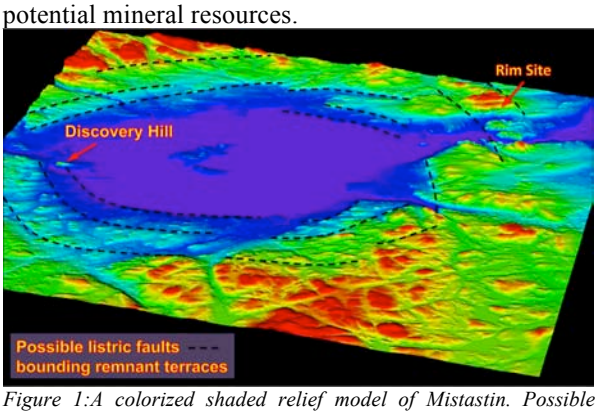

Figure 1:A colorized shaded relief model of Mistastin. Possible listric faults defining the terrace region are outlines in black dashed lines.

Overview of Analogue Mission Campaign: Our scientific approach mirrors exploration strategies for traditional geological exploration and field campaigns conducted on Earth, by 1) Using orbital and aerial data sets to assess geologic diversity, landing site selection, and accessibility/traverse planning; 2) Conducting reconnaissance surface mapping to get an overview of the site from the ground; 3) Follow-up detailed traverses, to study sites of interest in detail. Here we highlight this scientific process for a single landing site, Discovery Hill, situated on the southwest edge of Mistastin Lake (Fig. 1).

Site Selection Workshop, 2010: A site selection workshop was conducted prior to the deployments (results detailed in [5]). Three separate regions around the Mistastin Lake were chosen for reconnaissance exploration by the rover.

*Robotic Precursor Mission, Mistastin 2010***:** No mechanical robot was used on this deployment; instead, a field team of up to five people acted collectively as the robot – they made traverses with the instruments, collected data as requested by mission control, and sent the data to the remote mission control team using satellite communication [6]. At each site, instruments used in the field to characterize the regional context and then progressively focus the geographic area of study, included lidar, Gigapan camera, ground penetrating radar (GPR), mobile scene modeller (mSM), and X-ray fluorescence spectrometer (XRF).

Planning for a Human follow-on Mission: Following the robotic precursor mission, the data collected from the sites were reviewed. Two sites were chosen for further detailed work by human exploration: one site was located within the topographic high area surrounding Mistastin Lake, and the other was closer to the lakeshore and included a distinct topographic feature locally called Discovery Hill (see Fig. 1). Each of these regions are characterized by rugged terrain, and steep topographic relief.

Through the review of precursor data, Discovery Hill was determined to consist in part of a large outcrop of impact melt. The science team therefore focused on two hypotheses: 1) Discovery Hill melt is a portion of the continuous "melt sheet" from the crater floor, or 2) it is a discrete melt unit within the terraced rim section of the crater.

Human Exploration Mission, Mistastin 2011: Two PhD students acted as astronauts and explored the Discovery Hill site – one a geology graduate student with prior geological mapping field experience and specializing in impact cratering products (i.e. impactites), and the other a pilot with an engineering background and some geologic training (similar to many lunar astronauts). With only five days to explore the Discovery Hill area, a focused traverse strategy was developed for the human exploration that allowed for flexibility and adaptability to allow input from the astronauts.

Lessons Learned: Robotic reconnaissance has the potential to significantly improve scientific return from lunar surface exploration. In particular, data from robotic precursor missions can be used to narrow the scientific focus of a human mission (i.e. develop specific research questions and hypotheses to test), improve traverse planning, reduce operational risk, and increase crew productivity.

What key instruments and scientific data are needed from a robotic precursor mission to support human operations/sample return? We found that the main scientific value of a reconnaissance mission is providing surface geology visualization at resolutions and from viewpoints not achievable from orbit. High resolution surface imagery of surrounding areas on the scale of 10's of meters up to several km in extent. The most used data sets included large scale panoramic images that allowed a full contextual view of the surrounding area including exposure of rocks and traversibility of the area and lidar scans that provided range and scale information.

How do we adapt robotic precursor mission to specific site and science needs? The most useful data products were panoramic images and lidar scans taken from 'safe' vantage points looking at 1) steep topography (which allows would allow a cross-sectional view of stratigraphy within rocks) taken from below the rock exposure, 2) overview of landscape taken from a topographic high.

What surface mobility system should be used for a precursor mission? From this experience, it is suggested that the reconnaissance mobility can be more reduced then the mobility needed later for crew transport (i.e. crewrover). A 'small' rover with the ability to collect panoramic photography and lidar scans would meet baseline needs.

- Design rover to access low lying areas to view side of steep topography and reach high points to get pano of region

Recommendations: Focus reconnaissance science instrument/software development on 1) Visualization tools (m to km scale) including seamless data integration of high resolution imagery with lidar to measure distance and scale (e.g., imagery draped over high resolution lidar to create 3D scenes of landscape). Suggest including scale bar (e.g. by laser) in all collected imagery. 2) Instruments such as a multispectral sensor on the rover could further enhance the site selection process, provide remote mineralogical information, and provide scientific rational for prioritization at outcrop and sub-outcrop scales. 3) Data compression of high resolution imagery products (e.g. Gigapan and lidar) and/or communication architecture that allows for greater bandwidth to allow transfer of large files.

References: [1] Global Exploration Strategy (2007), The framework for coordination. [2] Fong et al. (2010). *Acta Astronautica 67*, 1176-1188. [3] Mader et al. (2010), Lunar Science 2010 Forum, Abstract. [4] Mader et al. (2011), LPSC abstract. [5] Grieve (1975) *Geol.Soc.of America Bull. 86*, 1617-1629. [5] Shankar et al. (2011), LPSC abstract. [6] Mader et al. (2011) The Importance of Solar System Sample Return Missionsto the Future of Planetary Science, Abstract.

Acknowledgments: Funding from the Canadian Space Agency (CSA) and the Northern Research Training Program (NSTP) are gratefully acknowledged. We'd like to thank Danielle Cormier, Allan Bassi, Alex Ozaruk, Salma Abou-Aoy, Jacky Clayton, Stephanie Blain and Nicky Barry for their participation during the 2011 deployments.

TOWARD CANADIAN CONTRIBUTIONS TO INTERNATIONAL LUNAR MISSIONS. Eric Martin[1], Jean-Claude Piedbœuf[1], Alain Ouellet[1], Martin Picard[1], Christian Lange[1] and Vicky Hipkin[1], [1]Canadian Space Agency, 6767 Route de l'Aéroport, St-Hubert, Québec, Canada, J3Y 8Y9, Eric.Martin@asc-csa.gc.ca.

Introduction: Canada is one of the fourteen signers of the Global Exploration Strategy that establishes in 2007 an international framework for the exploration of our Moon, Mars and beyond. The Canadian Space Agency (CSA) is evaluating potential participation in this renewed worldwide exploration effort building on its current expertise in space exploration. Canada has been involved in space exploration for more than 25 years with its robotics, science and astronaut corps contributions.

Planetary Exploration: The CSA's focus in planetary exploration is the robotic exploration of Mars, as well as participation in the robotic and human exploration of the Moon and the space between Earth and Moon (cis-lunar space). We also consider robotic asteroid missions and opportunistic missions to other destinations that are aligned with our signature technologies and our science expertise.

Lunar Exploration: The Moon is our nearest and most accessible neighbour; it is an extraordinary repository of the history of the Solar System, and could be a base to prepare for future human missions to Mars. The Moon represents an important opportunity for the Canadian scientific community to participate in planetary missions to prepare for the ultimate goal of Mars exploration.

Lunar missions will initially be robotic, but will eventually include astronauts. The Moon is the most likely destination to establish the first sustainable human base on a planetary body. Astronauts will be able to carry out investigations that are more complex and acquire the experience needed for human exploration of Mars.

Canadian scientists have an interest and expertise in several niche areas of lunar research including: impact processes and formation of the regolith (surface rock and dust layer); the structure and evolution of the lunar interior; and testing theories about heavy bombardment of the lunar surface by asteroids. The Canadian geology community is also interested in lunar exploration for the purpose of extracting resources, both minerals and ice.

Space agencies around the world are planning several missions to the Moon through the end of the decade. These missions combine precursor activities for human space flight with scientific objectives. The CSA is particularly interested in contributing key robotic infrastructure (such as rovers) for astronaut transportation or scientific investigation; robotic technologies for resource extraction; sub-systems for landing and navigation; and science instruments related to areas of Canadian expertise.

Exploration Core Program: To ensure its readiness for such future planetary exploration missions, in 2007, the CSA has launched an Exploration Core program. This program is developing the requirements for future space missions and deploys prototypes in terrestrial missions reproducing some of the characteristics of planetary missions. The Exploration Core is preparing both the scientific community and Canadian industry, enabling them to make scientific and technological advances that will position Canada to make informed decisions on a participation in the global exploration. When a mission of interest to Canada arises, the existence of the Exploration Core will ensure that the required science and technologies have matured to the appropriate level, minimizing risk and cost of a mission. The results of this broad effort will allow Canada to make more informed decisions concerning its contributions to, and participation in, the implementation of the Global Exploration Strategy.

Since its creation this program has funded more than 30 concepts studies, 15 prototyping contracts and 5 analogue deployments, all of them outside the Exploration Surface Mobility (ESM) project described below..

Exploration Surface Mobiliy: The Government of Canada Budget 2009 provided the CSA with $110 million over three years so that it can contribute to the development of terrestrial prototypes for space robotic vehicles, such as the Mars Lander and Lunar Rover. This funding was part of an overall strategy of establishing a Canadian capability to develop, build and eventually operate rovers on the Moon and Mars. Under the Exploration Surface Mobility (ESM) project, CSA has initiated more than 25 contracts to demonstrate the capabilities of prototypes of rovers and associated payloads for the Moon and Mars through field deployments. Terrestrial prototypes of three integrated rovers, two for Lunar Exploration and one for Mars, are being developed and are planned for analogue field deployments. These field deployments will evolve into one or more integrated analogue missions, where science, technical, and operational elements of a space mission will be simulated, tested, and validated in appropriate analogue field settings.

ILLUMINATION CONDITIONS OF THE LUNAR POLES TO 65 DEGREES LATITUDE FROM LUNAR ORBITER LASER ALTIMETER DATA. E. Mazarico[1,2], G.A. Neumann[2], D.E. Smith[1,2], M.T. Zuber[1] and M.H. Torrence[1,3]. [1]Massachusetts Institute of Technology, Cambridge MA, [2]NASA Goddard Space Flight Center, Greenbelt MD, [3]SGT Inc., Greenbelt MD.

Introduction: Although diurnal temperature variations over most of the Moon's surface can be extreme, the lunar polar regions have the potential to trap volatiles in permanently shadowed regions (PSRs). Because the Moon's spin axis is nearly perpendicular to the ecliptic plane, the Sun is always low on the horizon in the polar regions, and topographic relief such as impact craters can be sufficient to provide permanent shadow. Although the Moon obliquity has been larger in the past, many PSR regions have likely been stable over tens to hundreds of millions of years. This was recognized before good topographic knowledge of the polar regions existed **[1]**, and was confirmed by more recent studies using ground-based radar **[2]** or spacecraft data **[3,4,5,6]**.

Data: We use data collected by the Lunar Orbiter Laser Altimeter (LOLA) instrument **[7]** onboard the Lunar Reconnaissance Orbiter (LRO) **[8]**. With more than 4.67 billion LOLA altimetric measurements (as of September 1, 2011), and the polar orbit of the LRO spacecraft, the data coverage of the poles is excellent. We construct topographic maps of the lunar polar regions, from ~55° to the pole, at a resolution of 480 meters per pixel.

Method: The horizon method was described in detail in **[6]**. Horizon (angular) elevation maps are constructed for the region of interest (~80°-90°) for 720 azimuthal directions ($\delta\theta$=0.5°). The illumination conditions at any epoch can then be obtained by comparing the Sun elevation to that of the horizon (in the Sun direction).

Results: We conduct simulations with the LOLA topography to survey the extent of PSRs in both polar regions, down to 65° latitude. These regions are much larger than our previous work (down to 80°, **[6]**) and that of others. These calculations provide a nearly-complete survey of the lunar PSRs, with total areas of 21,866km^2 and 25,905km^2 in the North and South respectively. In addition to the average solar illumination, we also characterize the average and maximum incident flux. Those quantities are related to the illumination and energy budget of the lunar polar regions. We investigate how they relate to the LEND measurements **[9]**. Similarly to the LEND measured counts, the average, the average illumination decreases with increasing latitude, more steeply than what can be expected from a pure solar incidence effect.

References: [1] Watson K.B. et al. (1961) *JGR*, *66*, 3033. [2] Margot et al. (1999) *Science*, *284*, 1658. [3] Cook et al. (2000), *JGR*, *105*, 12023. [4] Noda et al. (2008), *GRL*, *35*, L24203. [5] Bussey et al. (2010), *Icarus*, *208*, 558. [6] Mazarico et al. (2011), *Icarus*, *211*, 1066. [7] Smith et al. (2010), *GRL*, *37*, L18204. [8] Chin et al. (2007), *Sp. Sci. Rev.*, *129*, 4. [9] Mitrofanov et al.(2010) Science, 330-6003, 483-486.

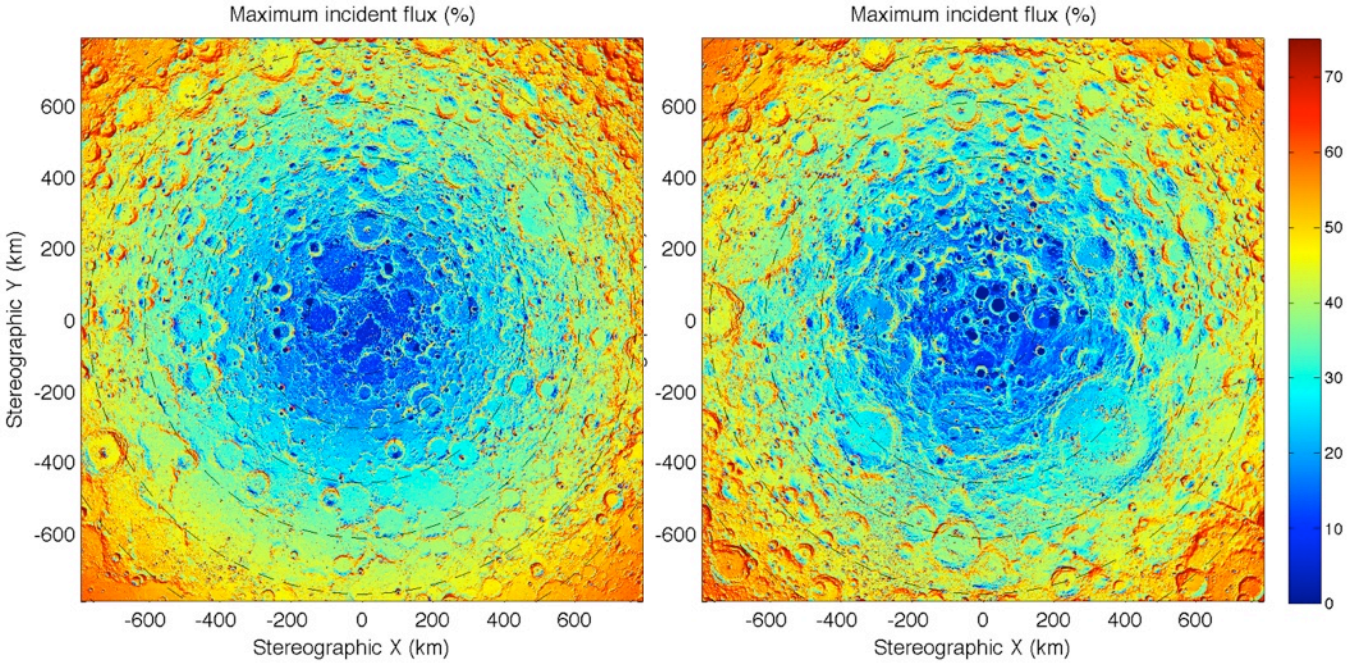

Figure 1. Maximum incident flux maps for the northern (left) and southern (right) polar regions. The simulation duration was one 18.6yr cycle, with a timestep of 6 hours. The latitude circles are every 5 degrees, down to 65° latitude.

TOPOGRAPHICALLY INDUCED THERMAL EFFECTS ON LUNAR HYDROGEN DISTRIBUTIONS: CORRELATED OBSERVATIONS FROM THE LRO LEND AND LOLA INSTRUMENTS. T.P. McClanahan[1] , I.G. Mitrofanov[2], W.V. Boynton[3], G. Chin[1], G. Droege[3], L.G. Evans[1,6], J. Garvin[1], K. Harshman[3], M.L. Litvak[2], A. Malakhov[2], G.M. Milikh[4], M. Namkung[1], G. Nandikotkur[5], G. Neumann[1], D. Smith[1,7], R. Sagdeev[6], A. G. Sanin[2], R.D. Starr[1,4], J.I. Trombka[1,5], M.T. Zuber[1,7], [1]Space Exploration Division, NASA Goddard Space Flight Center, Greenbelt, MD, USA., [2]Inst. for Space Research, Moscow, Russia, [3]Lunar and Planetary Laboratory, University of Arizona, Tucson, AZ, USA, [4]Catholic Univ., Washington , DC, USA. [5]Space Physics Dept., Univ. of Maryland, College Park, MD, [6]Computer Sciences Corp., Glenn Dale, MD, USA, [7]Dept. of Earth, Atmos., and Planet. Sci., MIT, Cambridge, MA, USA.

Introduction: The question of whether water exists on the Moon's surface has long been an enigma to Lunar researchers [1]. Largely, this was due to the thermally extreme lunar surface environment that would seem to preclude any long term maintenance, manufacture, transport or accumulation of hydrogen (H) volatiles over most of the lunar surface [2]. As a result, for many years the cold permanent shadow regions (PSR) in the bottoms of craters near the lunar poles appeared to provide the basic conditions at least for maintenance of lunar hydrogen. Importantly, recent discoveries indicate that there is some hydrogen at the poles [3]. However, the picture of the lunar hydrogen budget may be more complex than the PSR hypothesis has suggested. This evidence comes from observations by the Lunar Exploration Neutron Detector (LEND) onboard the Lunar Reconnaissance Orbiter (LRO) that indicate 1) some H concentrations lie outside PSR and 2) though a few of the larger PSR's have high hydrogen, PSR does not appear to be an independent factor influencing the large-scale suppression of polar epithermals observed by LEND and the Lunar Prospector Neutron Spectrometer [4, 5, 6].

In this research we investigate the possibility that the thermal contrast between pole-facing and equator facing-slopes is a factor influencing the surface distributions of lunar H. We perform this bulk correlated observation and study by developing a thermal proxy from slope data of the Lunar Orbiting Laser Altimiter (LOLA) digital elevation model (DEM) which is registered with the collimated LEND epithermal map [7]. From the LOLA transforms we impose a thermal functional decomposition and systematic statistical analysis of the LEND epithermal map. Our hypothesis testing suggests in most high latitude bands studied > ±45°: **Epithermal rates in pole-facing slopes are significantly lower than epithermal rates in equivalent equator-facing slopes**. As a control study, we find that there is no statistically significant difference between equivalent east and west facing slopes. This finding suggests topographic modulation of insolation is a factor influencing the lunar H budget. Importantly, this result is consistent with observations in terrestrial, Martian research.

Methods: Several important factors influence the design of the methods used in this series of experiments. 1) Due to LRO's polar coverage, LEND map uncertainties increase as a function of lower latitudes increasing correlation uncertainties with small-scale topographic features. 2) LEND maps are long duration accumulations ~2yrs, and diurnal, and seasonal thermal variations are convolved into the maps.

For factor 1) two approaches are used, 1a) use LOLA slope transforms to decompose and classify sets of LEND pixels and to perform class statistical comparisons. This technique takes advantage of the larger areas available in the low latitudes, thus minimizing the issue of uncertainties. 1b) Perform hypothesis testing of LEND epithermal classes as a function of discrete 5° latitude bands. For polar regions we implement 18 independent statistical t-tests (test of class mean differences), 18 F-tests (tests for class variance differences). For factor 2) We define a first-order assumption that the dominant solar irradiance direction *and the expected maximum local annual thermal conditions* for all LOLA DEM pixels occurs at local noon at polar summer solstice. This assumption fixes the solar direction along a given pixel's longitude and defines the requirement for deriving each pixel's slope orientation Φ. This defines a map with a slope orientation continuum with the following coding: [Φ = 0 is pole-facing, Φ =90= East, West-facing and Φ = equator-facing slopes]. Thus, we derive three parameters for each DEM pixel [latitude, slope°, slope angular orientation with respect to the pole-direction Φ].

From these meta-data we perform slope based classifications of LEND epithermal pixels. For experiment 1, we classify pole-facing (**PF**) and equator-facing pixels (**EF**) using the following conditions, 9-latitude bands, High-slope > 5° (to provide local thermal contrast), [**PF** = Φ < 15°, **EF** = Φ > 165°]. Contiguous pixels are region-grown into 'spots' to reduce high pixel spatial correlations and the ground clutter of numerous small spot areas << LEND's FOV = 10km FWHM = ~78 km^2. We only classify spot sizes > 10 km^2 [4]. The average epithermal rate over valid spots is obtained and entered as class sample, Figure 1.

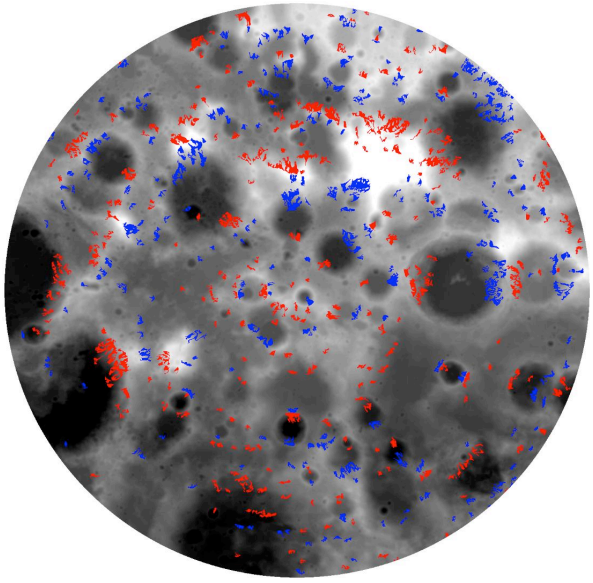

Figure 1: South Pole centered DEM -80:-90, of **PF** *blue* and **EF** *red* classified spots used in experiment 1. LEND epi's are averaged over spots. Spots ⊆ **Class**

Experiment 1 Results:

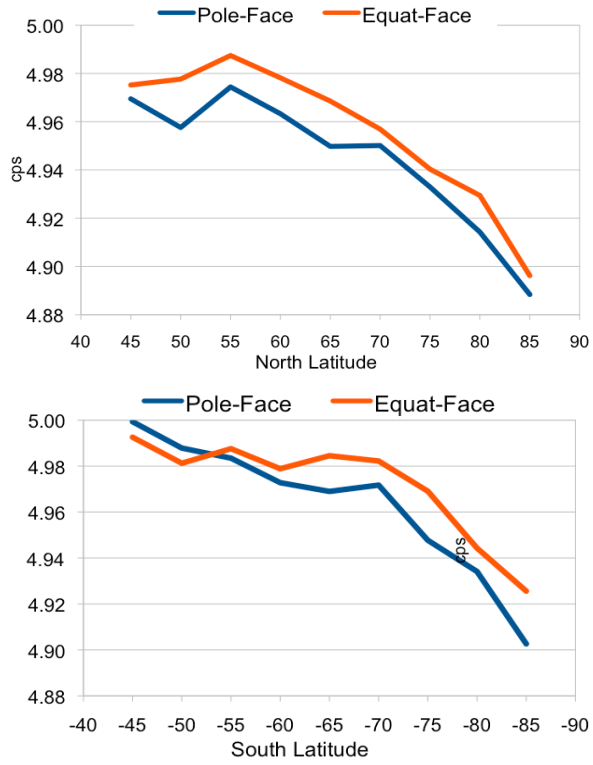

Figure 2a North, 2b South: 5° lat. band, pole-facing **PF** *blue* vs equator-facing **EF** *red* mean epi class rates.

Experiment 1: we evaluate our hypothesis that pole-facing slopes have lower epithermal rates than equator-facing slopes. For 16 of 18 North and South polar latitude bands pole-facing epi-rates were less than equator facing rates. Hypothesis testing using t-tests of the **PF**, **EF** class means in each band (which include latitude uncertainties) indicated 10 of the 16 were significant, *p*-values < α=0.05. From this result we conclude **PF** slopes have lower epithermal rates than **EF** classes in regions > ±60° latitude.

Experiment 2 Results:

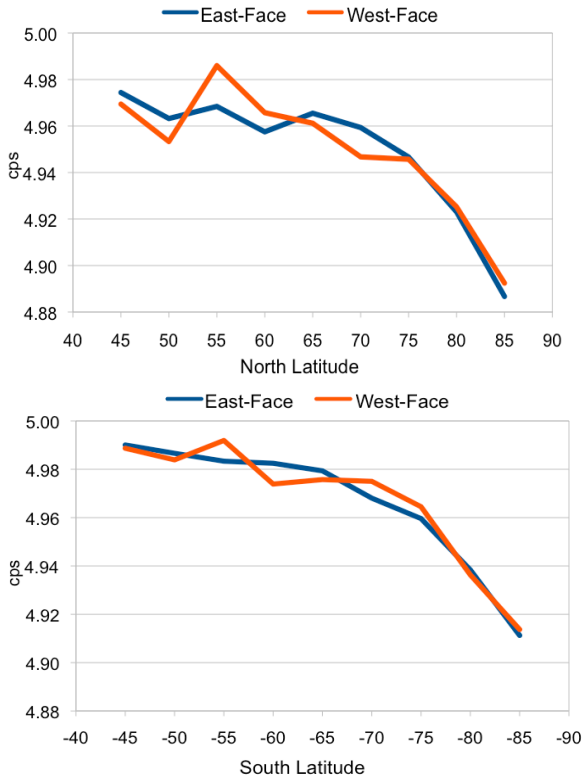

Figures 3a North, 3b South: North and South latitude > ±45°, study of **East** vs **West** facing slopes.

Experiment 2: is a control experiment and assumes similar irradiance and thermal conditions for East and West slopes. The hypothesis is that there should be no epi-rate differences in lat bands. Combined North and South evaluations observed in 10 of 18 cases of east vs. west-facing slopes, East-facing slopes had higher epithermal rates. Two low latit. values had significant p-values < 0.05, but 1 for **East**, 1 for **West**. We find no significant differences for **East** vs **West** epi-rates.

References: [1] Arnold (1979) *JGR*, #84, 5659-5668 [2] Vondrak and Crider (2003) *Amer. Sci.*, 9, 322-329 [3] Colaprete et al. (2010) Science, 330-463-468 [4] Mitrofanov et al.(2010) *Science*, 330-6003, 483-486 [5] Feldman et al.,(2001) *JGR*, 106-E10, 23231-23251 [6] Chin et al. (2007) *Sp. Sci. Rev.*, 150(1-4), 125-160 [7] Smith et al.(2010) *Sp. Sci. Rev., 150(1-4)*.

Radiation Risks for Future Manned and Robotic Missions: PREDICCS: Predictions of Radiation from REleASE, EMMREM, and Data Incorporating CRaTER, COSTEP, and other SEP Measurements – an Online Nowcasting and Forecasting System. J. F. Mislinski[1], N. A. Schwadron[1], L. Townsend[2], H. E. Spence[1], O. M. Rother[3], A. Posner[4], R. Squier[5], J. K. Wilson[1], A. P. Jordan[1], R. Anderson[1], T. Baker[1], K. A. Kozarev[6], C. Joyce[1]. [1]Institute for the Study of Earth, Oceans, and Space SCience (EOS), University of New Hampshire, Durham, NH, [2]Nuclear Engineering, University of Tennessee, Knoxville, Knoxville, TN, [3]Physics, University of Kiel, Kiel, Germany, [4]Heliophysics, NASA, Washington, D.C., [5]Computer Science, Georgetown University, Washington, D.C., [6]Astronomy, Boston University, Boston, Masschusetts.

Introduction: Future manned and robotic missions to the Moon, Mars, and beyond require accurate models for the radiation environment through the heliosphere. PREDICCS – Predictions of radiation from REleASE, EMMREM, and Data Incorporating CRaTER, COSTEP, and other SEP measurements – will be an on-line system to predict and forecast the radiation environment through interplanetary space. PREDICCS uses SEP (Solar Energetic Particle) measurements from the Cosmic Ray Telescope for the Effects of Radiation (CRaTER) [1] instrument currently on the Lunar Reconnaissance Orbiter (LRO) and data from the Comprehensive Suprathermal and Energetic Particle Analyzer (COSTEP) [2] and integrates two radiation environment models: The Earth-Moon-Mars Radiation Environment Module (EMMREM) [3] and the Relativistic Electron Alert System for Exploration (REleASE) [4]. REleASE very accurately forecasts SEP events up to one and a half hours ahead of the event. The EMMREM model predicts the real-time radiation environment using Energetic Particle Radiation Environment Module (EPREM) and the Baryon Transport Module (BRYNTRN). We combine these two models to nowcast and forecast the radiation environment at various observers – including the Earth, Moon, Mars, and at specific target observers such as comets and asteroids – and for future SEP events. Validation of these models requires data from CRaTER, COSTEP (EPHIN), and other SEP measurements. CRaTER characterizes the lunar radiation environment and its biological impacts with LET (Linear Energy Transfer) spectra of galactic and solar cosmic rays and COSTEP (EPHIN) measures relativistic electrons and deka-MeV protons and helium. Preliminary comparisons have been made of a recent, albeit small, SEP event from early June 2011 that has shown excellent agreement with EMMREM predictions. This event has been well observed by CRaTER and a number of other instruments. This has been the first "significant" event as we come out of the longest and deepest solar minimum in the space age. Additional observations of SEP events in the near future will help to fine tune the models in order to predict the radiation environment in interplanetary space with more confidence. This will be an invaluable resource for future manned and robotic missions.

References: [1] Spence, H., et al. (2010), CRaTER: The Cosmic Ray Telescope for the Effects of Radiation Experiment on the Lunar Reconnaissance Orbiter Mission, Space Science Reviews: Astronomy, Astrophysics, & Space Science, Springer Netherlands, ISSN 1572-9672, doi:10.1007/s11214-009-9584-8. [2] Müller-Mellin, R., et al. (1995), COSTEP – Comprehensive Suprathermal and Energetic Particle Analyser, Solar Physics, 162, ISSN 0038-0938, doi:10.1007/BF00733437. [3] Schwardon, N. A., et al. (2010), Earth-Moon-Mars Radiation Environment Module framework, Space Weather, 8, S00E02, doi:10.1029/2009SW00052. [4] Posner, A., S. Guetersloh, B. Heber, and O. Rother (2009), A New Trend in Forecasting Solar Radiation Hazards, Space Weather, 7, S05001, doi:10.1029/2009SW000476.

SCIENCE MISSION LUNA GLOB. I. G. Mitrofanov[1] , [1]Institute for Space Research of Russian Academy of Science, 117997 Moscow, Russia, imitrofa@space.ru,

The mission concept will be presented together with overview of scientific investigations in correspondence with the major scientific goals: studies of lunar poles and global investigations of lunar surface and exosphere.

LOCAL SPOTS OF LUNAR WATER-ICE PERMAFROST IN SHADDOW AND IN SUNLIGHT, AS SEEN BY LEND/LRO. I. G. Mitrofanov[1] , M. L. Litvak[1], A. B. Sanin[1], A. A. Malakhov[1], D. V. Golovin[1], W. Boynton[2], G. Droege[2], G. Chin[3], L. Evens[4], K. Harshman[2], J. Garvin[3], A. Kozyrev[1], T. McClanahan[3], G. Milikh[5], M. Mokrousov[1], R. Starr[5], R. Sagdeev[5], V. Shevchenko[7], V. Shvetsov[8], V. Tret'yakov[1], J. Trombka[5], A. Varenikov[1] and A. Vostrukhin[1]. [1]Institute for Space Research of Russian Academy of Science, 117997 Moscow, Russia, imitrofa@space.ru, [2]University of Arizona, Tucson, USA, [3]NASA Goddard Space Flight Center, Greenbelt, USA, [4]Computer Science Corporation, Greenbelt, USA, [5]University of Maryland, College Park, USA, [6]Catholic University, Washington DC, USA, [7]Sternberg Astronomical Institute of Moscow State University, Moscow, Russia, [8]Joint Institute of Nuclear Energy, Dubna, Moscow.

Introduction: The neutron telescope, LEND, was selected for NASA`s LRO mission for testing local spots of water-ice permafrost at lunar poles. This instrument maps epithermal neutron emission of lunar surface with high spatial resolution about 10 km from the orbit with altitude of 50 km [1, 2]. The epithermal neutrons are moderated in many collisions from original high energy neutrons with energy about 1 -20 MeV, which are produced by energetic particles of galactic cosmic rays. The leaking flux of epithermal neutrons depends on the content of hydrogen of the regolith, because more collisions with nuclei of hydrogen lead to faster moderation and thermalization of neutrons before leaking from subsurface. Observed suppression of emission of epithermal neutrons at some particular spot in comparison with the reference surface indicates enhanced content of hydrogen or water in the regolith.

Data analysis: To test for the presence of local suppression/excess spots, one should subtract the average count rate of the reference map smoothed with the scale of 230 km from count rate on the main map, and then test spatial distribution and amplitudes of residuals. If result of this test would be consistent with statistical fluctuation of counts, one should conclude that there are no local spots of water-ice permafrost as well as spots with chemical variations of the regolith which lead to variations of neutrons emission. On the other hand, the presence of such spots would be supported by experimental data provided statistical significant spots of neutron excess or suppression would be confidently detected on the surface of the Moon.

For selection of candidates for local spots with either negative (*Neutron Suppression Regions*, NSRs) or positive (*Neutron Excess Regions,* NERs) deviations over the testing map we use two thresholds ±0.0425 cps and ±0.085 cps for residuals with respect to the counting rate of the reference smoothed map at the same pixel. These thresholds correspond to 2.5% and 5% of the reference counts rate 1.7 cps, which is attributed for epithermal neutrons from lunar surface at the moderate latitudes [3]. The negative and positive thresholds determine the contours of potential candidates for NSRs and NERs, respectively. To test statistical confidence of each potential candidate spot, we sum up all counts of residuals of pixels inside the contour of a spot, and compare this value with the total statistical error estimated for initial counts of these pixels for the main map. We use 3standard deviation confidence selection criteria for candidate spots, which are used for further analysis of NSRs and NERs.

We decided to restrict this analysis of local candidate spots of NSRs or NERs by limiting their area to 2000 km^2, which corresponds to the spot's linear size about 40 – 50 km. Indeed, the reference map has a smoothing scale of about 230 km, so it does not contain variations with a moderate linear scale of about 100 km and less. On the other hand, these variations could be studied quite well by epithermal sensors with omni-directional field of view and large counting rate, and they are not proper observational targets for collimated sensors of LEND with narrow FOV.

So, we consider only candidate spots for NSRs and NERs, which are selected by thresholds criteria 2.5% and 5% , have confidence corresponding to 3σ or higher, and have the total area smaller than 2000 km^2.

Obtained results: Polar regions were tested above 70° at north and south by this method [4]. Twelve candidates were found including 8 NSRs and 4 NERs. These candidate were additionally validated by data from LOLA [5] and Diviner [6] instruments on LRO by testing the difference of solar irradiation and average surface temperature for areas inside and outside the candidate spots. It was found that 6 selected NSRs and 2 selected NERs are consistent with the phenomenological law "less/more heating – less/more neutrons", which prove that spots detected by LEND are real, because they are different from the surface at the nearest vicinity at the same latitude. This law could be related to the presence of hydrogen bearing volatiles in the regolith. When heating is small, regolith contains higher content of volatiles, and opposite – larger heating leads to less hydrogen in the subsurface.

The Shoemaker-Malapert territory is the most interesting case together with the crater of Cabeus of

possible water-rich permafrost detected with LEND data (see also [7]). The NSRs at this territory S1 and S3 have the total area of about 5300 km^2 (Figures 1 and 2). S1 includes the the spot with the largest local suppression 12.2 ± 2.6% at the *Permanent Shadow Region* (PSR) at the floor of Shoemaker crater (Figure 1). It is interesting, that accuracy of neutron imaging by LEND telescope is high enough to resolve the boundary if the permanent optical shadow at this spot.

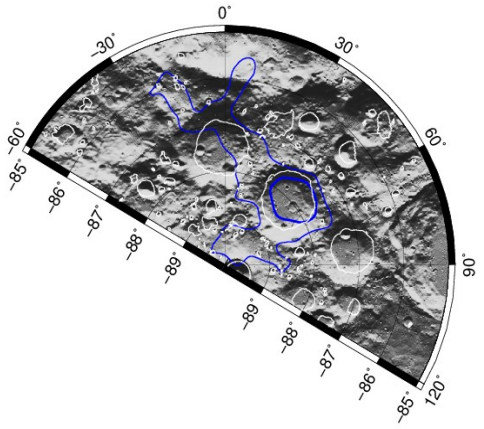

Figure 1. NSR S1 in Shoemaker with contours of suppression -2.5% (*thin blue*) and -5.5% (*thick blue*). White contours represent the boundaries of PSRs. PSR of Shoemaker is very well consistent with the contour of -5% suppression contour of NSR S1. Lunar landscape is shown in the Figures 1and 2 in accordance to LOLA altimetry and contours of PSRs are produced from this data also.

The contour of second NSR S3 at Shoemaker-Malapert territory has average neutron suppression even higher, 14.4 ± 4.1 %. The area of 650 km^2 includes part of Mountain Malapert with well-irradiared equator-facing spot together with large polefacing PSR (Figure 2). It is interesting, that average suppression of this spot with large fraction of sunlit surface is comparable with the suppression at Shoemaker, which is in the permanent shadow.

Conclusions: It is found that local NSRs is the real phenomenon at lunar poles [4, 8]. Comparison between selected NSRs and large PSRs lead to the conclusion that NSRs are not linked directly with PSRs, as has been commonly accepted before LEND investigation. One may conclude that favorable physical conditions for formation of NSRs at lunar poles are not directly related with the permanent shadow, but, on the other hand, the spot of permanent shadow could have larger suppression within the area of NSRs, which has been formed at this place.

The phenomenological law "more/less irradiation – more/less neutrons" leads to the hypothesis that irradiation and implantation of hydrogen from solar wind may work together, like chemical reactor, which produce water molecules during a sunlit time. We suggested to call this mechanism *Solar Water Chemical Reactor* (SWCR). A water molecule, which is produced at heated top layer from solar protons, could either diffuse down to cold subsurface for permanent trapping, or migrate out from the hot sunlit surface to cold shadow nearby for trapping there. The efficiency of SWCR depends on local landscape and on properties of the surface.

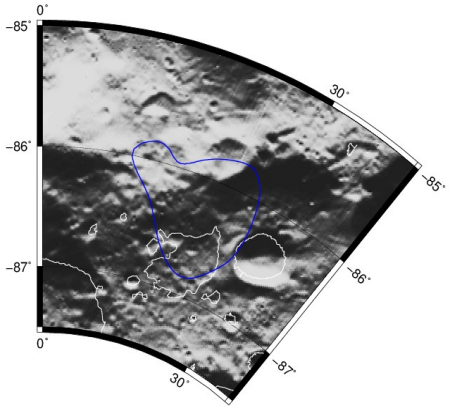

Figure 2. NSR S3 at south-east side of Malapert crater also has large fraction of the surface at PSR, and its another part is equator-looking slop of a rim.

There are two potential origins of lunar water, the *cometary water* delivered by comets and *solar water* produced by chemical reactions from protons of solar wind. In the first case water vapor from a comet would condense similarly at all cold traps of PSRs around the impact site. In this case one could expect that similar large PSRs should have similar deposits of water, and, *vise versa*, there should be no water deposits at sunlit surface outside the permanent shadow. Data presented above shows that it is not the case. This data is more favorable for the second choice, the *solar water* produced *in situ* from solar wind. In this case the difference between water-rich and water-poor PSRs could be explained by more or less favorable surface morphology for production of water at some local spots with SWCRs and for storage of water ice permafrost in the cold subsurface.

References: [1] Mitrofanov I. G. et al. (2008) *Astrobiol., 8,* 793. [2] Mitrofanov I. G; et al. (2010) *Space Sci. Rev. 150*, 183. [3] Litvak M. L. et al. (2011) subm. *JGR*. [4] Mitrofanov I.G. et al. (2011) subm. to *JGR*. [5] Smith D. et al. (2010) *GRL, 37*, 18. [6] Paige D.A. et al. (2010) *Space Sci. Rev. 150*, 125. [7] Mitrofanov I.G. et al. (2010*) Science 330*, 483. [8] Boynton W. et al. (2011) subm. to *JGR*.

CARBON AND RARE-EARTH ELEMENTS CONTENTS ON THE MOON: AS NEW RESOURCES. Yas. Miura, Yamaguchi University, Chuou 4-1-23, Yamaguchi753-0074, Japan (yasmiura@yamaguchi-u.ac.jp;moonyas@hotmail.com)

Introduction: Carbon, chlorine and rare-earth elements (REE) are remained in impact breccias on the Moon [1-4]. Although there are no "Earth-type mineral deposits" on the Moon due to few dynamic plate movements without sea-water and few dynamic convection process to transportation of light volatiles to the interior to produce multiple melting concentration of Earth-type mineral deposits, main melting process to produce elemental concentration of "Moon-type deposits" is considered to be" impact process" with vapor-liquid (fluid)-solid state changes [2-4]. The main purpose of the paper is to elucidate the Moon-type elemental concentration on carbon, chlorine and the REE anomalous Ca-rich plagioclase compositions with carbon, which will be one of main target for lunar space exploration [3, 4].

Carbon and REE deposits in the lunar rocks: In order to discuss the "impact process "of the rock types, the Apollo lunar rocks are only valuable samples to discuss the sampling points and thin-section textures in wide area. Figure 1 shows that carbon, chlorine and REE (Y, Ce and Nd etc.) contents are increased largely at the lunar polymict breccias among the highland troctolite, volcanic basalt, regolith soils and impact breccias as follows (Table 1).

1) All contents of carbon, chlorine and the REE are the most deficient in the highland rocks. This indicates that crystallized minerals do not include so much due to slower crystallization than other rocks.

2) Volcanic basalts shows lower contents, though the REE contents of Y elements are higher contents.

3) Regolith soils show higher contents of carbon, chlorine and the REE (especially Y element). This suggests that regolith soils are mainly originated from basaltic rocks (at the Apollo sampling sites of the near side with major Mare basalts).

4) Polymict breccias shows the highest contents of these elements, especially the REE of Ce and Nd. This indicates that Ce contents is considered to be significant indicator of impact mixing , though high Nd contents has contribution for magnetic properties around the impact craters due to its high magnetic properties.

Table 1. Anomalous data of lunar plagioclases .
1) Carbon, chlorine and the REE:
The highest contents in the polymict breccias.
2) Y and Ce contents of the REE:
Clear increase of Y contents in polymict breccias .

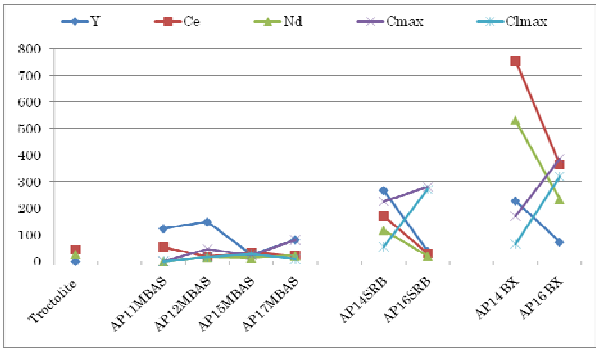

Fig.1. Average contents of carbon, chlorine and the REE-Y, Ce and Nd in the Apollo samples of the troctolite, basalts, regolith soils and breccias [1-4].

Estimated amounts of the REE deposits: Significant deposits of the REE (17 elements) contents are estimated as ca. 20 million ton (in regolith soils in 10 m thickness) and ca. 13300 million ton (in breccias in 2km thickness) on overall surface of the Moon. This large amounts of the REE are considered to be new resources in the airless Moon with impact surface.

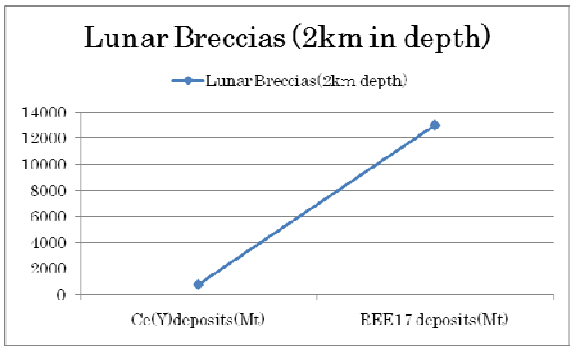

Fig. 2. Estimated amounts of the lunar REE (Ce, Y) deposits in the reported data of the Apollo samples.

Summary: The lunar Apollo breccias contain the highest amounts of the REE (esp. Ce) deposits, which will be strong candidate for the lunar resources.

References: [1] Heiken G., Vaniman D. & French B. (1991): L*unar source book* (Cambridge Univ.Press). 468-474. [2] Miura Y. (2009). LPI Contrib. No. 1515 (LEAG 2009), 2042, 2043. [3] Miura Y. (2011): PTMS-2 (Ottawa), pp.2 (in press). [4] Miura Y. et al. (2011): Report of ISAS-JAXA Plasma Research, pp.4 (in Japanese; in press).

EFFECT OF SOLAR ACTIVITY ON THE NEUTRON FLUX DETECTED BY LEND. G. Nandikotkur[1] , G. M. Milikh[1], R. Sagdeev[1], G. Chin[2], W. Boynton[3], K. Harshman[3], J. G. Droege[3], I. G. Mitrofanov[4], M. L. Litvak[4], A. B. Sanin[4], D. Golovin[4], L. G. Evans[5], R. Starr[6], T. McClanahan[2], [1]University of Maryland, College Park MD (giridhar@physics.umd.edu), [2]NASA-Goddard Space Flight Center, Greenbelt, MD, [3]University of Arizona, Tucson, Arizona, [4] Institute for Space Research of Russian Academy of Sciences, Moscow, Russia, [5]Computer Sciences Corporation, Greenbelt, MD, [6]Catholic University of America, Washington DC.

Introduction: The Lunar Exploration Neutron Detector (LEND) onboard Lunar Reconnaissance Orbiter (LRO) [1] measures the flux of neutrons from the lunar surface, produced by the bombardment within the surface by Galactic Cosmic Rays (GCR) whose variability is associated with the Solar Cycle. The objective of this paper is to make an assessment of the effect of solar activity on the neutron flux radiated by the moon. The model will be then checked against the LEND data gathered during 2009-2011 period, as well as against other relevant observations such the neutron data collected at Mars and Earth.

Approach: In our analysis we use the results by *McKinney et al.* [2] who computed the lunar differential neutron leakage by using MCNPX code with the flux of galactic cosmic rays (GCR) as an input. The model results were then checked against *in situ* neutron measurements made during the Apollo 17 mission. The Apollo 17 Lunar Neutron Probe Experiment (LPNE) provided a unique set of in situ data on the production of neutrons within the top 2 meters of the Lunar regolith bombarded by GCR, and serves as an invaluable "ground-truth" in the age of orbital remote sensing. Moreover a model of the GCR flux was presented in [3, 4] where the key role is played by the solar modulation potential Φ which describes the effect of solar magnetic field on the GCR flux. The potential ranges from 100 MeV in a local interstellar medium to more than 900 MeV in periods of Solar Grand Maximum [4].

Results: The initial phase of LRO mission 07/09 – 05/10 took place during the period of a very quiet sun. As suggested by [4] since Φ = 100 MeV is used for a local interstellar spectrum, such modulation potential could be used during extreme solar minimum periods such as the Maunder Minimum (1645-1715). Moreover the analysis [5] shows that the current solar cycle is similar to the three cycles that occurred during the Dalton minimum in the early nineteenth century. The minima of those cycles could be described by the potential Φ = 200-250 MeV which is the average between the absolute minimum of 100 MeV at the Maunder Minimum and a "regular minimum" of 300-400 MeV such as happened in the 1980s and 1990s. The value of Φ = 200-250 MeV can serve as a conservative estimate for the early part of the LRO mission (07/09 – 05/10). Furthermore the total neutron flux was found by integrating the GCR flux with the neutron production rate per particle adapted from [2]. The neutron flux was then obtained as a function of the solar modulation potential. The model was checked against the neutron count rates for each of four collimated LEND sensors collected during LRO mission and against the GCR counts collected by the Mars Odyssey. A good correlation was found between the model results and the temporal behavior of the Lunar and Martian count rates.

References:

[1] Mitrofanov, et al. (2008), Experiment LEND of the NASA Lunar Reconnaissance Orbiter for High-Resolution Mapping of Neutron Emission of the Moon, *Astrobiology,8*,DOI:10.1089/ast.2007.0158. [2] McKinney, G.W., et al. (2006), MCNPX benchmark for cosmic ray interactions with the Moon, *J. Geophys.Res.,111*,E06004,doi:10.1029/2005JE002551 [3] Masarik, J. and R.C. Reedy (1996), Gamma ray production and transport in Mars, *J. Geophys. Res., 101*, E8, 18891. [4] Castagnoli, J. and D. Lal (1980) Solar modulation effects in terrestrial production of Carbon-14, *Radiocarbon, 22*, 133. [5] Turner, R. (2011), Solar Cycle Slow to Get Going: What Does It Mean for Space Weather?, *Space Weather, 9*, S04004, doi:10.1029/2011SW000671.

Establishing a Lunar Geophysical Network for Exploration and Solar System Science. C. R. Neal[1], [1]Department of Civil Eng. & Geological Sciences, University of Notre Dame, Notre Dame, IN 46556, USA (neal.1@nd.edu)

Introduction: After the announcement by President Bush of the Vision for Space Exploration in 2004, the years immediately thereafter sparked a tremendous and international refocusing on the Moon and lunar exploration. From the science side, one of the important aspects of exploring the Moon was to establish a global geophysical network to truly understand the interior of our nearest neighbor. Such a mission requires multiple landers including some on the lunar farside, which resulted in cost estimates that were in the billion dollar range. This led to the development of the International Lunar Network (ILN) mission (http://science.nasa.gov/missions/iln/) whereby NASA with international partners would establish several nodes of a geophysical network on the Moon, with NASA establishing 4 anchor nodes [1].

The change of administration in 2009 changed NASA's direction and the Moon was by-passed in favor or near Earth asteroid exploration. This change of emphasis has dulled enthusiasm at NASA for the ILN. However, NASA's Planetary Sciences Division underwent its decadal survey in 2010 [2]. Due to community input, a New Frontiers class mission to establish a Lunar Geophysical Network was recommended.

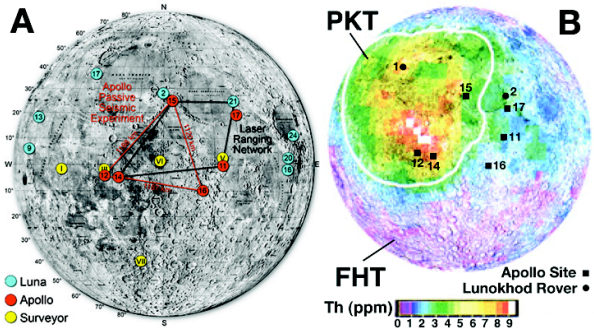

Fig. 1: ***A*** *– Map of human and robotic lunar landing sites;* ***B*** *– Map of Apollo and Lunokhod landing sites relative to lunar terranes. PKT = Procellarum KREEP Terrane; FHT = Feldspathic Highlands Terrane.*

The Lunar Geophysical Network (LGN): Seismic, heat flow, laser ranging, and magnetic field/electromagnetic sounding data are critical for understanding the Moon's interior [2], but multiple stations are needed across the lunar surface covering a much wider footprint that the Apollo stations did (Fig. 1A).

Importance of the LGN for Lunar Science: Establishing a global geophysical network is critical for understanding the crustal structure within the different lunar terranes [3; Fig. 1B], as well as the deep mantle structure and confirming the tantalizing results about the lunar core [4]. The Moon represents the initial end-member of terrestrial planet differentiation because it is the smallest differentiated body in the inner solarsystem. A globally distributed network of stations, well within terrane boundaries and returning data outlined above, would allow the thermal and chemical nature of the lunar core, mantle and crust to be elucidated.

Implications for Astrohpysics: A relay orbiter would enable not only the emplacement of landers on the farside, but could also radio astronomy because the farside hemisphere is shielded from terrestrial radio interference, and during the lunar night the farside is also shielded from solar emissions. For these reasons, the farside of the Moon has been considered to be an excellent site for low-frequency radio astronomy [5,6]. The two Radio Astronomy Explorer satellites launched in 1968 and 1973 are the only spacecraft to have made low frequency radio measurements in the frequency range of 0.02 to 13.1 MHz. From the collected data (total flux only), these spacecraft could study only solar, Jovian and terrestrial radio emissions [7].

Implications for Exploration: Although not ideal, the Apollo network (Fig. 1) identified issues that have particular relevance for long-term human exploration of the Moon. Of the 4 types of lunar seismic events recorded, shallow moonquakes are the most enigmatic and potentially dangerous for any outpost [e.g., 8]. The Apollo passive seismic network (1972-1977) recorded 28 such events, which are of higher frequency than the other types, and 7 of these were of body wave magnitude ≥5. As the Moon has a much higher seimic Q than the Earth [9], it means the maximum amplitude of moonquakes exist for tens of minutes. While these moonquakes are classified as "shallow," (50-200 km) the exact depths and locations are poorly known because all were outside the Apollo network. Obviously, siting a Moonbase in regions where shallow moonquakes occur would be disastrous! However, the causes of these "high frequency teleseismic events" [10] is unknown. The LGN mission would go a long way to defining the causes and locations of these mysterious and potentially catastrophic seismic events.

References: [1] ILN SDT Report (2009) http://iln.arc.nasa.gov/. [2] Vision & Voyages for Planetary Science in the Decade 2013-2022. NAS http://www.nap.edu/catalog/13117.html. [3] Jolliff et al. (2000) *JGR* **105**, 4197-4216. [4] Weber et al. (2011) *Science* **331**, 309-312. [5] Mimoun et al. (2011) *Exp. Astron.* (in press). [6] Jester & Falcke (2009) *New Astron. Rev.* **53**, 1-26. [7] Alexander et al. (1975) *Astron. Astrophys.* **40**, 365-371. [8] Neal (2005) SRR-LEAG Joint mtg. Abs. 2065. [9] Nakamura & Koyama J. (1982) *JGR* **87**, 4855-4861. [10] Nakamura (1977) *PEPI* **14**, 217-223.

VIRTUAL SWIRLS: HIGHLIGHTS FROM NLSI'S FIRST WORKSHOP WITHOUT WALLS. C.D. Neish[1], S. Besse[2], G. Kramer[3], W. Farrell[4], C. Pieters[5], M. Horanyi[6], Y. Pendleton[7], [1]The Johns Hopkins University Applied Physics Laboratory, Laurel, MD, 20723 (catherine.neish@jhuapl.edu), [2]The University of Maryland, College Park, MD, 20742, [3]Lunar and Planetary Institute, Houston, TX, 77058, [4]NASA Goddard Spaceflight Center, Greenbelt, MD, 20770, [5]Brown University, Providence, RI, 02912, [6]University of Colorado, Boulder, CO, 80309, [7]NASA Lunar Science Institute, Moffett Field, CA, 94035.

Introduction: Swirls are among the most puzzling features on the surface of the Moon. Their bright, looping patterns are unlike anything seen in the solar system (Figure 1). The origin of the lunar swirls has been discussed for many years, but a universally accepted explanation for their formation remains elusive [1,2,3, 4].

Current space missions are returning new views of the lunar swirls, at resolutions and wavelengths never before considered. These new data have the potential to provide tremendous new insights into swirl formation. We therefore organized an informal one day "Workshop without Walls" on lunar swirls using NASA Lunar Science Institute (NLSI) remote communications tools. The workshop was held on September 7, 2011 and was open to interested persons from all over the world. This represents NLSI's first virtual workshop, based on previously successful workshops sponsored by the NASA Astrobiology Institute (NAI).

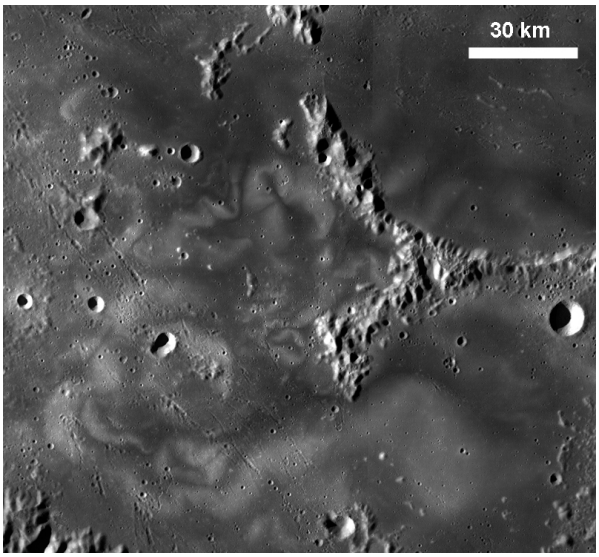

Figure 1: LROC WAC image of the swirls at Mare Ingenii (credit: NASA/GSFC/Arizona State University).

The Workshop: The purpose of the meeting was to bring together an international group of experts from various disciplines (geology, plasma physics, magnetism, remote sensing, etc.) to share their knowledge of the many processes related to lunar swirl formation. In the course of the workshop, it was hoped that we could identify new links between these processes that may explain the origin of the lunar swirls. The processes discussed during the meeting included the origin of lunar magnetic anomalies, the interaction between the solar wind and magnetic anomalies, dust transport, and space weathering. We also presented the latest data from the flotilla of international spacecraft that have been studying the Moon over the last few years. These data provide information about the swirls at wavelengths and resolutions previously unavailable to the scientific community. Complementary laboratory experiments were discussed addressing the charging and mobilization of dust on surfaces, and the interaction of plasma flows with localized magnetic fields.

The workshop featured eighteen presenters from six countries, representing eight instruments on three spacecraft (LRO, Chandrayaan-1, and Kaguya), as well as one future spacecraft (LADEE). In addition, we had over 150 registered participants from 18 countries, who actively engaged in discussions over the phone line and in the online chat window (Figure 2).

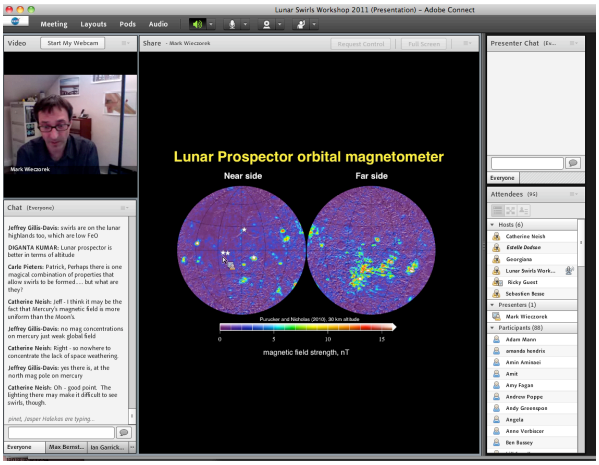

Figure 2: Mark Wieczorek discusses the origin of lunar magnetic anomalies at NLSI's first Workshop Without Walls. A chat window at lower left facilitated discussions between participants during the event.

Results: During the course of the workshop, speakers compared and contrasted the primary models for swirl formation. These include cometary impacts [1], differential space weathering [2], dust levitation

[3], and exo-ion congregation [4]. Experts in fields ranging from remote sensing to plasma physics discussed these theories in the context of new data presented from an international set of investigators. Some of the new results presented during the meeting included:

1) Data from several instruments, including the LROC NAC and Kaguya Terrain Camera (TC), demonstrated conclusively that Reiner Gamma and other swirls lack any observable topography.

2) There is no signature of the swirls in the radar data collected by Mini-RF on LRO, suggesting that the swirls are a surficial coating, less than a meter thick.

3) There is evidence of craters in LROC NAC images that have 'punched through' a thin bright layer to reveal a dark substrate beneath.

4) Data from Diviner on LRO do not indicate substantial thermal anomalies associated with the swirls, inconsistent with the presence of thick deposits of dust.

5) Laboratory experimental results indicated the generation of localized electric fields near magnetic anomalies, and the transport of charged dust near boundaries of lit and dark regions.

6) Several presentations support the idea that swirl material represents some of the most immature material on the lunar surface.

7) Data from the M^3 instrument on Chandrayaan-1 suggests that there is a decrease in OH ions on swirl compared with surrounding regions, implying that whatever process forms the swirls also controls the surficial OH.

8) Kaguya magnetometer data demonstrated that the horizontal component of the magnetic field lines up remarkably well with the surface markings of the swirls, at the 10 km scale.

Although no official consensus was reached during the meeting, much of the data presented above is consistent with an origin for the swirls linked to the interaction between the solar wind and the lunar magnetic anomalies. However, more work will be required to fully understand the origin of the lunar swirls. Some of the future research directions identified in the workshop include:

1) What is the ultimate source of the lunar magnetic anomalies?

2) What is the chronology of swirl emplacement relative to the surrounding geology? How can we use new data available on fresh, small craters to place the swirls in sequence?

3) Why are swirls visible at some magnetic anomalies, but not all magnetic anomalies?

4) What causes the unusually bright albedo characteristic of the lunar swirls? How might laboratory experiments help us to understand this process?

5) How does the magnetic signature at orbital altitudes (> 50 km) map to the detailed swirl structure at the surface?

6) What future missions (either orbital or in-situ) would be required to determine the electrical and magnetic environment at the swirls? What observations could be done from orbit, and what measurements could only be done on the surface?

It is our hope that the presentations and discussions from this workshop will encourage future collaborations between the participants, leading to a new understanding of the enigmatic lunar swirls. The workshop itself will also serve as a model for future meetings, saving time and money by eliminating the need for travel (Figure 3). This is especially important for fostering international collaboration, where travel may be prohibitive to participation.

Figure 3: NLSI Teams from the University of Colorado, Brown University, NASA Ames, and NASA Goddard (clockwise from top left) participated in the workshop using video teleconferencing (credit: E. Dodson).

References: [1] Schultz P.H. and Srnka L.J. (1980) *Nature, 284*, 22-26. [2] Hood L. and Schubert G. (1980) *Science, 208*, 49-51. [3] Garrick-Bethell I. et al. (2011) *Icarus, 212*, 480-492. [4] Keller J. et al. (2011) LPSC XLII, Abstract #1817.

VOLUME OF IMPACT MELT GENERATED BY THE FORMATION OF THE SOUTH POLE-AITKEN BASIN. N. E. Petro, NASA Goddard, Planetary Geodynamics Branch, Greenbelt, MD (Noah.E.Petro@nasa.gov).

Introduction: The South Pole-Aitken Basin (SPA) is the largest, deepest, and oldest identified basin on the Moon and as such contains surfaces that are unique due to their age, composition, and depth of origin in the lunar crust [1-5] (Figure 1). SPA has been a target of intense interest as an area for robotic sample return in order to determine the age of the basin and the composition and origin of its interior [6-8]. In response to this interest there have been several efforts to estimate the likely provenance of regolith material within central SPA [9-12]. These model estimates suggest that, despite the formation of basins and craters following SPA, the regolith within SPA is dominated by locally derived material. An assumption of these models has been that the locally derived material is primarily SPA impact-melt as opposed to local basement material (*e.g.* unmelted lower crust). However, the definitive identification of SPA derived impact melt on the basin floor, either by remote sensing [5, 13] or via photogeology [2, 14] is extremely difficult due to the number of subsequent impacts and volcanic activity [4].

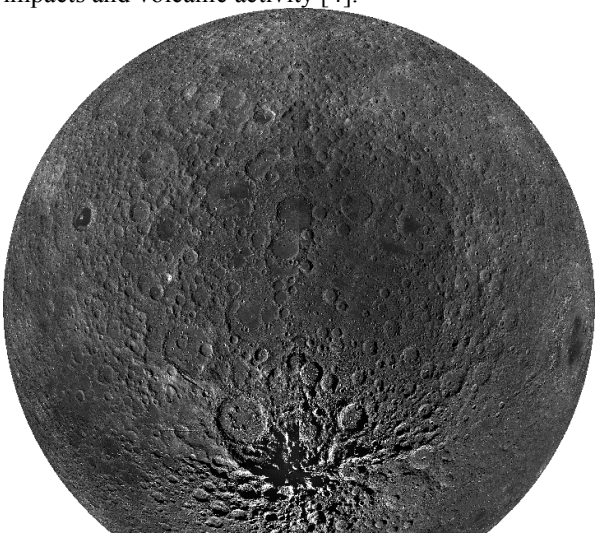

Figure 1. LRO Wide Angle Camera mosaic centered on SPA. Interior of SPA contains several smooth, flat regions (Figure 2), interpreted to contain either ancient mare basalts or SPA melt.

Here, the total volume of impact melt generated by the formation of SPA is estimated based on existing crater scaling models, as well as the relative proportion of melt retained within the basin [15, 16]. The ultimate distribution of melt, based on these models, will also be described.

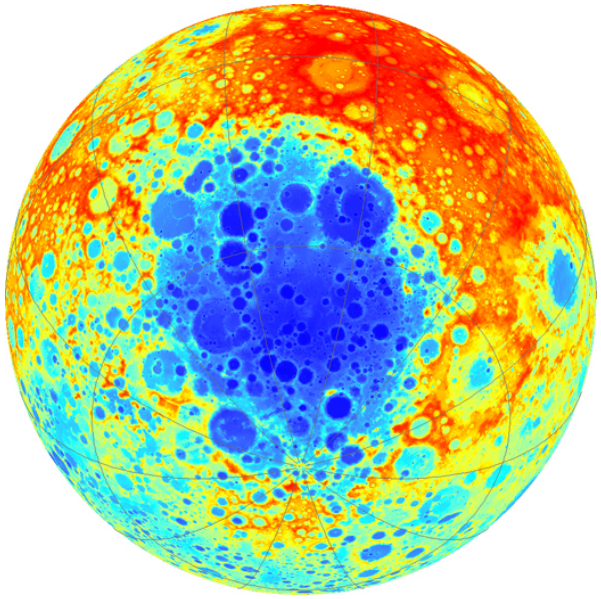

Figure 2. LOLA Topography centered on SPA. Models of impact melt generation predict that the deepest, central portion of the basin is almost completely covered by melt produced by SPA's formation.

Volume of Melt Produced by SPA: Prior studies of the production of SPA impact melt [16] focused on the depth of melting and the possible amount of mantle melted during basin formation. Warren et al. [16] concluded that, assuming a transient cavity 1,170 km in diameter, melt produced by SPA would be nearly completely of mantle origin, and that SPA melt (from both crust and mantle) would comprise approximately one-third of the total ejecta volume. However, how much melt is retained within SPA proper?

Cintala and Grieve [15] state that "…the relative volume of impact melt remaining inside the final crater increases with crater size." Subsequently, they show that, for craters larger than 10 km in diameter, the volume of melt retained within the crater is larger than 40% of the total melt. Extrapolating their data out to a basin the size of SPA (Figure 3), and assuming a transient cavity diameter of 2,099 km [17] suggests that nearly 80% of the impact melt that is produced is retained within SPA. Clearly such models, applied to a basin as large and unusual as SPA, should be treated carefully. However, even if the formation of is more like a smaller basin, then perhaps only 60% of the melt is retained [15]. Even in this extreme case a significant volume of the roughly 8×10^8 km^3 of melt would still be retained. Assuming that 80% of the melt is indeed retained within SPA, that volume is roughly 50% of

the entire volume of the transient cavity. Such melting would likely reach deep into the mantle, which would be incorporated into SPA's melt.

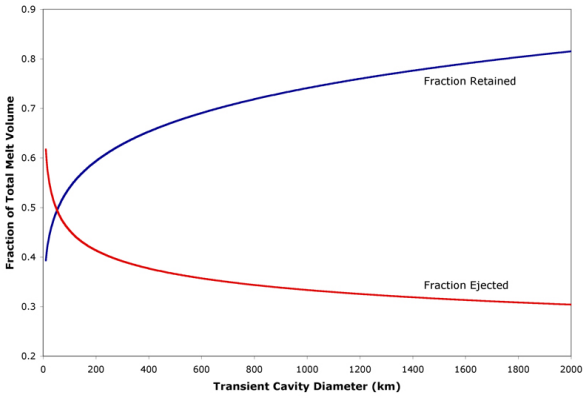

Figure 3. Estimated fraction of melt ejected and retained within the final crater, based on the modeling of Cintala and Grieve [15]. Here the curves have been extended well beyond the original modeling, in order to illustrate the melt fate for a basin as large as SPA.

Melt Distribution Within SPA: As stated above the definitive identification of SPA is difficult, however, by comparison to other large basins, such as Orientale [18], we assume that much of the interior of SPA was covered by impact melt. Based on the above conclusion that much of the melt generated by SPA was derived from the lower crust or upper mantle, we infer that the melt from SPA would be iron rich. Indeed the interior of SPA is well known to be iron rich (Figure 4), yet lacks significant deposits of mare basalt [4, 5, 19, 20]. Some portion of the iron enhancement may be due to ancient basalts [4, 5].

Conclusions: A large volume of material was melted during the formation of SPA, and a significant proportion, a modeled 80% is retained within the basin. The origin of melt, likely lower crust or upper mantle, is a likely source for the iron enhancement across the basin. Given the relatively minor contamination by subsequent events [9, 10, 11], it is very likely that the regolith inside SPA, in many areas, is dominated by melt from the SPA event.

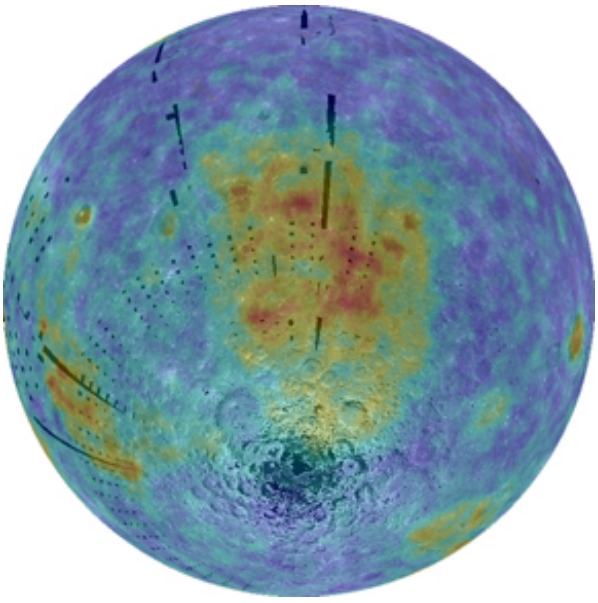

Figure 4. Map of FeO abundance, from Lunar Prospector, showing the enhancement of iron within SPA.

References: [1] Wilhelms, D. E., (1987) *The Geologic History of the Moon*, 327 p. [2] Wilhelms, D. E., et al., (1979) Geologic map of the South side of the Moon, I-1162. [3] Haruyama, J., et al., (2009) *Science*, 323, 905-908. [4] Petro, N. E., et al., (2011) *Recent Advances and Current Research Issues in Lunar Stratigraphy: Geological Society of America Special Paper 477,*, Geomorphic terrains and evidence for ancient volcanism within northeastern South Pole–Aitken basin, doi:10.1130/2011.2477(1106). [5] Pieters, C. M., et al., (2001) *JGR*, 106, 28001-28022. [6] Jolliff, B., et al., (2010) MoonRise: A US Robotic Sample-Return Mission to Address Solar System Wide Processes, 42, [7] Jolliff, B. L., et al., (2010) *AGU Fall Meeting Abstracts*, 43, 01. [8] Jolliff, B. L., et al., (2010) *LPI Contributions*, 1595, 31. [9] Haskin, L. A., et al., (2003) *LPSC*, 34, 1434. [10] Haskin, L. A., et al., (2003) *MAPS*, 38, 13-33. [11] Petro, N. E. and C. M. Pieters, (2004) *Journal of Geophysical Research*, 109(E6), E06004, doi:06010.01029/02003JE002182. [12] Petro, N. E. and B. L. Jolliff, (2011) Basin and Crater Ejecta Contributions to the South Pole-Aitken Basin (SPA) Regolith: Positive Implications for Robotic Surface Samples, 42, 2637. [13] Lucey, P. G., et al., (1998) *JGR*, 103, 3701-3708. [14] Stuart-Alexander, D. E., (1978) Geologic map of the central far side of the Moon, I-1047. [15] Cintala, M. J. and R. A. F. Grieve, (1998) *MAPS*, 33, 889-912. [16] Warren, P. H., et al., (1996) *GSA Special Paper*, 307, 105-124. [17] Wieczorek, M. A. and R. J. Phillips, (1999) *Icarus*, 139, 246-259. [18] Head, J. W., (1974) *Moon*, 11, 327-356. [19] Yingst, R. A. and J. W. Head, (1999) *JGR*, 104, 18957-18979. [20] Jolliff, B., et al., (2000) *JGR*, 105, 4197-4216.

SCIENTIFIC BREAKTHROUGHS FROM THE MOON MINERALOGY MAPPER. C. M. Pieters[1] and the Moon Mineralogy Mapper Team, [1]Department of Geological Sciences, Brown University, Providence, RI 02912 (Carle_Pieters@brown.edu).

Introduction: The Moon Mineralogy Mapper (M^3) is a state-of-the-art visible and near-infrared imaging spectrometer that was a guest instrument on Chandrayaan-1, the Indian Space Research Organization's (ISRO) first mission to the Moon. The instrument was designed to measure the diagnostic mineral absorption bands of solar radiation reflected from the lunar surface with a spatial resolution and coverage to provide geologic context. During operations, M^3 demonstrated excellent instrument uniformity and performance. Although the mission lasted for only10 months, global coverage was achieved in the M^3 low-resolution mode. Unfortunately, the spacecraft thermal environment exceeded requirements, forsing mission operations to be intermittent and under highly variable conditions. The last three months of operation were without star-trackers and from a higher altitude (200km vs 100km). Nevertheless, M^3 was the first imaging spectrometer to orbit the Moon and collect detailed near-infrared spectroscopic data (500 – 3000 nm) for mineral assessment. Highlighted below are examples of the valuable breakthroughs provided by M3 on Chandrayaan-1.

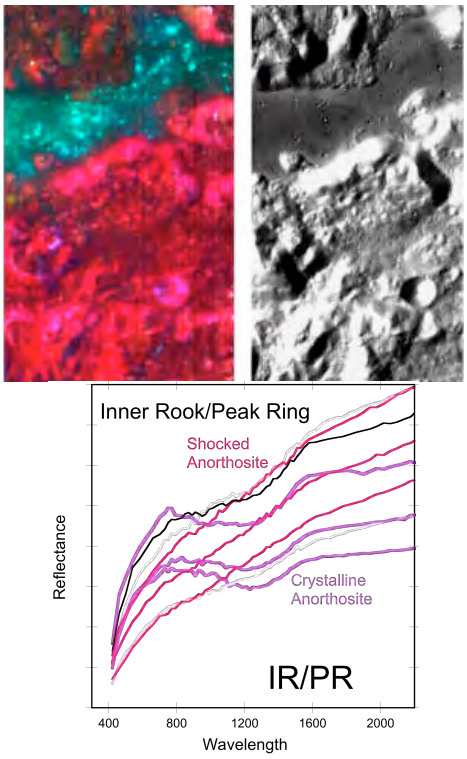

Figure1. **Massive and extensive anorthosite** is identified (in crystalline and shocked anorthosite form) as comprising the Inner Rook Mountains. This exposure is extraordinary strong evidence for the Magma Ocean hypothesis of lunar crust formation. [e.g. Pieters et al 2009, lpsc]

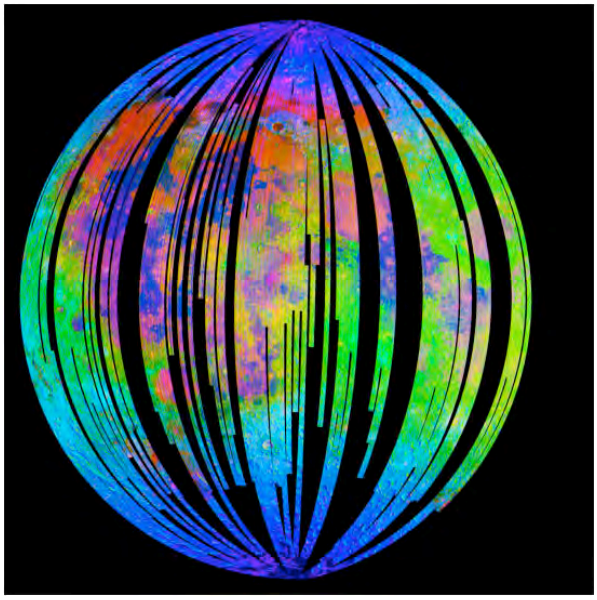

Figure 2. **Surficial OH/H2O** is found to be widespread across the Moon (most readily detected in cooler environments near the poles or terminator). [Pieters et al 2009, Science; Clark 2011, lunar volatiles workshop]

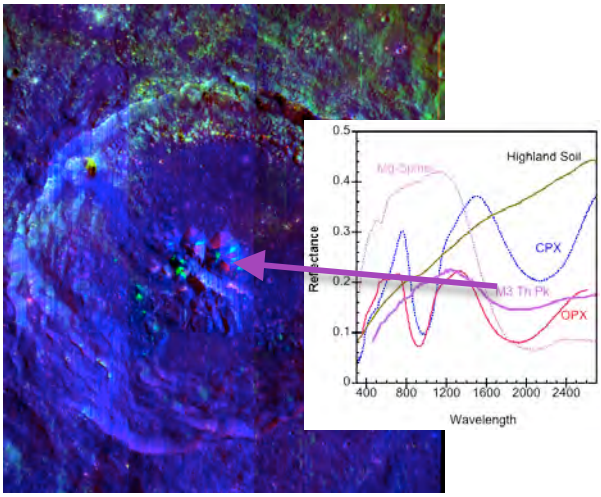

Figure 3. **New Mg-spinel Rock Type** discovered in farside feldspathic Moscoviense Basin and at Theophilius central peaks (shown here) [Pieters et al 2011 JGR; Dhingra et al 2011 GRL] This discovery and its deep-seated origin indicates this new rock type is an important part of lunar crustal stratigraphy.

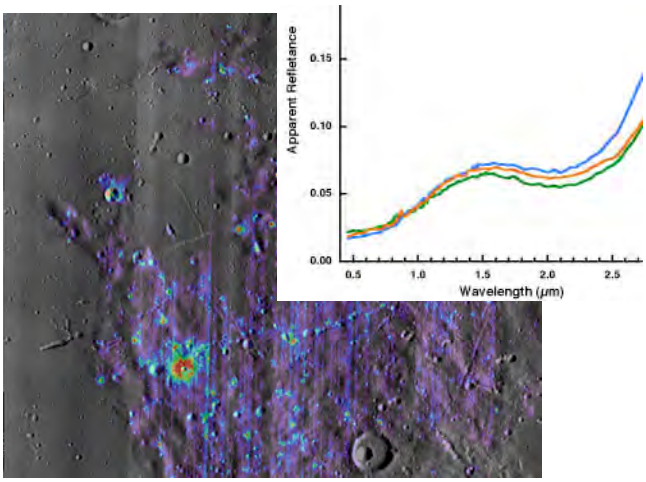

Figure 4. ***New*** **Pyroclastic** ***Mineralogy*** found at regional nearside Dark Mantle Deposits: Cr-spinel dominates the optical properties of Sinus Aestuum DMD. [see Sunshine et al., 2010, lpsc]

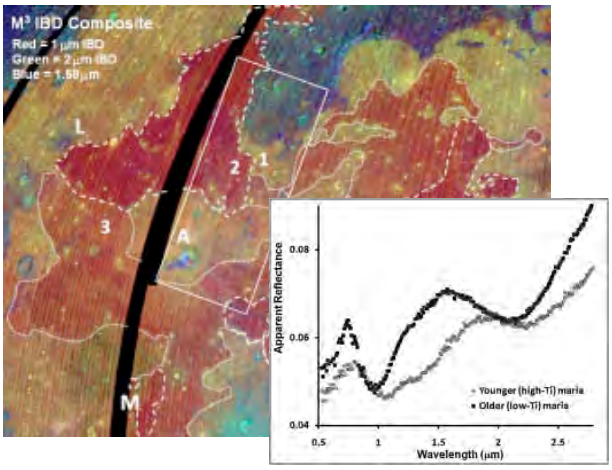

Figure 5. **Young** ***picritic*** **basalts**. The western Ti-rich basalts (red in this composite) contain abundant olivine. [see Staid et al., JGR 2011]

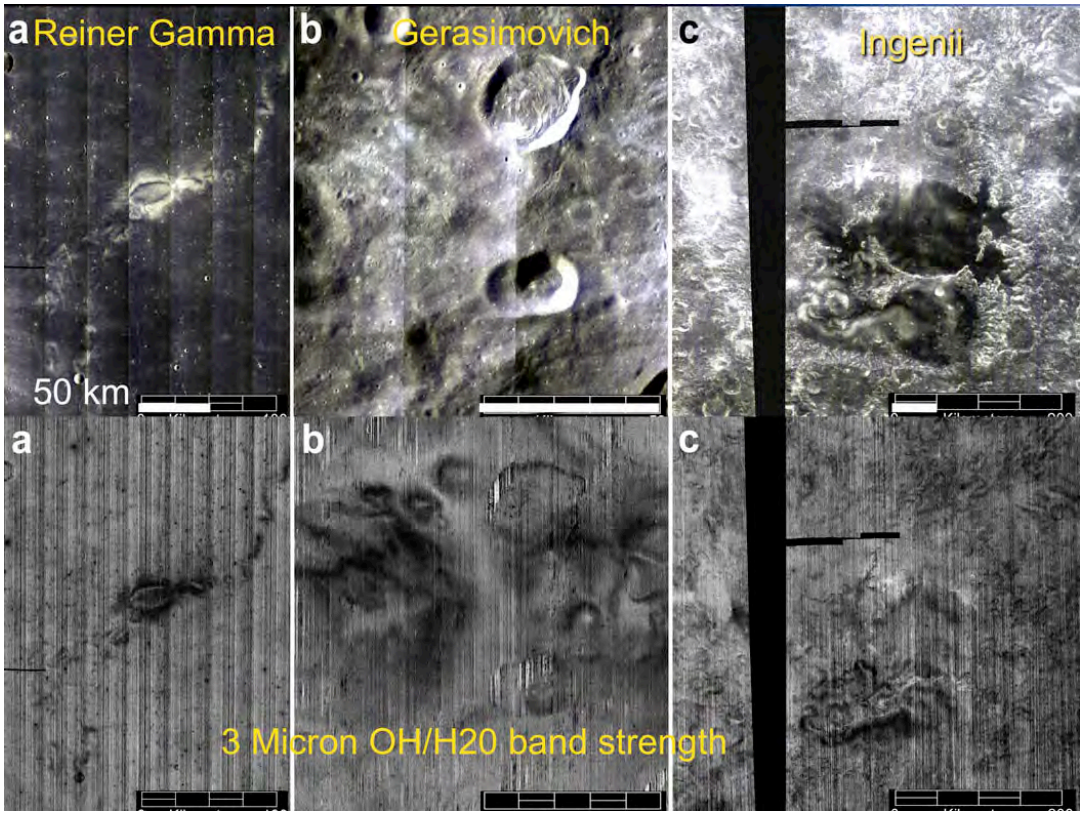

Figure 6. **Dry Swirls**. The high albedo component of lunar swirls are unusually DRY! (linked to local environment). [see Kramer et al., JGR 2011] Scale bar is 50 km in each.

WHAT'S NEXT? BUILDING ON RECENT RESULTS C. M. Pieters[1] [1]Department of Geological Sciences, Brown University, Providence, RI 02912 (Carle_Pieters@brown.edu).

Introduction: After the long awaited pulse of new data from the international armada of missions to the Moon (Kaguya, Changé, Chandrayaan-1, LRO), new discoveries and scientific insights are being revealed in abundance. What is left to do?

LOTS!

As in all good exploration endeavors, this influx of new data and information about the Moon, its surface, and its environment has opened abundant new areas of research and broad fundamental questions that need to be addressed.

This discussion will outline several small to modest missions that address questions that were unknown a decade ago, but now beg to be explored with modern instruments on orbiters, landers/rovers, and with targeted sample return. These are unprioritized examples, but certainly not a complete list!

Rover:

Traverse a swirl. What is the surface texture across bright and dark swirl markings? What is the magnitude of surficial magnetic field and how does it vary across swirl markings? How does the intensity of the solar wind vary across a swirl? How does OH/H2O vary across the swirls? Key experiments include: High resolution stereo camera, in-situ magnetometer, solar wind monitor, dust detector, mass spectrometer, etc.

Landed:

Target nearside sample return. With new lithologies identified in remotly sensed data, several readily accessible nearside areas are excellent targets for automated sample return. Each of the examples below will provide samples that do currently not exist in our sample collections.

Copernicus. The central peaks exhibit diverse deep-seated lithologies: troctolite (olivine + plagioclase), plagioclase, and now also Mg-spinel. In addition, impact melt is widespread and may improve traficability across the floor.

Theophilius. The central peaks exhibit one of the best exposures of Mg-spinel lithology to date.

Sinus Aestuum. This area of regional dark mantling material (volatile driven pyroclastic deposits) contains abundant Cr-spinel either as a crystallized product or as mantle xenoliths.

Young picritic basalt. Several of the western young Ti-rich basalt regions contain extensive olivine and are an important unsampled basalt type.

Orbital:

Track the Water. What is the nature and abundance of the widespread surficial water? How does it vary with time? How is it linked to different surface environments (composition, regolith, temperature, illumination, etc.)? Key experiments include: Next generation Moon Mineralogy Mapper, Thermal infrared imaging spectrometer, Solar wind monitor and particle reflectance, etc.

Read the geologic record at high resolution. What are the primary compositional constituents of the lunar crust? What is their distribution laterally and vertically? What do local, regional, and global geologic relations between lithologies imply about planetary processes active on the Moon? How has the compositional diversity evolved? Key experiments include: Next generation Moon Mineralogy Mapper, Thermal infrared imaging spectrometer, Next generation X-ray spectrometer, etc.

LRO-Lyman Alpha Mapping Project (LAMP) Far-UV Maps of the Lunar Poles. **K. D. Retherford** (1), G. R. Gladstone (1), S. A. Stern (2), A. F. Egan (2), P. F. Miles (1), J. Wm. Parker (2), D. E. Kaufmann (2), D. G. Horvath (1), T. K. Greathouse (1), M. H. Versteeg (1), A. J. Steffl (2), J. Mukherjee (1), M. W. Davis (1), D. C. Slater (1), A. J. Bayless (1), P. M. Rojas (1), P. D. Feldman (3), D. M. Hurley (4), W. R. Pryor (5), and A. R. Hendrix (6); (1) Southwest Research Institute, San Antonio, TX (kretherford@swri.edu), (2) Southwest Research Institute, Boulder, CO, (3) Johns Hopkins University, Baltimore, MD, (4) Johns Hopkins University Applied Physics Laboratory, Laurel, MD, (5) Central Arizona University, Coolidge, AZ, (6) Jet Propulsion Laboratory, Pasadena, CA.

Abstract. Maps of polar far ultraviolet (FUV) albedo are being produced using the Lunar Reconnaissance Orbiter (LRO) Lyman Alpha Mapping Project (LAMP)'s innovative nightside observing technique. Similar dayside FUV maps are also being produced using more traditional photometry techniques. The quality of these maps increases with every UV photon collected from the surface. Importantly, the nightside technique allows us to peer into the permanently shaded regions (PSRs) near the poles, and determine their UV albedos. LAMP measurements indicate ~1-2% surface water frost abundances in a few PSRs based on spectral color comparisons, and we find that many PSRs may have porosities of ~0.9 based on relatively low albedos at Lyman-α [1]. We also briefly report results from a new lab study of the UV reflectance properties of lunar simulants and water ice samples that are helping us pioneer these new techniques in UV spectroscopy for investigating lunar volatiles.

Observations. The LRO-LAMP is a UV spectrograph (Figure 1) that addresses how water is formed on the Moon, transported through the lunar atmosphere, and deposited in permanently shaded regions (PSRs)[2,3]. LAMP far-ultraviolet (FUV) albedo maps are being produced to investigate the intriguing albedo differences that occur within PSRs.

LRO's polar orbit provides repeated observations of PSRs, enabling accumulation of UV signal with the photon-counting LAMP instrument over these locations. Lyman-α albedo maps obtained during the nominal ESMD mission and part of the first SMD mission phase (Sept. 2009 to Feb. 2011) are shown in Figure 2 for the north and south poles.

Figure 1: LAMP instrument prior to LRO integration.

The LAMP instrument covers the 57-196 nm passband. Its 6°×0.3° slit, nominally pointed nadir, scans the surface in push-broom style, similar to other LRO instruments. LAMP routinely observes the Lunar nightside. The lunar dayside is also observed by switching to a pinhole mode following terminator crossings each orbit.

LAMP data products include nightside brightness maps of polar regions over specific wavelength ranges, similarly constructed albedo maps (i.e., brightness maps normalized by the varying illumination), and on-band to off-band ratio maps (i.e., on and off the expected FUV absorption band for water frost). See refs. [1&4] for details on how the maps are created. LAMP nightside maps are produced monthly, and these are combined for best-quality compilations as shown in Figure 2. A few instrument-related artifacts are removed as part of our data calibration and mapping pipelines, with time-dependent microchannel plate detector gain sag and low pulse amplitude signals the primary (flat-field) issues being remedied.

Current Results. The Lyman-α albedo maps shown in Figure 2 reveal lower albedo (darker blue here) regions within craters. The lower albedo regions are roughly correlated with the coldest PSR regions. This albedo darkening at Lyman-α is consistent with high porosity (~0.9), based on modeling using functions described in Hapke 2008 [3]. Maps of reflected starlight at wavelengths longer than Lyman-α (121.6 nm) are also produced. They are of lower signal quality owing to the dimmer source of light at these wavelengths and the need to subtract detector background. However, regions within these longer wavelength maps are averaged over known PSR areas [6] to provide reasonable comparisons with models of lunar surface reflectance [7]. We find the spectral variations of a few PSRs are well fit with 1-2% water ice abundances. This water ice necessarily resides directly on the surface. Revised estimates of the long-term stability of water frost to UV-photolysis reinforce this conclusion [1].

Polar maps of dayside FUV albedos will be presented. Comparisons between the nightside and dayside photometry techniques used for producing these respective maps help validate the use of Lyman-α and starlight as illumination sources. Similarly, a new lab

study of the FUV reflectance properties of lunar simulants and water ice samples is underway to further characterize the UV photometry and test our photometry model-based conclusions. Initial maps of the equatorial region are also currently being computed. All of these LAMP map products are being compared with other LRO datasets to search for large scale trends and for interpretation of a few key sites [4].

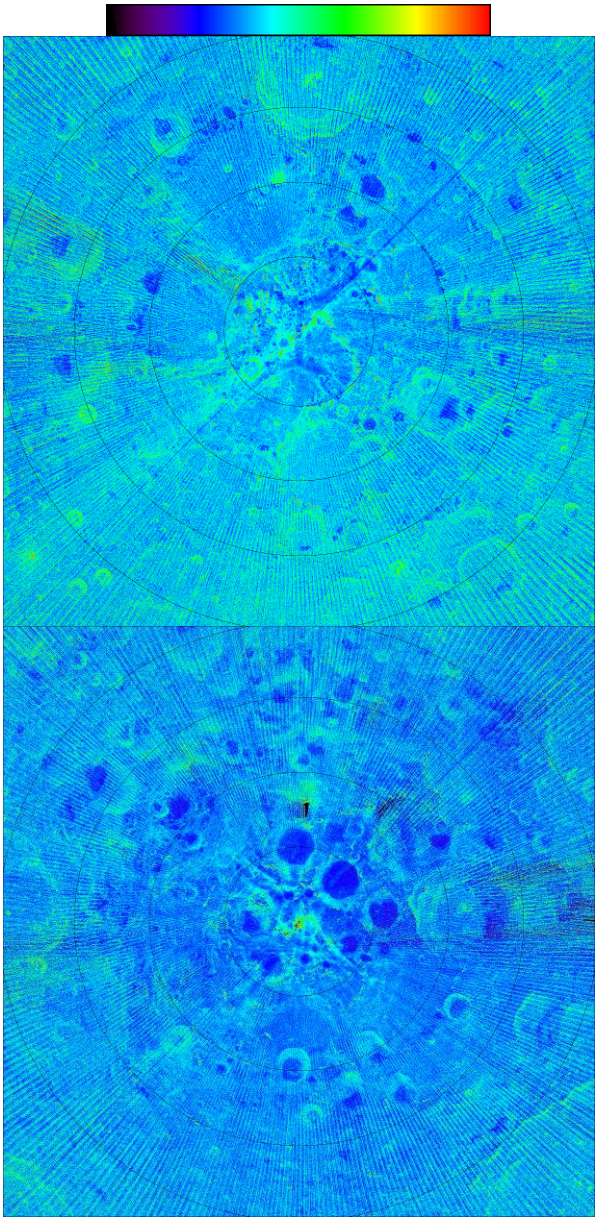

Figure 2: LAMP Lyman-α albedo maps, North (top) and South (bottom). Black circles indicate 2.5° latitude increments from the poles. Color-bar runs from 0 to 10% albedo.

Extended Mission. We plan to capitalize and expand upon these recent discoveries in the proposed LRO mission extension through Sept. 2014. More EUV/FUV data (60-190 nm) at a variety of incident and emission angles is needed to improve signal, spectral, and photometric quality and further develop our innovative nightside UV reflectance technique for determining surface porosity. We plan to target UV-interesting regions and focus on key PSRs identified by LRO/LEND and MiniRF as potentially water-rich to obtain these crucial data with improved sensitivity. Global searches of water signatures *outside of PSRs* with LAMP will confirm and/or elucidate the findings of surface water/hydroxyl and its variability with infrared Chandryaan-M3/Cassini-VIMS/EPOXI data. EUV (60-110 nm) albedos, photometry, and potential space-weathering signatures of solar system bodies are largely unknown – LAMP Moon measurements with better EUV calibration in the extended mission will be the baseline for comparative studies, and will aide calibration for all EUV astronomy. Collaborative LAMP-Juno/UVS observations are planned in 2013 when these similar spectrographs will provide a unique, simultaneous two-angle vantage point for understanding the phase angle influence on EUV/FUV photometry.

References

[1] Gladstone, G. R. et al., Far-Ultraviolet Reflectance Properites of the Moon's Permanently Shadowed Regions, submitted to *JGR*, 2011.

[2] Gladstone, G. R., and 15 coauthors, LAMP: The Lyman Alpha Mapping Project on NASA's Lunar Reconnaissance Orbiter Mission, *Space Sci. Rev., 150*, 161-181, 2010.

[3] Gladstone, G. R. et al., LRO-LAMP Observations of the LCROSS Impact Plume, *Science, 330,* 472-476, 2010.

[4] Retherford, K. D., et al., LRO/LAMP Far-UV Albedo Maps of the Lunar Poles, in prep, 2011.

[5] Hapke, B. Bidirectional reflectance spectroscopy 6. Effects of porosity, *Icarus, 195*, 918–926, 2008.

[6] Mazarico et al. 2011, Illumination conditions of the lunar polar regions using LOLA topography, *Icarus, 211*, 1066–1081.

[7] Mishchenko, M. I., et al., Bidirectional reflectance of flat, optically thick particulate layers: An efficient radiative transfer solution and applications to snow and soil surfaces, *J. Quant. Spectrosc. Rad. Transf., 63*, 409–432, 1999.

THE LUNAR RECONNAISSANCE ORBITER CAMERA: TWO YEARS EXPLORING THE MOON. M. S. Robinson[1] and the LROC Team, [1]School of Earth and Space Exploration, Arizona State University, Tempe, AZ.

Introduction: The Lunar Reconnaissance Orbiter Camera [**1**] acquired its first Wide Angle Camera (WAC) image of the Moon 30 June 2009 at 15:08:17.555 UTC and its first Narrow Angle Camera (NAC) on the same day a few minutes later (15:11:03.741 UTC). Since that exciting day the WACs have returned over 183,630 images and the NACs 408,287 images. Of these 114,000 WAC images and 367,000 NAC images cover the illuminated surface (as of 14 September 2011). The remaining observations are of the night side and looking into space (including Earth views) for calibration purposes.

The WAC images represent more than twenty complete near-global maps with pixel scales of ~100 m, each with unique lighting conditions, comprising the most complete photometric dataset [**2**] for any Solar System body besides the Earth. Since the WAC field-of-view (61° in color mode) has >50% overlap at the equator global stereo coverage exists providing the means to complete a 100-m pixel scale near-global Digital Elevation Model (DEM) [**3**]. Due to persistent shadowing at the poles the DEM covers latitudes 80°S to 80°N (*Fig. 1*).

From the 50-km mapping orbit the NACs have imaged 34% of the equatorial region (45°S to 45°N) with pixel scales ~50 cm. Within that same equatorial region 17% of surface was imaged with beta angles (angle between the Sun line and spacecraft orbit plane) less than 45° (high Sun) and 20% coverage for beta angles between 45° and 80°. Total coverage of the equatorial region with beta angles 0° to 80° is 34%. By slewing the spacecraft from two orbits and imaging the same area the NACs have returned over 750 stereo observations. The stereo pairs enable DEM production with 1.5-m to 2.0-m pixel scales and elevation precision of 1-m and accuracy better than 10-m (*Fig. 2*) [**4**].

These new data have lead to many discoveries, and will continue to do so for decades to come. A few highlights are presented in the following paragraphs.

Impact Melt: LROC NAC images of fresh impact melts show well-preserved sub-meter detail [**5**]. For craters smaller than 15-km in diameter impact melts can occur as thin veneers, ponds, sheets, or lava-like flows. Two types of impact deposits have been identified: 1) a lower reflectance and smooth material (LSM), and 2) deposits of moderate to higher reflectance and often rubblier material (MRM). Melt ponds often have variable albedo, both from crater to crater and sometimes within the same crater. LSM ponds typically appear fresh, with no superposed craters from later impacts, have smooth and undulating surfaces, and often have cooling cracks. MRM floor deposits occur as flat-lying, hummocks, or mounds, implying that there may be different types of MRM associated with impact craters. In some craters, LSM melt veneer coats the crater interior on the side opposite the most prominent LSM exterior melt, consistent with an oblique impact. Impact melt flows have been identified within one crater diameter of impact craters as small as 3-km in diameter. Craters with floor MRMs more frequently have superposed craters, suggesting that some MRM craters may be older than those with LSM. Impact melts can be used to infer the properties of the target material, and can be used to infer freshness of an impact crater. Small mare and highlands craters allow investigation of the influence of target material and strength on the development and distribution of impact melt and interior deposit morphology.

Farside Extensional Tectonism: Linear and arcuate rilles associated with nearside basins are related to extensional stresses induced by the mare fill. This basin-related extension ceased at ~3.6 Ga while contractional tectonic activity that formed mare ridges continued to ~1.2 Ga. Although small-scale, relatively young (<1 Ga) contractional lobate scarps were previously known, no evidence of extensional landforms in the highlands beyond the influence of mare filled basins were known to occur. NAC images reveal small-scale graben in the farside highlands and in nearside mare basalts. The lack of superposed craters, crosscut impact craters with diameters as small as ~10 m, and depths as shallow as 1 m suggest these graben are <50 Ma. In order for the small-scale graben to form, extensional stresses must locally exceed the global compressional stress that resulted in the young lobate scarps. The formation of these young graben suggests relatively low compressional background stresses [**6**].

Farside Silicic Volcanism: Images from the Wide and Narrow Angle Cameras and derived DEMs provide evidence that a small volcanic complex occurs at the center of the Compton-Belkovich "thorium anomaly." Morphologies seen at high resolution, including domes with slopes exceeding 20° and collapse features, are consistent with a near-surface intrusion that developed late-stage silicic lavas, which then erupted to form domes ranging from 500-m to 6-km base diameters. Comparison of the topographic expression of this volcanism and bright reflectance associated with silicic material further suggests some pyroclastic dispersal of late-stage material. The Compton-Belkovich volcanic complex is the only known occurrence of silicic volcanism on the lunar farside [**7**].

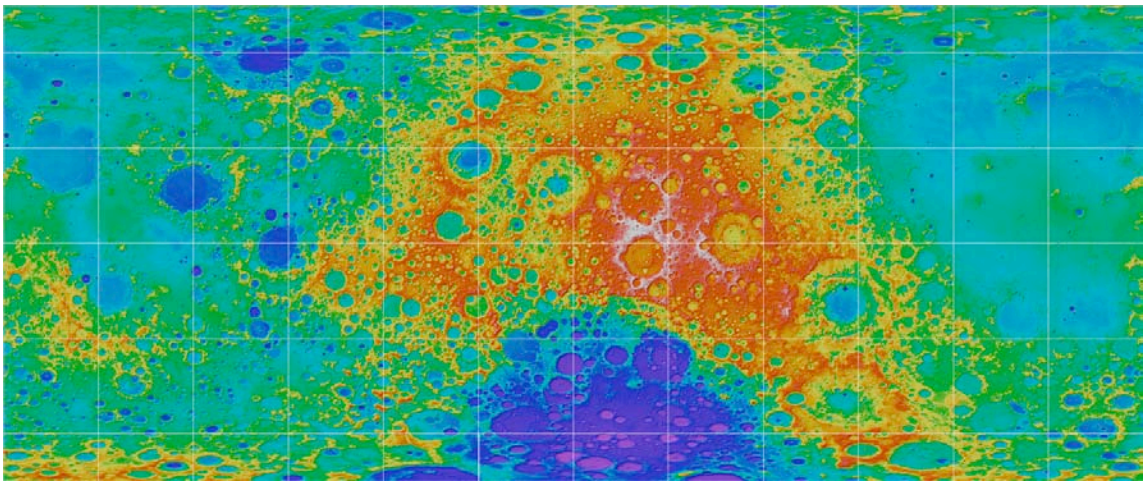

Figure 1. LROC WAC DEM from 75°S to 75°N and 0-360°E, full resolution product is sampled at 100 m.

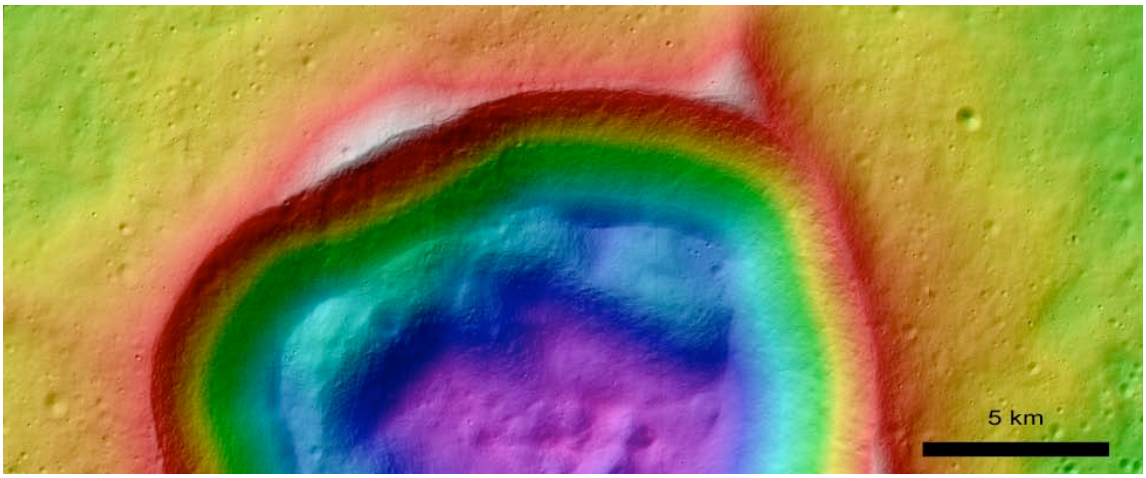

Figure 2. Small portion LROC NAC stereo-derived DEM of central Lichtenberg crater, total relief is 2831 m.

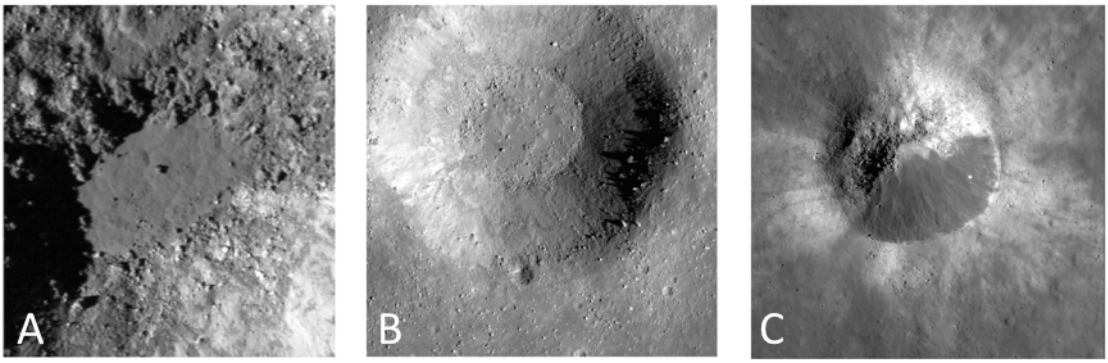

Figure 3. A) A fresh, smooth ~100 m LSM melt pond in a 700-m crater exhibiting an undulatory surface texture. **B)** A 940 m crater with MRM floor deposits, crater superposed on the rim, and less visible ejecta rays. **C)** A fresh 550 m crater with asymmetric distribution of melt veneer.

References: [1] Robinson, M. S. et al. (2010) *Space Sci. Rev., 150*, 81-124. [2] Sato, H. et al (2011) *LPSC*, abstract 1974. [3] Scholten, F. et al. (2011) *LPSC*, abstract 2046. [4] Tran, T. et al. (2010) *ISPRS Commission VI, WG VI/4*, abstract. [5] Stopar et al, this meeting. [6] Watters et al, *Nature Geosciences*, in press. [7] Jolliff et al. (2011) *Nature Geosciences* 4, 566–571.

INTREPID: LUNAR ROVING PROSPECTOR PROVIDING GROUND TRUTH AND ENABLING FUTURE EXPLORATION. M. S. Robinson[1], S. J. Lawrence[1], E. J. Speyerer[1], J. Stopar[1], School of Earth and Space Exploration, Arizona State University, Tempe, AZ (mrobinson@asu.edu).

Introduction: As noted by the Decadal Survey and the Lunar Exploration Roadmap [1,2], critical science and exploration measurements are needed from the lunar surface. Orbiting spacecraft (i.e. Lunar Reconnaissance Orbiter (LRO), Clementine, Lunar Prospector, and others) and impactors like the Lunar Crater Observation and Sensing Satellite (LCROSS) were designed to provide key information about potential landing sites, identify potential resources, and characterize the lunar regolith. However, these missions cannot provide the ground truth required to tie these remote sensing datasets to physical characteristics on the lunar surface. We propose a Lunar Roving Prospector, *Intrepid*, to collect essential measurements to address key scientific questions, obtain important measurements to enable future human exploration, and demonstrate technology required for future exploration of the Moon and other terrestrial bodies.

Science Measurement Objectives: The Intrepid rover will investigate twenty major (and hundreds of minor) scientific sites over 1000 km during two Earth years. This mobility will enable Intrepid to acquire measurements over a broad areas and address many key scientific objectives, including:

- Provide ground truth for all terrain types measured by orbiting spacecraft.
- Characterize the composition of the components of the lunar regolith in order to provide important constraints on the lithologic diversity of the crust.
- Characterize the lunar surface to investigate volcanic processes and increase our understanding of the evolution of the lunar crust.
- Investigate and quantify possible magnetic anomalies and lunar surface swirls.
- Create a sample cache that could be retrieved by future human and robotic exploration systems.

Exploration Opportunities: In addition to providing key measurements for scientific studies, Intrepid will provide measurements essential for future robotic and human missions to lunar surface, including:

- Detect, assay, and map potential resources (identifying and quantifying ISRU potential).
- Quantify the nature of dust, its environments, and interactions with systems.
- Measure the radiation environment (primary and secondary) present on the lunar surface.

Mission Concept: The *Intrepid* rover is designed to be highly mobile with a baseline traverse of over 1000 km, over a two year nominal mission. This long range rover enables measurements to be collected over a variety of geologic terrains (i.e. mare and highlands). To enable this mobility, Intrepid is designed to acquire measurements in three traverse modes: cruise, roam, and focused investigation. In the cruise mode, in which Intrepid will predominately be traveling to different discrete scientific sites, the rover will mainly take measurements while in motion (for example, passive magnetometer measurements). However, infrequent stops will be made to provide basic measurements that cannot be acquired while the rover is motion (i.e. Pancam, LIBS – ChemCam, etc.). In the roam mode, the rover will make more frequent stops during its traverse to acquire more science measurements. In the focused investigation mode, Intrepid will acquire measurements with a higher frequency (less than every 10 meters) to enable focused analysis of the scientific sites of interest. An advanced sliding autonomous navigation system will enable the rover to traverse in all three operating modes with little interaction with human drivers. However, humans will be able to intervene if sites of opportunities are identified in the live feeds.

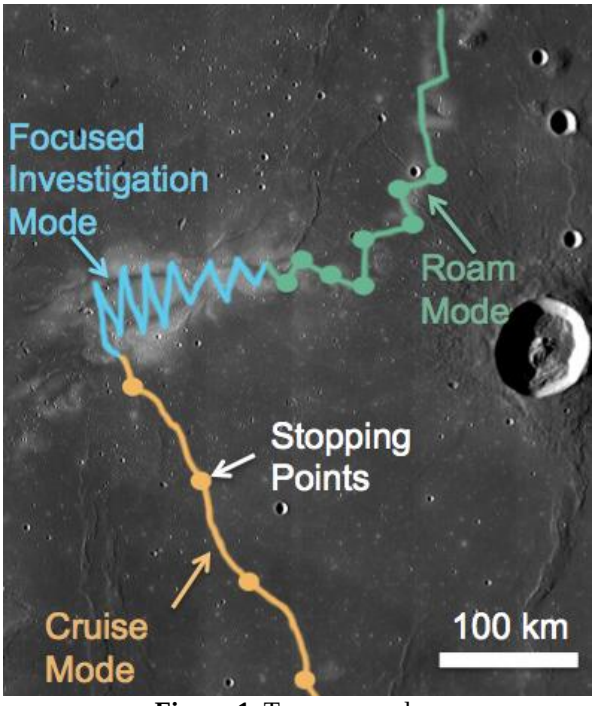

Figure 1. Traverse modes

Notional Instrument Suite: The proposed emphasis on mobility in the Intrepid concept makes stand-off measurements a critical concept for Intrepid operations. We have baselined a notional instrument suite consisting of a multispectral stereo imaging system, a narrow angle FARCAM for long-distance imaging of potential targets, a Raman spectrometer, an APXS for major element chemistry determinations, a magnetometer, and a radiation environment sensor.

Traverse Options: With a range of 1000 km, a series of high-priority targets will answer both scientific and exploration questions in a single mission. Leveraging data returned by the Lunar Reconnaissance Orbiter, we are in the process of defining several high-value scientific traverses on the lunar nearside. For example, one high value traverse initiates in southern Oceanus Procellarum near the Reiner Gamma Constellation Region of Interest, continues through the Marius Hills volcanic complex, proceeds northward along the youngest mare basalts as defined by crater statistics [3], and concludes with an in-depth exploration of the Aristarchus plateau. This traverse would include diverse lithologies, regions of unexplained albedo, color, and magnetic anomalies, a full range of lunar volcanic types and ages, and includes four Constellation Regions of Interest (Reiner Gamma, Marius Hills, Aristarchus 1 and 2), providing critical data for further scientific studies.

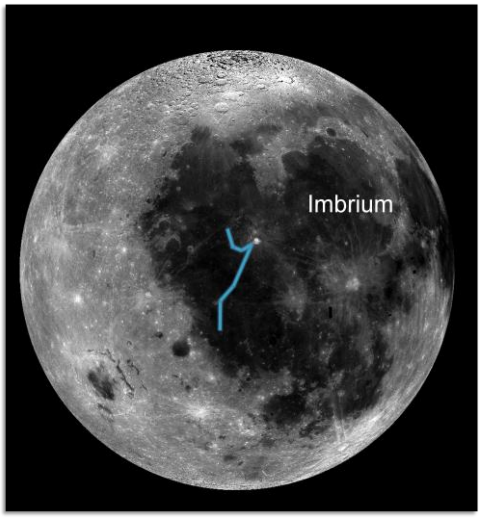

Figure 2. Traverse option for the Intrepid rover

Rovers offer many operational advantages over static landers, which lack the capability to perform investigations beyond a limited distance from the original landing site. Intrepid offers the flexibility and the capability to perform wide-scale investigations that characterize the composition and properties of the lunar regolith over hundreds of square kilometers to address key science and exploration objectives. For example, with respect to studies designed to address in-situ resource utilization assessment, mobility allows assessment of *grade and tonnage* of an ore body – essential information for planning ISRU.

Opportunities to Develop Technologies: Future explorers (to the Moon and beyond) will require new technologies, and the Moon is an ideal location to develop and validate them. One of the highest priorities identified in the decadal survey for near-term multi-mission technology investment is for the completion and validation of the Advanced Stirling Radioisotope Generator (ASRG). An ASRG/solar hybrid rover enables electronics to survive and operate in the extreme lunar environment. In addition, Intrepid offers other opportunities to test technologies essential for future robotic and human exploration, including precision autonomous landing instrumentation, automated precision landing systems and surface navigation, instrument development, and tele-operations.

Leveraging existing remote datasets: In the past two decades, orbital satellites have collected datasets essential for planning future missions to the Moon. One of the main objectives of LRO is to provide datasets to enable future ground based exploration activities. The Lunar Reconnaissance Orbiter Camera (LROC) acquires high-resolution and synoptic images that provide high resolution maps, digital elevation models, and illumination maps. Datasets from other instruments onboard LRO and other satellites (Clementine, Lunar Prospector, Chandrayaan, Chang'e, SMART-1, and future orbiters) will be used in traverse planning and identifying features of scientific and exploration interest and potential hazards that could disrupt rover operations.

Participatory Exploration: The proposed Intrepid rover has outstanding opportunities for immersive public engagement with both passive (live high-definition video streams, 3-D surface panoramas, and daily views of Earth) and participatory (remote rover driving and imaging, collective data analysis, and communication via social media) participation throughout the two-year nominal mission. Intrepid operations and data analysis will also contribute to developing NASA's future workforce (undergraduates, graduates, and postdocs).

References: [1]Committee on the Planetary Science Decadal Survey; National Research Council, 2011 [2] LEAG Exploration Roadmap (2011) [3] Hiesenger et al. (2010), *J. Geophys. Res., 115, E03003.*

The Lunar Radiation Environment from the Cosmic Ray Telescope for the Effects of Radiation (CRaTER) and from Earth-Moon-Mars Radiation Environment Modules (EMMREM)

N. A. Schwadron[1], A. W. Case[2], M. Golightly[1], A. Jordan[1], C. Joyce[1], J. Kasper[2], K. Kozarev[2], J. Mazur[3], J. Mislinski,[1] H. E. Spence[1], L. W. Townsend[4] , and J. Wilson[1]

[1] Univerisity of New Hampshire, Institute for the study of Earth, Oceans and Space (8 College Road, Durham NH, n.schwadron@unh.edu);
[2] Harvard-Smithsonian Center for Astrophysics, Cambridge, MA 02138, USA;
[3] The Aerospace Corporation, CH3/210, 15049 Conference Center Drive, Chantilly, VA 20151
[4] Department of Nuclear Engineering, University of Tennessee, Knoxville, Tennessee, USA

The Cosmic Ray Telescope for the Effects of Radiation (CRaTER) is actively measuring lineal energy transfer by Galactic Cosmic Rays (GCRs) and Solar Energetic Particles (SEPs) on the Lunar Reconnaissance Orbiter (LRO) Mission, which is in a near cirular, polar lunar orbit. Major advances in physics-based numerical models of the coupled Sun-to-Earth system now provide unprecedented opportunities to predict the lunar radiation environment and to compare these predictions with CRaTER observations. The Sun is slowly emerging from a deep and prolonged solar minimum between solar cycles 23 and 24. The Galactic Cosmic Ray (GCR) levels remain at almost the highest levels ever observed during the space age, while activity has just begun to elevate as we observe some of the first Solar Energetic Particle (SEP) events from the this peculiar solar cycle 24. To date, the largest SEP event observed by CRaTER occurred on June 8, 2011 (day-of-year 157). We compare model predictions by the Earth-Moon-Mars Radiation Environment Module (EMMREM) for both dose rates from GCRs and SEPs during the June 8 event with observations from CRaTER. We demonstrate the remarkable agreement between these models and the CRaTER dose rates, which shows the accuracy of EMMREM, and its suitability for a real-time space weather system. We find further that flux levels of GCRs and their associated dose rates were likely at the highest levels in the space age very near the time that CRaTER began taking data. This maximum in GCR dose rate observed by CRaTER in mid-2009 was almost 60% higher than the previous solar maximum GCR dose rate of in 1998 in the solar minimum between cycles 22 and 23. These historic highs in GCR dose rates in the anomalously long and deep solar minimum between cycles 23 and 24 reinforce the fact that the Sun and space environment are experiencing remarkable changes.

Exploring a "New" Moon Now and Preparing for Future Lunar Exploration. A Consortium Study of "Special" Lunar Samples. C.K. Shearer[1], C.R. Neal[2], R. Christoffersen[3], L. P. Keller[3], S. J. Clemett[3], and S.K. Noble[4]. [1]Institute of Meteoritics and Department of Earth and Planetary Sciences, University of New Mexico, Albuquerque, NM 87131 (cshearer@unm.edu). [2]University of Notre Dame, Notre Dame, IN 46556. [3]NASA Johnson Space Center, Houston, TX 77058. [4] NASA Goddard Space Flight Center, Greenbelt, MD 20771.

Introduction: The results from a variety of recent lunar missions carried out by NASA and other national space agencies together with numerous terrestrial laboratory studies provide a new view of the Moon that differs from assessments made prior to and immediately following the Apollo Program. This new view of the Moon will influence the further human exploration of the Moon and beyond. For example, many of these new missions and studies have questioned our understanding of the characteristics and distribution of lunar volatile reservoirs. By reducing launch mass to the lunar surface in support of human exploration, along with other benefits these volatile reservoirs could be a high value resource for future human exploration and eventual colonization [e.g. 1-3]. In addition, deciphering the origin and composition of these reservoirs has a high science value that is fundamental to understanding early Solar System processes and the evolution of the Earth-Moon system. The collection and return of new samples from robotic missions specifically designed to further understand these new scientific and exploration views of the Moon would be valuable, but appears unlikely in the near future. However, the far-sightedness of those associated with the Apollo Program over 4 decades ago has resulted in the preservation of potentially important samples that have current scientific and exploration importance. These "special" lunar samples may provide guidance for future decades of lunar exploration. The purpose of this abstract-presentation is to (1) identify potential science and engineering studies of these samples that could be conducted in a consortium framework, and (2) illustrate pathways for studying these valuable samples.

Special samples: During the Apollo Program samples were returned to Earth in several different types of sample containers. The containers were designed based on several requirements, but the success in meeting these requirements was variable [4,5]. Details of samples containers were documented by [4] and a list of examples follows: (1) A large volume of lunar samples were returned in Apollo Lunar Sample Return Containers (ALSRC). Two ALSRCs were used on each Apollo mission. (2) Drive tube core samples were sealed in a Core Sample Vacuum Container on the A-16 and A-17 missions. (3) The Special Environmental Sample Container was designed to ensure that samples were not exposed to terrestrial atmosphere or spacecraft cabin gases. (4) The Gas Analysis Sample Container used on A-11 and A-12 was designed to hold a small amount of lunar soil within a large volume. On Earth, most samples were stored under specific conditions selected to limit contamination and best preserve their integrity [5]. However, a subset of samples was stored under significantly different conditions for over 38 years (i.e. freezer samples, stored in He or vacuum). Some of these uniquely collected, stored, and curated lunar samples remain unopened and unstudied. They are very relevant to both current missions and future sampling as they potentially preserve lunar characteristics no longer preserved in most of the Apollo collection. Further, they illustrate alternative approaches to sampling and curating lunar materials.

Consortium studies:

Science goals. The first goal is to evaluate the nature of the samples to see if they are (relatively) uncompromised. If they are, a large number of measurements may be made that will provide a better understanding of volatiles on the lunar surface. For example: (1) gas composition in the container head space; (2) solar wind volatile species, some of which may be weakly bound to mineral surfaces; (3) volatile species in the lunar regolith that have limited terrestrial contamination; (4) other environmentally sensitive or fragile surface coatings on mineral and glass surfaces.

Exploration and engineering goals. The study of "special" samples provides high value for engineering and exploration as sample handling, processing, and experimental design can be taken into account these goals. For example: (1) reactivity of mineral surfaces that may be highly relevant to health issues and resource issues, (2) resource exploration (3) organic background for planetary protection, (4) dust studies, (5) design of sample containers that will preserve environmentally sensitive planetary samples.

Access to samples for consortium studies: Any consortium assembled to study these special samples will be required to provide a well-defined science and engineering rationale. A consortium study must define sample handling-processing protocols that will not compromise samples and define a logical sequence for conducting analyses-experiments.

References: [1] Jolliff et al. (2007) LEAG Workshop on Enabling Exploration. abst. # 3056. [2] Neal et al., (2007) LEAG Workshop on Enabling Exploration. abst. # 2109. [3] Committee on the Scientific Context for Exploration of the Moon, National Research Council (2008) 97pp. [4] Alton (1989) JSC-23454 97pp. [5] Lofgren (2011) Wet-Dry Moon Workshop, abst. # 6041.

Chlorine isotope composition and carbon mineralogy of "rusty rock" 66095. Implications for the petrogenesis of rusty rock, origin of "rusty" alteration, and volatile element behavior on the Moon. C.K. Shearer[1,2], Z.D. Sharp[2], F. McCubbin[1,2], and A. Steele[3]. [1] Institute of Meteoritics, Department of Earth and Planetary Sciences, University of New Mexico. Albuquerque, New Mexico 87131 (cshearer@unm.edu), [2] Department of Earth and Planetary Sciences, University of New Mexico. Albuquerque, New Mexico 87131, [3] Geophysical Laboratory, Carnegie Institute of Washington, Washington DC 20015

Introduction: "Rusty Rock" 66095 has yielded significant confusion concerning its origin, yet it has and will continue to reveal significant insights into the behavior of volatiles on the Moon. Most of 66095 is composed of a fine-grained, subophitic to ophitic impact melt-rock, which also contains a wide variety of lithic clasts [1,2]. Alteration is found in the interior as well as on the surface of 66095. A brownish alteration extends from margins of metallic iron grains into the adjacent silicates and consists of a variety of relatively low-temperature minerals [1-6]. The origin of this alteration and hydrogen and oxygen isotopic signatures have been attributed to alteration on the Moon [7,8] to "terrestrial" alteration during or following transport to Earth [4,9]. Another interesting aspect of 66095 is its enrichment in ^{204}Pb, Cd, Bi, Br, I, Ge, Sb, Tl, Zn, and Cl indicating that portions of this sample contain substantial sublimates [e.g.10-14]. The chloride mineralogy has not been fully described [8]. The origins of these enrichments have been attributed to fumarolic-hydrothermal [14], magmatic, or impact processes [11,12]. Here, we examine the Cl isotope composition of 66095 and selected regolith at the Apollo 16 site and the carbon mineralogy of 66095 to gain additional insights into the petrogenesis of the rusty rock, the origin of the "rusty" alteration, and transport of volatiles in the lunar crust and on the lunar surface.

Analytical Approach: The δ^{37}Cl (Where $\delta^{37}Cl = (R_{sample}/R_{standard} - 1)1000$ and $R = {}^{37}Cl/{}^{35}Cl$) was determined for 66095 and A16 soils using the method of Sharp et al [15]. All data are reported relative to SMOC (Standard Mean Ocean Chloride with a δ^{37}Cl value of 0‰). The carbon mineralogy of 66095 was explored using Raman Spectroscopy following the approaches outlined in Steele et al. [16].

Cl isotope composition of 66095 and A16 soils: In 66095, the leachate had a Cl isotope composition of +14.0‰, whereas the non-leachable Cl has a composition of +15.6‰. The A16 soils that were analyzed included mature soil 64501,232 (I_s/FeO=61) and immature soil 61220,39 (I_s/FeO=9.2). The leachate from mature soil (64501) had a Cl isotope composition of +5.6‰ and a non-leachable Cl composition of +15.7‰. The immature soil has a similar Cl isotope composition with the leachate with a Cl isotope composition of +6.1‰ and the non-leachable Cl composition of +14.3‰. Like all the other lunar lithologies analyzed [15], the leachates have a lower δ^{37}Cl than the non-leachable Cl. There is no apparent correlation between δ^{37}Cl and other stable isotopes (δ^{34}S, δ^{13}C).

Carbon Mineralogy: Previously, carbon compound cohenite (Fe_3C) in metallic iron was described [5]. Raman spectra collected on fresh fracture surfaces of 66095 indicate the possible presence of a carbon compound that are associated with the alteration veins. The suspected C-compound is closely associated with oxides and hydroxides, including goethite. Further analyses are being conducted to characterize the suspected C-compound.

Discussion: Sharp et al [15] observed that unlike the Earth and most other materials in the solar system, samples from the Moon exhibited an extremely wide range of δ^{37}Cl. They concluded that the bulk Moon had a δ^{37}Cl that was similar to Earth (~ 0 ‰) and that the wide variation of δ^{37}Cl (-0.7 to 24.5‰) was produced by volatilization of metal halides during the eruption of low H basalts and/or following the loss of H from lunar basalts. In the case of rusty rock 66095, fumarolic activity is more likely to fractionate the Cl more so than either impact or magmatic processes. The few Apollo 16 soil samples must have a Cl component derived from "rusty rock" lithologies. The Cl isotopic fractionation observed in these soils is not a product of different degrees of soil maturity. The appearance of C closely associated with the "rusty" alteration does have implications for the origin of this alteration.

References: [1] Garrison and Taylor (1980) In Proc. Conf. Lunar Highland Crust (ed. Papike and Merrill). 395-417. GCA Supp. 12, Lunar Planetary Institute, Houston. [2] Hunter and Taylor (1981) *Proc. 12th Lunar Planet. Sci. Conf.* 253-259. [3] Hunter and Taylor (1981) *Proc. 12th Lunar Planet. Sci. Conf.* 261-280. [4] Taylor et al. (1974) *Geology* **2**, 429-432. [5] El Goresy et al. (1973) *Proc. 4th Lunar Sci. Conf.* 733-750. [6] Taylor et al. (1973) *Proc. 4th Lunar Sci. Conf.* 829-839. [7] Freidman et al. (1974) *Science* **185,** 346-349. [8] Lunar Sample Compendium. http://curator.jsc.nasa.gov/ lunar/lsc/66095.pdf. [9] Epstein and Taylor (1974) *Proc. 5th Lunar Sci. Conf.* 1839-1854. [10] Nunes and Tatsumoto (1973) Science 182, 916-920. [11] Allen et al. (1973) *Proc. 6th Lunar Sci. Conf.* 2271-2279. [12] Hughes et al. (1973) Lunar Sci. IV 400-402. [13] Jovanovic and Reed (1981) P*roc. 12th Lunar and Planet. Sci. Conf.* 2271-2279. [14] Krahenbuhl et al. (1973) *Proc. 4th Lunar Sci. Conf.* 1325-1348. [15] Sharp et al. (2010) *Science* 329, 1050-1053. [16] Steele et al. (2007*) Meteoritics and Planetary Science* 42, 1549-1566.

IMPACT MELT AND PALAEOREGOLITH DEPOSITS AS IMPORTANT SOURCES OF INFORMATION ABOUT LUNAR HISTORY. M. P. Sinitsyn, Moscow State University, Sternberg Astronomical Institute, Universitetsky prospect,13, Moscow 119992 Russia (msinitsyn.sai@gmail.com)

Introduction: It is well known that among the inner planets of the Solar system, only Mercury and the Moon are atmospherless bodies. This means that they are exposed to a wide range of external radiation. The rays, which leave traces in the lunar regolith can be divided into the following main components: galactic cosmic rays (GCR), solar cosmic rays (SCR) and solar wind (SW). As a consequence we expect that the lunar regolith contains information about the external radiation for the period of exposure. Each of these three types of radiation leaves traces in the form of tracks of protons and alpha particles. Moreover, these tracks are at different depths: SW penetrates to a depth of several microns; SCR – a few inches; GCR – a few meters. In addition, the regolith layer thickness of 1 meter builds up about 1 billion years.

Thus, making the vertical column of the lunar soil up to 4 meters may receive information about changing the content of external radiation in the history of lunar evolution. Unfortunately, in the process of meteorite bombardment (gardening) of regolith on the Moon thickness of 3-5 meters is largely homogenous. The column of regolith, delivered the spacecraft Apollo-12 demonstrated this. It consists of much of the mixed soil, which exposed a few times and then immersed as a result of gardening. Thus, to restore the history of the solar evolution and history of sun's rotation around the galactic center is very important to obtain a layer of the regolith, which was exposed only once in a certain historical period (palaeoregolith). So it is important to find a place where there is access to the palaeoregolith deposits. But now there is an opportunity to explore the surface layers, where gardening of the last 20-200 million years ago did not have time to play a significant role. Such places are apparently melts formed during impact processes.

Lunar immature impact formations

On the lunar surface there are a number of immature formations whose age is suitable to study the vertical cores of soil**.** Studies of impact processes have shown that at typical speeds of meteoroids (10-30 km/sec) impact melt is formed.

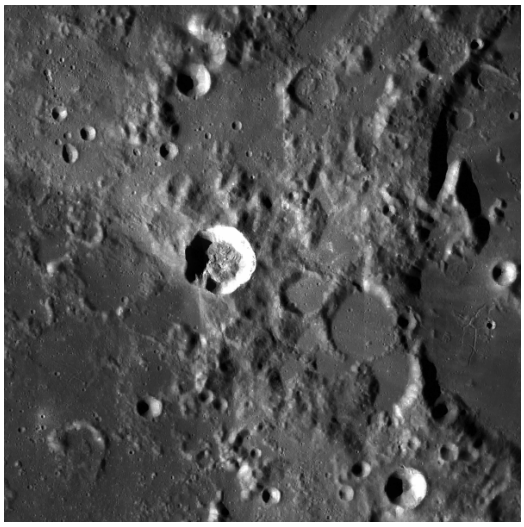

Fig.1 The area of the crater Proclus (LROC camera). Age of the crater is estimated at 20 million years. He is one of the extremely immature formations. Impact melt is visible at the bottom of the crater.

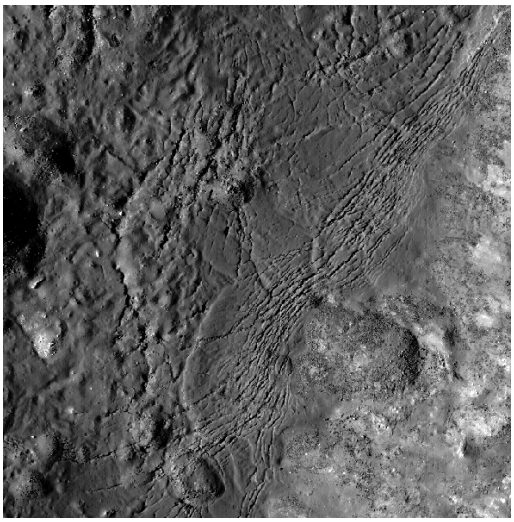

Fig.2 The characteristic form of impact melt on the crater Necho (LROC camera), located on the far side of the Moon.

Figure 2 shows the typical image of impact melt. The following well-known formations: Proclus (Fig.1), Aristarchus, Plinius and some other can be attributed for immature impact formations (up to age 200 million years). This limit due to the fact that the melt will not

have time to undergo a large extent the process of mixing.

Hydrogen anomalies in areas of immature impact formations

It should be noted that immature impact craters on the lunar surface are extremely rare. Based on the distribution of hydrogen produced by Lunar Prospector Neutron Spectrometer (LPNS)[2], we found an abnormal correlation of increased concentration of hydrogen with many immature impact craters. Figure 3 shows the hydrogen anomaly corresponding to the location of the crater Aristarchus

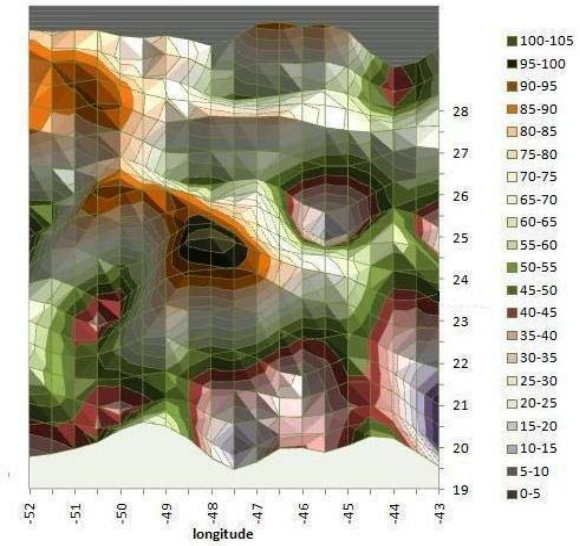

Fig.3 Concentration of hydrogen in the Aristarchus crater by LPNS data [2].

The figure clearly shows significant increased hydrogen content even up to 100 ppm. This is a large value not only for the equatorial region (where is the crater Aristarchus), but even for the polar regions.

We have several such correlations. They indicate that the immature surface formation may have a high concentration of hydrogen. For more accurate recording of these anomalies would be helpful to their confirmation by spectrometer LEND installed on the LRO spacecraft.

It is possible that these anomalies are the realy traces of any cosmic events that have occurred over the past tens millions years of lunar history. Obviously, the traces these events were reflected at the shock melt.

The potential scientific results from study of impact melts and palaeoregolith

In the study of GCR in the long-term scales (> 1 billion years) is possible to trace the rate of star formation in the Galaxy [1]. Traces of the SCR on time scales up to 4 billion years have important information about the early evolution of the Sun. Study the changes of the SW will provide an opportunity to confirm and adjust models of the evolution of the Sun as a main-sequence stars. Information obtained at shorter time intervals, especially reflecting the past 200 million years, can be an opportunity to trace the movement of the Sun through the spiral arms of the Galaxy and supernova explosions in the vicinity of the Sun [1]. Information received from all external radiation on the short and long time scales can be very useful for modeling the evolution of life on Earth.

Because with very high information content of the palaeoregolith deposits and impact melt we consider an important finding and cataloging of these objects for the sampling of them in the future space missions.

References: [1] Crawford, I. A. et al, 2010, Earth Moon Planets, 107, 75-85; [2] http://pdsgescences.wustl.edu/missions/lunarp/reduced_special.html

SURFACE ROUGHNESS AND SLOPES ON THE MOON AT 5-METER SCALE. D. E. Smith[1], M. T. Zuber[1], G. A. Neumann[2], E. Mazarico[1], J. W. Head III[3], and the LOLA Science Tean, [1]MIT, Cambridge, MA 02139 smithde@mit.edu, zuber@mit.edu, [2]NASA Goddard Space Flight Center, Greenbelt, MD 20771, [3]Brown Univ., Providence, RI 02912.

Introduction: The multi-beam laser altimeter (LOLA) on the Lunar Reconnaisance Orbiter (LRO) spacecraft has been mapping the lunar topography for over two years. In addition, LOLA is acquiring laser pulsewidth data that we are using to map the slopes and surface roughness on a 5-m scale, the size of the laser footprint of each beam on the lunar surface.

LOLA Data: The altimeter has 5 beams and makes altimeter and pulsewidth at 28Hz on each of the 5 beams. The width of the laser spots on the surface from 50 km is 5 meters and the measurement of pulse width provides a measure of the topographic variation within the spot which we can interpret with caution as a roughness on the scale of the footprint. The quality of the pulsespread measurement is limited by the instrument to about 20 to 30 cm on a single measurement so we usually average 5 or 10 measurements, equivalent to a spatial average of the 5-meter scale measurments over 50 to 100 meters.

Roughness Variation: The most prominent variation in surface roughnes at these small scales is between surfaces inside relatively young craters and basins compared to some of the maria. The smoother areas indicate a roughness of approximatey 1 meter or less, and for the roughest areas suggest values of approximately 4 meters, possibly indicative or a boulder type enviroment.

References:

[1] Smith D. E. et al (2010) *GRL,* doi:10.1029/2010GL043751.

USING THE RESOURCES OF THE MOON TO CREATE A PERMANENT, CISLUNAR SPACE FARING SYSTEM. P. D. Spudis[1] and T. Lavoie[2], [1]Lunar and Planetary Institute, 3600 Bay Area Blvd., Houston TX 77058 spudis@lpi.usra.edu [2]NASA Marshall Space Flight Center, Huntsville AL 35812 tony.lavoie@nasa.gov

We have previously described an architecture that extends human reach beyond low Earth orbit by creating a permanent space transportation system with reusable and refuelable vehicles [1]. Such a system is made possible by establishing an outpost on the Moon that harvests water and produces rocket propellant from the ice deposits of the permanently dark areas near the poles. Our plan is affordable, flexible and not tied to any specific launch vehicle or family of vehicles. Robotic assets are teleoperated from Earth to prospect, demonstrate and produce water from local resources. These robots are launched separately over several years, allowing the program to be implemented under constrained and uncertain funding conditions. In addition, the stepwise, incremental approach encourages and facilitates international and commercial participation. Humans arrive only after we have begun water production. Once there, the human mission begins to explore the potential for possible, practical, and affordable use of regolith for material production for outpost sustainment and growth. Consistent with the overarching goal to see if we can learn how to live off-planet, another objective of human activity on the Moon will be the experimentation of biological systems and their interaction and performance in the lunar environment. Our arbitrarily defined end stage is a fully functional, human-tended lunar outpost producing 150 metric tonnes of water per year – enough to export water from the Moon and create a permanent, extensible reusable transportation system that allows routine access for people and machines to all points of cislunar space. This cost-effective architecture advances technology and builds a sustainable space transportation infrastructure. By eliminating the need to launch everything from the surface of the Earth, we fundamentally change the paradigm of spaceflight. This lunar outpost serves as the vanguard for studying the practical employment of techniques, processes, and systems that allow humanity to effectively extend its reach off-planet.

Reference [1] Spudis P.D. and Lavoie T. (2011) An affordable lunar return architecture. *Space Manufacturing* **14**, NASA-Ames Research Center, October, 2010, in press.

IMPACT MELT PROPERTIES AND CHARACTERISTICS AS OBSERVED WITH THE LROC NARROW ANGLE CAMERAS. J. D. Stopar[1] B. W. Denevi[2], M. S. Robinson[1], B. R. Hawke[3], S. J. Lawrence[1], and S. Koeber[1] [1]SESE, Arizona State University, Tempe, AZ, [2]Johns Hopkins University Applied Physics Laboratory, Laurel, MD, [3]Hawaii Institute of Geophysics and Planetology, University of Hawaii, Honolulu, HI.

Introduction: Impact craters are ubiquitous on the surface of the Moon, and any future lunar surface activities will encounter the products of impacts. Therefore, the new views of impact craters provided by the Lunar Reconnaissance Orbiter (LRO) suite of science instruments will play a key role in characterizing and utilizing surface materials. The Lunar Reconnaissance Orbiter Camera (LROC) Narrow Angle Cameras (NACs) provides sub-meter pixel scale insights into the products and distribution of glassy melt products including impact melt flows and sprays [1-3] and impact melt ponds [4-5]. The physical properties and dynamics within these materials can be inferred from these images [3,5]. Impact melts can occur as thin veneers, ponds, sheets, or lava-like flows [e.g., 6-7]. Here we present new LROC NAC images of fresh impact melt materials and characterize the different types of impact melt deposits observed from meter to kilometer scale craters, with a focus on sub-kilometer craters.

Methods: More than 800 fresh, randomly distributed impact craters (D<15km) were identified for study based on their Clementine maturity parameter, albedo, presence of ejecta rays, radar properties, and by visual inspection of LROC images. About 20% of these craters have been imaged with the NAC. A pair of NAC images provides ~0.5 m/pixel scale at 50-km altitude with a combined swath width of 5 km and length of 26 km [8]. For craters greater than a few kilometers in diameter, more than one NAC image pair is required for complete coverage. Melt flows and ponds were digitized using ArcGIS for spatial analysis and, when combined with the LROC Wide Angle Camera (WAC)-derived Digital Elevation Model (DEM), topographic analysis. Limited NAC DEMs are currently available.

Results and Discussion: Sub-meter detail of diverse impact melt materials are well preserved in many fresh impact craters. At least two types of impact deposits have thus far been identified based on morphology and reflectance: 1) a lower reflectance and smooth material (LSM), and 2) deposits of moderate to higher reflectance and often rubblier material (MRM) (Fig. 1). The LSM is interpreted to be impact melt and is typically found near the crater rim, in the crater, and occasionally as thin stringers, or rays, up to roughly one crater radius in length. The MRM typically extends over a larger area and in some cases displays flow lobes similar in form to low-viscosity terrestrial lava flows. In other cases, MRM can be difficult to distinguish from granular ejecta. Therefore, MRM could be a mix of melt and non-melt ejecta. We cannot yet rule out that the flow forms are a granular material deposited in a fluidized manner. Further study will investigate the relationship between these melt types, target material, impact dynamics, melt volumes, and underlying slope and topography to address the distribution of these two types of melt and their most likely composition.

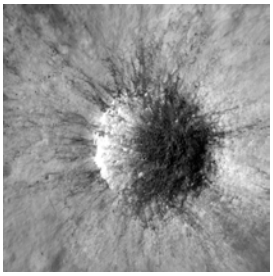

Figure 1: 480 m fresh impact crater (161.25° E, 16.26° N) with low reflectance stringers (interpreted as melt rich) apparently superposed on a higher reflectance veneer.

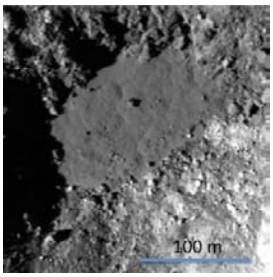

Figure 2: A fresh, smooth ~100 m LSM melt pond in a 700-m crater (348.52° E, 15.54° N) exhibiting an undulatory surface texture. This pond is too small to have cooling cracks.

Melt Ponds. In this study, impact melt ponds have thus far been unambiguously detected in craters with diameters as small as ~450 m, and [4] identified impact melt ponds in the bottoms of craters with diameters as small as ~200 m. Melt ponds often have variable albedo, both from crater to crater and sometimes within the same crater. LSM ponds typically appear fresh, with no superposed craters from later impacts, have smooth and undulatory surfaces, and often have cooling cracks (Fig. 2). MRM floor deposits occur as flat-lying, hummocks, or mounds, implying that there may be different types of MRM associated with impact craters. Smaller craters with interior MRMs generally do not display cooling cracks. Craters with MRMs more frequently have superposed craters, suggesting that some MRM craters are older than those with LSM (Fig. 3). Many of the radar-bright craters of [9] are correlated with large blocks mixed with melt on the floors of craters (Fig. 4). Future work will investigate

why some craters have more boulders than melt on the floor.

Melt Veneers. Impact melt veneers occur in many fresh craters but are seen very clearly in several oblique craters with asymmetric ejecta distributions. In these craters, the LSM melt veneer coats the interior of the crater on the side opposite the most prominent LSM exterior melt (Fig. 5), consistent with an oblique impact [e.g., 6-7]. Some craters have deposits of MRM that also resemble melt veneers, but it is not clear whether or not these materials are composed, at least in part, of melted ejecta. They may also be granular "flows" particularly on the interior slopes of crater walls [e.g., 4] (Fig. 6).

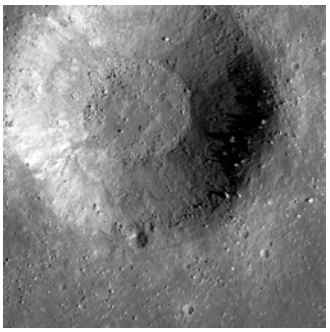

Figure 3: A 940 m crater (62.7°E, 12.9°N) with MRM floor deposits. A crater superposed on the rim and less visible ejecta rays suggest that this crater is less fresh those in Figs. 1, 2, 4, and 5.

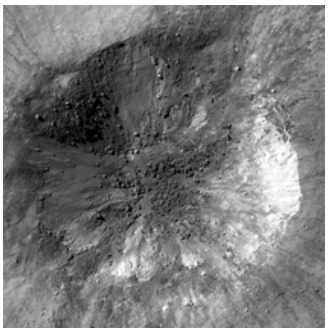

Figure 4: A fresh 1.4 km radar-bright impact crater (17.23° E, 33.72° S) with large boulders on crater interior and floor mixed with extensive LSM melt.

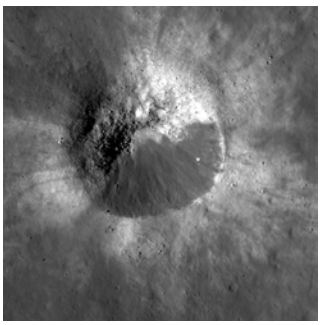

Figure 5: A fresh 550 m crater (336.01° E, 15.53° N) with asymmetric melt distribution. A thin veneer coats the interior crater wall opposite the LSM ejecta to the NW, suggesting an oblique impact.

Melt Flows. Impact melt flows have been identified within one crater diameter of impact craters as small as 3-km in diameter [1-4, 6-7]. Given that the volumes of impact melts are expected to scale with the size of the crater [10], it is perhaps surprising that craters this small can produce sufficient melt to form flows. [7] found a correlation between impact melt flows and craters with asymmetric melt distribution, in some cases, likely due to topographic controls on melt coalescence, and this finding is now supported by [3]. Impact melt flows sometimes entrain rubbly ejecta materials along their flow margins, implying that these flows of melt occurred after the deposition of rubbly ejecta, consistent with previous models [6,11]. Many of the flows have channels.

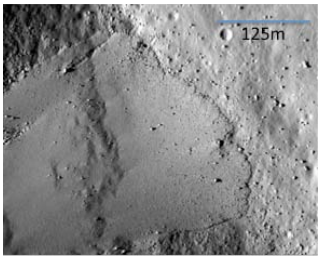

Figure 6: Probable debris flow, but possibly melt, covering part of MRM floor deposits in a 12.4 km crater (354.78° E, 3.22° S).

Discussion and Summary: Characterization of the types and morphologies of impact melt and ejecta materials is useful in the characterization of future exploration sites. Observations from the NAC images have shown that impact melt products are more extensive than previously thought and can be found beyond 1 crater radius [e.g., 4,12]. Impact melts can be used to infer the properties of the target material [e.g., 8], and can be used to infer freshness of an impact crater. Different types of impact melt associated with a single crater may suggest multiple generations of melt as in [5]. Small mare and highlands craters allow investigation of the influence of target material and strength on the development and distribution of impact melt and interior deposit morphology. NAC images show that even relatively fresh impact craters can have significant degradation due to mass wasting.

Acknowledgements: The authors thank the LROC Team, LROC Science Operations Center staff, and LROC students for their assistance.

References: [1] Hawke, B. R., et al. (2010) LPSC #1611. [2] Hawke, B. R., et al. (2011) LPSC #2347. [3] Denevi, B. W., et al. (in prep). [4] Plescia, J. B., et al. (2011) LPSC #2033. [5] Bray, V. J., et al. (2010) GRL 37: L21202. [6] Howard, K. and Wilshire, H. (1975) J. Res. U.S. Geol. Surv. 3, p. 237-251. [7] Hawke, B. R. and Head, J. (1977) in *Impact and Explosion Cratering*, p. 889-912. [8] Robinson, M. S., et al. (2010) Space Sci. Rev. 150: 81-124. [9] Thompson, T., et al. (1981) Icarus 46: 201-225. [10] Cintala, M. and Grieve, R. (1998) Met. Plan. Sci. 33: 889-912. [11] El-Baz, F. (1972) in *Apollo 16: Prelim. Sci. Rep*., p. 29-62 – 29-70. [12] Robinson, M. S., et al. (2011) LPSC #2511.

The Lunar Reconnaissance Orbiter: Plans for the Science Phase R. R. Vondrak[1], J. W. Keller[1], G. Chin[1], J. B. Garvin[1], J. W. Rice Jr.[1], N. E. Petro[1], [1]Goddard Space Flight Center, Greenbelt MD 20771.

Introduction: The Lunar Reconnaissance Orbiter spacecraft (LRO), launched on June 18, 2009, began with the goal of seeking safe landing sites for future robotic missions or the return of humans to the Moon as part of NASA's Exploration Systems Mission Directorate (ESMD). In addition, LRO's objectives included the search for surface resources and to investigate the Lunar radiation environment. After spacecraft commissioning, the ESMD phase of the mission began on September 15, 2009 and completed on September 15, 2010 when operational responsibility for LRO was transferred to NASA's Science Mission Directorate (SMD). The SMD mission is scheduled for 2 years and will be completed in 2012 with an opportunity for an extended mission. Under SMD, the mission focuses on a new set of goals related to understanding the geologic history of the Moon, its current state, and what it can tell us about the evolution of the Solar System.

Having marked the two-year anniversary, we will review here the major results from the LRO mission for both exploration and science and discuss plans and objectives going forward. Results from the LRO mission include but are not limited to the developent of comprehensive high resolution maps and digital terrain models of the lunar surface; discoveries on the nature of hydrogen distribution, and by extension water, at the lunar poles; measurement of the day and night time temperature of the lunar surface including temperature down below 30 K in permanently shadowed regions (PSRs); direct measurement of Hg, H_2, and CO deposits in the PSRs, evidence for recent tectonic activity on the Moon, and high resolution maps of the illuminication conditions as the poles.

The objectives for the second phase of the mission under SMD include: 1) understanding the bombardment history of the Moon, 2) interpreting Lunar geologic processes, 3) mapping the global Lunar regolith, 4) identifying volatiles on the Moon, and 5) measuring the Lunar atmosphere and radiation environment.

The instruments, which were describe in detail previously[1], include ***Lunar Orbiter Laser Altimeter (LOLA)***, PI, David Smith, NASA Goddard Space Flight Center, Greenbelt, MD, ***Lunar Reconnaissance Orbiter Camera (LROC)***, PI, Mark Robinson, Arizona State University, Tempe, Arizona, ***Lunar Exploration Neutron Detector (LEND)***, PI, Igor Mitrofanov, Institute for Space Research, and Federal Space Agency, Moscow, ***Diviner Lunar Radiometer Experiment (DLRE),*** PI, David Paige, University of California, Los Angeles, ***Lyman-Alpha Mapping Project (LAMP)***, PI, Alan Stern, Southwest Research Institute, Boulder, Colorado, ***Cosmic Ray Telescope for the Effects of Radiation (CRaTER)***, PI, Harlan Spence, University of New Hampshire, New Hampshire, and ***Mini Radio-Frequency Technology Demonstration (Mini-RF)***, P.I. Ben Bussey, Applied Physics Laboratory, Maryland.

Figure 1 The fully assembled and thermal blanketed spacecraft.

Data Access: All of the LRO data are added to the Planetary Data System on three month intervals, with no data or data products older than 6 months. As of September 15 2011 more than 250 TBytes of data have been made available to the science community.

References: [1] Vondrak, R.R., Keller, J.W., and Russell, C.T., (Ed.s), 2010, Lunar Reconnaissance Orbiter Mission, New York, Springer.

FIRST COSMIC RAY ALBEDO PROTON MAP OF THE MOON. J. K. Wilson[1], H. E. Spence[1], A. W. Case[2], J. B. Blake[3], M. J. Golightly[1], J. Kasper[2], M. D. Looper[3], J. E. Mazur[3], N. Schwadron[1], L. W. Townsend[4], C. Zeitlin[5], [1]Space Science Center, University of New Hampshire, Durham, NH, (jody.wilson@unh.edu), [2]High Energy Astrophysics Division, Harvard CFA, Cambridge, MA, [3]The Aerospace Corporation, Los Angeles, CA, [4]Department of Nuclear Engineering, University of Tennessee, Knoxville, TN, [5]Southwest Research Institute, Boulder, CO.

Introduction: High energy cosmic rays are constantly bombarding the lunar regolith, producing secondary "albedo" particles like protons and neutrons, some of which escape back to space. Two lunar missions, Lunar Prospector and LRO, have shown that the energy distribution of albedo neutrons in particular is modulated by the elemental composition of the lunar regolith[1], [2]. In particular, reduced neutron fluxes near the lunar poles appear to be the result of collisions with hydrogen nuclei in ice deposits[3] in permanently shadowed craters. We explore the possibility that the flux of escaping lunar protons might also be dependent on regional compositional variations, either due to spallation yields or to energy loss in secondary collisions.

CRaTER Instrument: The Lunar Reconnaissance Orbiter (LRO) has been observing the surface and environment of the Moon since June of 2009. The CRaTER instrument (Cosmic Ray Telescope for the Effects of Radiation) on LRO is designed to characterize the lunar radiation environment and its effects on simulated human tissue. CRaTER's multiple solid-state detectors can be used to discriminate the different elements in the galactic cosmic ray (GCR) population above ~10 MeV/nucleon, and can also distinguish between primary GCR protons arriving from deep space and albedo particles propagating up from the lunar surface.

Summary of Results: We use albedo protons with energies greater than 60 MeV to construct a cosmic ray albedo proton map of the Moon. The yield of albedo protons is proportional to the rate of lunar proton detections divided by the rate of incoming GCR detections. The map accounts for time variation in the albedo particles driven by time variations in the primary GCR population, thus revealing any true spatial variation of the albedo proton yield.

We find no obvious albedo features corresponding to regional differences in elemental composition of the regolith, such as between maria and highlands. The distribution of albedo values resembles the Poisson distribution that is expected for ~330,000 detected protons, meaning the map is consistent with a spatially uniform albedo. More data will improve the counting statistics and lower the detection threshold for any proton albedo features.

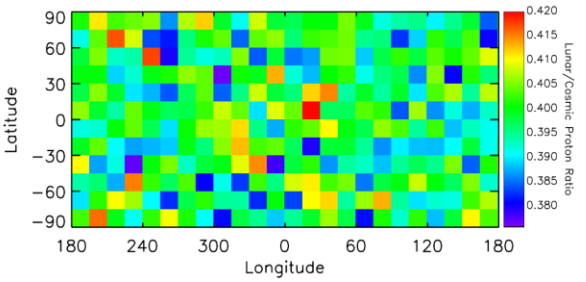

Figure 1. Map of the lunar albedo proton "yield."

References: [1] Feldman W. C. et al. (1998) *Science, 281*, 1496. [2] Mitrofanov I. G. et al. (2010) *Science, 330*, 483. [3] Feldman W. C. et al. (1997) *JGR, 102*, 25565.

DEVELOPMENT AND TESTING OF GAS ASSISTED DRILL FOR THE EMPLACEMENT OF THE CORNER CUBE REFLECTOR SYSTEM ON THE MOON. K. Zacny[1], D. Currie[2], G. Paulsen[3], A. Avanesyan[4], P. Chu[5], T. Makai[6], T. Szwarc[7], [1]Honeybee Robotics (zacny@honeybeerobotics.com), [2]University of Maryland, [3-6]Honeybee Robotics, [7] Stanfod University

Introduction: The Lunar Laser Ranging Retroreflector Array for the 21st Century (LLRRA-21) in combination with a Lunar Laser Ranging (LLR) program within the International Laser Ranging Service (ILRS) would provide extensive new information on the lunar interior, General Relativity and cosmology. Since the Apollo, the ground stations improved the ranging accuracy by 200x and now the Apollo arrays located on the lunar surface provide a significant limitation of the LRR accuracy. One of the objectives of the current program is to provide for the further improvement in ground station accuracy over the next few decades.

During the day/night lunar cycle, the regolith will rise and fall by almost 500 µm. Yet, it is estimated that the thermal variation 0.5 m - 1 m below the surface is less than 0.1 °C throughout the month. Thus to achieve 10 µm ranging performance, the CCRs must be anchored to that thermally stable mass at 0.5 m or greater depth.

Pneumatic Drilling Approach: The proposed emplacement approach uses gas-powered drill consisting of a 1 m long, slim hollow rod with perforated anchor-cone at its lower end and the CCR mounted to the top. Gas supplied from a small tank is directed into and down the rod and out through the cone lofting the soil out of the hole and allowing the rod to sink to 0.5 m depth.

Laboratory Tests: We conducted a number of tests in compacted JSC-1a lunar soil simulant and inside a vacuum chamber (see Figure 1). In all tests, the rod with a cone at the end (see Figure 2) was placed on the top of the soil surface. Once vacuum was reached, the soil bin was temporarily vibrated to compact the soil.

The test involved opening and monitoring gas flow and recording the rate of the rod sinkage into the soil. The rod and the CCR can on top weighed 1.6 kg. This mass provided the only vertical force (16 Newton) to the cone.

In several tests, the rod successfully sunk to a 50 cm depth in 4-6 minutes. The gas pressure was 101kPa absolute and the mass of gas used was 10-20 grams.

The gas-ejected soil particles travel up the hole (between the hole and the rod), and were effectively deflected sideways by the shield.

These tests successfully demonstrated the gas assisted drilling approach. Thus, the LLRRA-21 will require no power and could be deployed from lightweight lunar platforms.

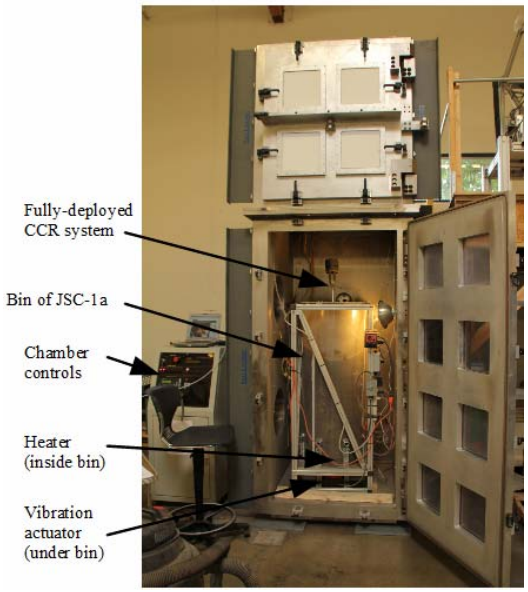

Figure 1. The CCR system was successfully deployed to 50 cm depth into compacted JSC-1a soil inside a vacuum chamber.

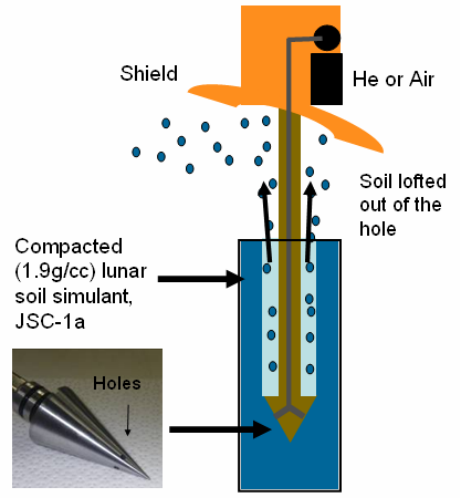

Figure 2. The details of the cone experimental set up.

Acknowledgement: This project is funded by the NLSI Lunar University Network for Astrophysics Research (LUNAR) project (PI. Jack Burns).

TESTING OF A PNEUMATIC PROBOSCIS HEAT FLOW PROBE IN A VACUUM CHAMBER AND JSC-1A LUNAR SOIL SIMULANT. K. Zacny[1], G. Paulsen[1], J. Shasho[1], J. Craft[1], M. Hedlund[1], B. Mellerowicz[1], T. Makai[1], T. Szwarc[2], S. Nagihara[3], P. Taylor[4], B. Milam[4], [1]Honeybee Robotics (zacny@honeybeerobotics.com); [2]Stanford University, [3]Texas Tech University, [4]NASA GSFC

Introduction: A heat-flow probe directly addresses the goal of the Lunar Geophysical Network, which is to understand the interior structure and composition of the Moon [1].

To place 1 kg on the surface of the Moon costs ~$50k to $100k. Thus, any scientific instruments must be efficient with respect to limited spacecraft resources such as mass, power, and volume without compromising THE scientific quality OF THE measurements.

A key challenge for heat flow measurement is to install thermal sensors to A DEPTH LEAST A OF ~3 m SO that THEY are not influenced by the diurnal, annual, and longer-term fluctuations of the surface thermal environment. In addition, once deployed, the heat flow probe should cause little disturbance to the thermal regime of the surrounding regolith.

Pneumatic Proboscis Heat-Flow Probe Concept: OUR heat flow probe system uses a pneumatic (gas) approach to lower the temperature and thermal conductivity sensors attached to a bi-convex tape to >3 meters. ThIS system is a revolutionary innovation for small landers as it has extremely low mass, volume, and simple deployment.

The pneumatic heat flow architecture implements concave/convex tapes in a different manner to arrive at a bi-convex (lenticular) shape. A set of two tapes are arranged in a biconvex configuration and bound together, forming a rigid rod capable of pressing the needle tip into the soil. RTDs are AN integral PART OF the tape. The tape is coiled around a deployment drum similar to how a tape measure functions. The full length of the heat flow probe can then be packaged in a small form factor around the drum. Compressed gas is plumbed to the nozzle at the end of the tape which provides the mechanism for penetration into the regolith. A heating needle with an RTD protruding from below the cone measures the temperature and conductivity of undisturbed regolith ahead of the cone.

Helium gas, used for pressurizing liquid propellant and typically vented once on the surface, THEY can be scavenged from the lander propulsion system, making OUR thermal probe system lighter. Honeybee demonstrated that 1 gram of N2 at 5 psia can lift 6000g of JSC-1a in lunar conditions (vacuum, 1/6g) [3]. Thus, only a small amount of gas would be required.

Testing: We tested the heat flow probe in compacted (1.9 g/cc JSC-1) lunar soil simulant inside a vacuum chamber, Figure 1. The probe reached a maximum possible depth of 70 cm and acquired BOTH thermal GRADIENT as well as thermal conductivity DATA using THE needle heater AT THE BASE OF the cone. The thermal conductivity was calculated to be ~0.04 W/m/K, which is in the range of the conductivities of the REGOLITH at that pressure [4].

The concept of the heat flow probe deployment is shown in Figure 2. The probe is mounted along the leg of the lander (*i.e.*, closer to the ground) and deployed upon LANDING. The required gas is provided in the form of pressurant Helium from the propulsion system.

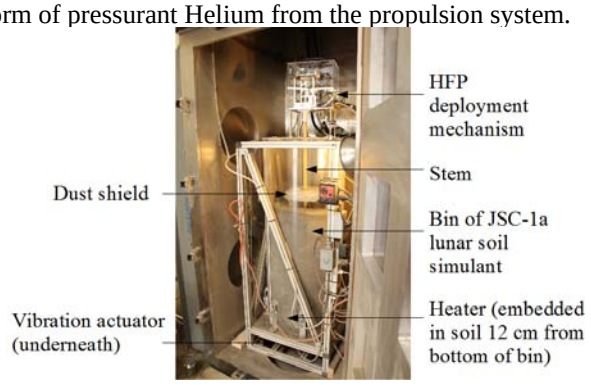

Figure 1. Pneumatic Proboscis heat flow probe being tested inside vacuum chamber in compacted JSC-1a lunar soil simulant.

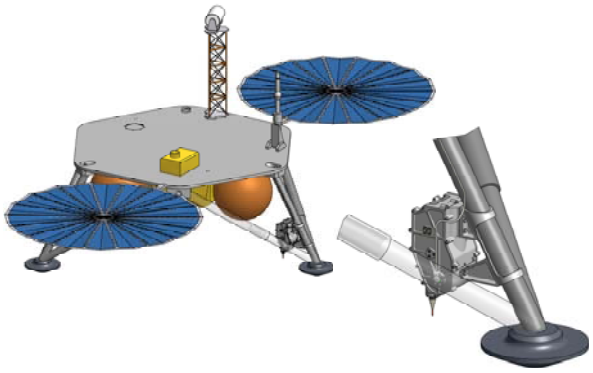

Figure 2. Conceptual Design of the Heat Flow Probe mounted on Spacecraft Landing System

References: [1] Science Definition Team for the ILN Anchor Nodes, ILN Final Report (2009). [2] Zacny, K. Methods and Considerations for Heat Flow Probe Deployment, NLSI (2009). [3] Zacny, K. (2009) *LPSC XXXX*, Abstract #1070.[4] Heiken, G. et al. (1991) Lunar Source Book, 37-38.

A NEW HYPOTHESIS FOR MARE BASALT VOLCANISM, VOLATILE DISTRIBUTION IN THE LUNAR MANTLE, AND MOONQUAKES, S. J. Zhong, Department of Physics, University of Colorado at Boulder, Boulder, Colorado 80309, USA (szhong@colorado.edu)

Introduction: Lunar basalt volcanism, deep moonquakes, and heterogeneities in volatile concentration (water) in the lunar mantle are distinct features of the Moon. They occur in different spatial and temporal domains. The goal of this study is to explore the possible relationship between them.

Mare basalts. Mare basalt volcanism occurred around 3.8 Ga ago and lasted for more than 1 Ga. Mare basalt volcanism is probably the most important volcanic and tectonic event in the lunar geological history after the formation of the lunar anorthositic crust that resulted from solidification of the lunar magma ocean [1]. Two characteristics of mare basalt volcanism are important for understanding the origin of the volcanism. The first is its hemispherically asymmetric distribution, that is, the volcanism predominantly occurred on the nearside of the Moon (Fig. 1) [2]. The second is that the distribution of rare earth elements of bare basalts is complementary to that of the anorthositic crust, suggesting that mare basalts were derived from remelting the melt residue that crystallized contemporaneously with the anorthositic crust [3]. There is also evidence that indicates a deep source region of mare basalts, possibly at ~500 km depth [4].

Deep Moonquakes. Moonquakes recorded by seismometers deployed in Apollo missions in 1970s display a couple of important characteristics. First, they mostly occur at large depths (~800 km) as clusters and on the nearside of the Moon (Fig. 1) [5-10]. They are correlated with mare basalt distribution [5], as recently quantified [11]. Second, the deep moonquakes show correlations with Earth-Moon tides [12-14]. Although it is possible that the occurrence of moonquakes in the nearside is partially attributed to the uneven distribution of the limited number of seismometers (i.e., all of the four seismometers were on the nearside) [8], a cluster of moonquakes, A33, from the farside were detected from the seismometers [8-10], indicating the capability of the seismometers in locating moonquakes from the farside.

Volatiles and water. Recent spacecraft studies of lunar surfaces [15-17] and laboratory analyses lunar rock samples [18] suggest that the Moon contains significant amount of water at its surface and in the lunar interiors. The water has significant effects on both elastic and viscous deformation of rocks [19,20]. Therefore, the discovery of significant amount of water in the interior of the Moon has implications for the early evolution of the Moon and as well as recent lunar tectonic activities such as moonquakes.

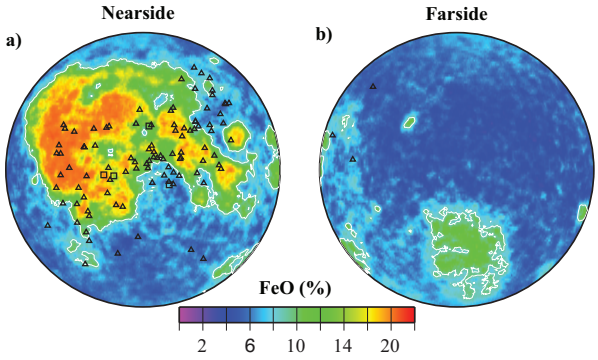

Fig. 1. The surface distribution of FeO on the (A) nearside and (B) farside of the Moon [2]. High concentration of FeO is indicative of mare basalts. Deep moonquakes are also plotted as symbols [10].

Previous Studies and Outstanding Questions: To account for the chemical characteristics and the hemispheric asymmetry of mare basalt volcanism, a number of studies have considered lunar mantle dynamics that may lead to hemispherically asymmetric structure in melt residue materials that are remelted due to temperature anomalies [21-23]. In one of the models [22], the remelting of the melt residue materials was suggested to be caused by dynamically developed upwellings in one hemisphere. While such models lead to hemispherically asymmetric distributions of not only surface volcanism but also the mantle interior structure, these studies did not explore time evolution of lunar mantle structure from the early lunar history (~3.8 Ga ago when the mare basalt volcanism occurred) to the present-day.

Moonquakes are poorly understood. Tidal deformation models have been formulated to explain the characteristics of some moonquakes [11-14]. These tidal deformation models often assume elastic parameters that vary only in the radial direction with no lateral variability which enable simple analytic solution approaches. However, three features of moonquakes present challenges to simple tidal models. First, moonquakes occur in highly localized regions and form clusters [10], while predicted tidal deformation tends to be of long-wavelength and smoothly varying. Second, tidal deformation is always symmetric, but moon-

quakes clearly show much higher concentration on the nearside than on the farside. Third, tidal stress tends to be small in magnitude, and it is unclear whether tidal stress is large enough to cause moonquakes at large depths [10]. Frohlich and Nakamura [10] recently suggested that fluids may play an important role in causing moonquakes in dynamic interaction with tidal stresses. However, to test this idea is beyond the current tidal deformation models.

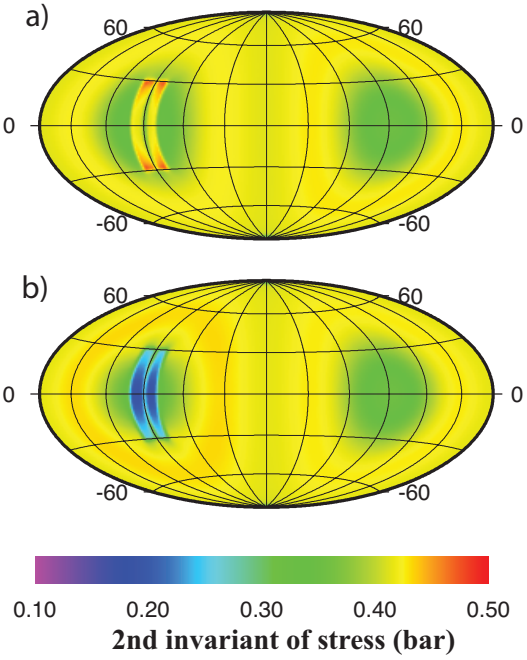

Fig. 2. Tidal stress at a depth of 1000 km from 3-dimensional tidal deformation model calculations with a) shear modulus on nearside in a 10^{o}x60^{o} region is reduced by 50% and b) increased by 50%. Notice that stress is enhanced with reduced shear modulus on the nearside.

A New Hypothesis: I propose a new hypothesis for lunar mantle structure evolution and its control on moonquake occurrence in interaction with tidal deformation. I also outline strategies to test this hypothesis and present preliminary results. I hypothesize that accompanying the mare basalt volcanism, the lunar mantle temperature, volatiles and fluids develop globally asymmetric distributions such that the nearside of the Moon has acquired a higher temperature and higher concentration of volatiles. Such distributions have been maintained throughout the lunar geological history to the present-day and are responsible for the high concentration of clusters of moonquakes on the nearside of the Moon as the asymmetric mantle structure interacts with the tidal forces.

To test this hypothesis, I have formulated preliminary tidal deformation models that differ from previous models in incorporating realistic three-dimension elastic parameters to account for the possible effects of fluids and volatiles. I use three-dimension viscoelastic finite element code CitcomSVE that was developed to study earth's post-glacial rebound [24,25]. The new models capable to include rapid variations in elastic parameters caused by fluids enable determinations of tidal stress variations over small length-scales that are comparable with those of moonquake clusters. Preliminary results (Fig. 2) show that three-dimension elastic parameters may influence tidal stress and stress rate significantly. Particularly, regions with reduced elastic parameters (e.g., shear modulus) show enhanced stresses, thus having implications for deep moonquakes.

References: [1] Ringwood A.E. & S.E. Kesson (1976) LPSC 7, 1697-1722. [2] Lawrence et al. (2002), JGR, 107, doi:10.1029/2011JE001530. [3] Taylor R.S. (1982) *A lunar perspective*, LPI, 481 pp. [4] Delano J.W. (1986) *JGR* 91, 201-213. [5] Lammlein D.R. et al. (1974) *Rev. Geophys. Space Phys*. 12, 1–21. [6] Nakamura, Y. et al. (1973) *Science* 181, 49–51. [7] Nakamura, Y. (2003) *PEPI* 139, 197–205. [8] Nakamura, Y. (2005) *JGR* 110, E0100. [9] Bulow, R.C et al. (2007) *JGR* 112, E09003. [10] Frohlich C. & Y. Nakamura (2009) *PEPI 173,* 365-374. [11] Muirhead & Zhong (2011), LPSC. [12] Latham G. et al. (1971) *Science* 174, 687-692. [13] Cheng C.H. & Toksöz M.N. (1978) *JGR* 83, 845–853. [14] Minshull, T.A. & Goulty N.R. (1988) *PEPI* 52, 41–55. [15] Pieters C. M. et al. (2009) *Science* 326, 568-572 [16] Sunshine J.M. et al. (2009) *Science* 326, 565-568. [17] Clark R.N. (2009) *Science* 326, 562-564. [18] Saal, A.E., et al. (2008) *Nature* 454, 192-195. [19] Karato S. (1986) *Nature*, 319, 309-310. [20] Hirth G. & D. L. Kohlstedt (1995) *EPSL* 144, 93-108. [21] Hess P.C. & E.M. Parmentier (1995) *EPSL* 134, 501-514. [22] Zhong S. et al. (2000) *EPSL* 177 131-140 [23] Parmentier E.M. et al. (2002) *EPSL* 201, 473-480. [24] Zhong S. et al. (2003) *GJI* 155, 679-695. [25] Paulson et al. (2005) *GJI* 163, 357-371.

UPDATE ON THE GRAIL TWIN SPACECRAFT MISSION TO THE MOON. M. T. Zuber[1], D. E. Smith[1], M. Watkins[2], and S. Asmar[2], [1]MIT Cambridge, MA 02139 zuber@mit.edu, smithde@mit.edu, [2]JPL Pasadena, CA 91109.

The twin GRAIL spacecraft were successfully launched to the Moon at 1308 GMT on Sept 10, 2011 in a trajectory that will place the two spacecraft in lunar orbit on December 31 this year and on Jan 1, 2012. After approximately 2 months of refining the orbits of the two spacecraft the science phase will begin with the spacraft approximately 60 km apart in a near cirular polar orbit at 55 km avaregae altitude above the lunar surface. For 82 days the spaecraft will map the lunar gravity field in unprecedented detail.

The status of the mssion, the twin spacecraft, and the anticipated scientific return will be presented.

NOTES

NOTES